Santana Barros, K.; Martí Calatayud, MC.; Scarazzato, T.; Moura Bernardes, A.; Espinosa, DCR.; Pérez-Herranz, V. (2021). Investigation of ion-exchange membranes by means of chronopotentiometry: A comprehensive review on this highly informative and multipurpose technique. Advances in Colloid and Interface Science. 293:1-31. https://doi.org/10.1016/j.cis.2021.102439

Investigation of ion-exchange membranes by means of chronopotentiometry: a comprehensive review on this highly informative and multipurpose technique

Kayo Santana Barros [1]; Manuel César Martí-Calatayud [2]; Tatiana Scarazzato [3]; Andréa Moura Bernardes [4], Denise Crocce Romano Espinosa [5], Valentín Pérez-Herranz [6]

[1,5] Department of Chemical Engineering, University of São Paulo (USP). Address: Av. Professor Lineu Prestes, 580, Bloco 18 – Conjunto das Químicas, 05434-070. São Paulo – SP. Brazil.

[1,2,6] IEC Group, ISIRYM, Universitat Politècnica de València – Spain. Address: Camí de Vera s/n, 46022, P.O. Box 22012, València E-46071, Spain

[3,4] Department of Materials Engineering, Federal University of Rio Grande do Sul (UFRGS). Address: Av. Bento Gonçalves, 9500, 91501-970, Porto Alegre, Brazil

[1]Corresponding author: kayobarros@alumni.usp.br
[2] mcmarti@iqn.upv.es
[3] tatiana.scarazzato@gmail.com
[4] amb@ufrgs.br
[5] espinosa@usp.br
[6] vperez@iqn.upv.es

Abstract: Electrodialysis is mostly used for drinking water production but it has gained applicability in different new fields in recent decades. Membrane characteristics and ion transport properties strongly influence the efficiency of electrodialysis and must be evaluated to avoid an intense energy consumption and ensure long membrane times of usage. To this aim, conducting studies on ion transport across membranes is essential. Several dynamic characterization methods can be employed, among which, chronopotentiometry has shown special relevance because it allows a direct access to the contribution of the potential in different states of the membrane/solution system. The present paper provides a critical review on the use of chronopotentiometry to determine the main membrane transport properties and to evaluate mass transfer phenomena. Properties, such as limiting current density, electrical resistances, plateau length, transport number of counter-ions in the membrane, transition times, and apparent fraction of membrane conductive area have been intensively discussed in the literature and are presented in this review. Some of the phenomena evaluated using this technique are concentration polarization, gravitational convection, electroconvection, water dissociation, and fouling/scaling, all of them also shown herein. Mathematical and experimental studies were considered. New trends in chronopotentiometric studies should include ion-exchange membranes that have been recently developed (presenting anti-fouling, anti-microbial, and monovalent-selective properties) and a deeper discussion on the behaviour of complex solutions that have been often treated by electrodialysis, such as municipal wastewaters. New mathematical models, especially 3D ones, are also expected to be developed in the coming years.

Keywords: Electrodialysis; chronopotentiometry; current-voltage curve, overlimiting phenomena; electroconvection.

1. Introduction

Electrodialysis is a membrane separation process that allows the extraction and recovery of ions from an electrolyte solution by applying an electrical potential difference between different compartments separated by ion-selective membranes. Considering an ideal system, cation-exchange membranes (CEMs) are polymeric films that allow only the passage of cations between compartments, while they block the transfer of anions. In turn, anion-exchange membranes (AEMs) allow the transfer of anions and block the passage of cations. One of the first applications of electrodialysis was proposed by Maigrot and Sabates in 1890, who suggested using an electrodialysis system to demineralize sugar syrup using permanganate paper as membrane [1]. From the 1950s, electrodialysis has often been used to produce drinking water from brackish water sources, and it still plays an important role in this field. Electrodialysis has become a highly adaptable, multifunctional process, being applied in industrial effluent treatment, in the pharmaceutical and food industry, and for producing organic acids and ultrapure water [2]. Parallel to the evolution of electrodialysis systems, membranes rendering more efficient ion transport have also been developed, that is, membranes with improved selectivity, reduced resistance, and low manufacturing cost. Dynamic characterization techniques are essential to compare the wide variety of new membrane materials under diverse operating conditions and applied to different electrolyte systems. Several dynamic characterization methods can be used for determining the transport properties of ions through the membranes, such as impedance spectroscopy, cyclic voltammetry, linear sweep voltammetry (potential sweeps) and chronopotentiometry.

Chronopotentiometry is an electrochemical method widely used to investigate mass transfer and reactions taking place in electrolytic solutions near electrodes [3–5] and ion-exchange membranes [6–8]. For the latter, a current density (i) is applied to a system composed of an ion-exchange membrane flanked by an electrolytic solution at both sides. The current is imposed between a working and a counter electrode that are placed at both ends of the electrochemical cell, while the variation in voltage (potential drop) between both sides of the membrane is measured over time using two reference electrodes. Chronopotentiometry provides valuable information on the progress of ion transport through the membranes, such as the ohmic contribution to the system resistance and the development of concentration polarization. The latter is a phenomenon responsible for the saturation of the current density when ion concentration vanishes at the membrane-

solution interface. The current density from which an intense polarization concentration occurs is called limiting current density, whereas the time required for the ion depletion during this phenomenon is called transition time. Both can be determined by chronopotentiometry. This technique can also be used to determine the apparent fraction of membrane conductive area and the transport number of counter-ions in the membrane phase, which indicates the fraction of the current that is carried by a specific type of ions that cross the membrane. In addition to the dynamic monitoring of ion transport through ion-exchange membranes, the steady-state behavior of membrane systems can be also obtained by means of chronopotentiometry. This is represented in the form of current-voltage curves (or polarization curves), from which the limiting current density, the electrical resistance of the membrane system under different current regimes, and the plateau length can be obtained [9]. Yet, the potential of chronopotentiometry is not merely restricted to the quantitative evaluation of ion conduction across different membrane materials; this technique has shown its applicability in a variety of qualitative studies focused on the investigation of mass transfer mechanisms, for example, in the characterization of competitive ion transport in complex electrolyte mixtures, or as a tool to gather information on the development of fouling and scaling phenomena.

In spite of the numerous theoretical and experimental studies carried out in the last decades on membrane characterization and ion transport phenomena, from the best of our knowledge, there is no critical review about the use of chronopotentiometry for the investigation of ion transport processes in electrodialysis systems. The most recent papers with reviews on chronopotentiometry were published in the 1970's and are focused on electrode studies [10,11]. Hence, the present article aims to provide a comprehensive review on the determination of ion transport properties and on the assessment of mass transfer mechanisms in electrodialysis by means of this useful and widely used technique.

2. Ion-exchange membranes and electrodialysis

2.1. Ion-exchange membranes: types and properties

Different types of membranes can be found in the market and in scientific literature, being their differences originated from the density of the polymer chain, the concentration and type of fixed charges, or its hydrophobic or hydrophilic character [2]. In general, the

most desirable membrane properties are: high selectivity to counter-ions, low electrical resistance to guarantee low potential drops, high mechanical stability, moderate degree of swelling, good chemical stability to allow applications in a wide pH range and in the presence of oxidizing agents, thermal stability to support large temperature differences and low production costs [12,13].

The choice of membranes is the key factor in electrodialysis, since they allow or block the transport of ions, depending on the purpose of the separation. Figure 1 presents a scheme of the main types of membranes; as shown, they can be classified as a function of their heterogeneity and polarity.

Concerning heterogeneity of the membrane structure, two main types of membranes can be found: the homogeneous and the heterogeneous ones. In homogeneous membranes, the fixed functional groups are uniformly distributed throughout the polymer matrix, whereas in the heterogeneous ones, the fixed groups are non-uniformly distributed and separated by uncharged binding polymer, which enhances membrane mechanical resistance [14]. Figure 2 shows a schematic drawing illustrating a counter-ion pathway through homogeneous and heterogeneous membranes, whereas Figure 3 shows images of the structure of a heterogeneous (HDX100/IONSEP-HC-C, Hangzhou Iontech Environmental Technology Co., Ltd., China) and a homogeneous cation-exchange membrane (PC-SK, PolymerChemie Altmeier GmbH, Germany) obtained by scanning electron microscopy [15]. Counter-ion pathway is more tortuous in heterogeneous membranes, as isolating regions are impermeable to ions. In Figure 3, the heterogeneous membrane has its structure characterized by distinct conductive (red arrows) and non-conductive regions (blue arrows), since there are dispersed agglomerates of ion-exchange particles. In turn, the homogeneous membrane shows a uniform structure without distinction between conductive and non-conductive regions. As it will be shown later, the apparent fraction of conductive area of the membranes can be determined by chronopotentiometry.

Concerning polarity, the two main types of membranes are the monopolar and the bipolar ones. Monopolar membranes have either cation- or anion-exchange groups that allow the passage of counter-ions and the exclusion of co-ions. The cation-exchange membranes have fixed groups with negative charges, and anion-exchange membranes have fixed groups with positive charges. The fixed charge groups commonly present in

CEMs are sulfonic acid ($-SO_3^-$), carboxylic acid ($-COO^-$), phosphoryl ($-PO_3^{2-}$), and phosphonic acid ($-PO_3H^-$). For AEMs, the most common fixed charge groups are ammonium ($-NH_3^+$), secondary amine ($-NRH_2^+$), tertiary amine ($-NR_2H^+$), and quaternary amine ($-NR_3^+$) [16,17]. In cation-exchange membranes, the fixed anionic groups are in equilibrium with cations of the solution, which are called counter-ions. In turn, anions of the solution, which are called co-ions for cation-exchange membranes, are repelled by the charges of the CEMs. In contrast, in anion-exchange membranes, cations are the co-ions and anions are the counter-ions [13]. The phenomenon of ion exclusion by electrostatic repulsion is known as Donnan exclusion and occurs to satisfy the electroneutrality condition between the charges of the polymeric matrix and the ions in solution. Figure 4 shows a scheme of a polymer matrix of a cation-exchange membrane with cations and anions from a solution to be treated by electrodialysis. It can be seen that the amount of anions present in the membrane matrix is much lower than that of cations. The ion exchange phenomenon that occurs in membrane/electrolyte systems may be described in a simple way by the "charged sponge" model; in this analogy, the ion exchanger (membrane) immersed in an electrolyte acts as a sponge, absorbing and releasing ions until reaching an equilibrium [18]. Figure 5 shows a representation of a typical electrodialysis cell with cation- and anion-exchange membranes.

Bipolar membranes (BM) are composed of a combination of a cation- and anion-exchange layer, as represented in Figure 6, and have received great attention since they are able to convert salts into conjugated acids and alkalis. Some of the studies carried out using bipolar membrane electrodialysis (BMED) have focused on production of acetic acid [19,20], gluconic acid [21,22], citric acid [23] and organic acids in general [24,25,34,35,26–33]. In these systems, dissociation of water occurs at the junction layer of a bipolar membrane according to the second Wien effect [36]. The generated H^+ and OH^- ions bind to the salts and produce the conjugate acid and alkali on each side of the BM. Figure 7 shows a representation of a typical bipolar membrane electrodialysis cell.

Two other types of membranes are the mosaic and amphoteric ones. The former is composed of both cation- and anion-exchange domains randomly distributed in a neutral polymer matrix [17,37], whereas amphoteric membranes present randomly distributed weak acid and weak basic groups [38].

2.2. Ion transport in electrodialysis cells

The transport rate of a type of ion in the membrane and in solution is determined by its concentration, mobility, and by the applied driving force [2]. Generally, the transport of an ion *j* in the solution or in the membrane is described by the extended Nernst-Plank equation adapted with the convective term [39], which is represented by Equation 1.

$$\vec{J_j} = -D_j\left(\nabla C_j + z_j C_j \frac{F}{RT}\nabla\varphi\right) + C_j\vec{v} \qquad \text{Equation 1}$$

In Equation 1, $\vec{J_j}$, D_j, z_j, and C_j represent the flux density, diffusion coefficient, charge and concentration of the ionic species *j*, respectively; φ is the electric potential, $\vec{v}$ is the velocity vector of the fluid; *F*, *R*, *T* are the Faraday constant, the gas constant and the temperature, respectively. The first term on the right side of Equation 1 represents the transport of ions by diffusion, the second one the migration and the third one the convection. Equation 1 can be used under consideration of several assumptions. First, the effect of concentration gradients on activity coefficients is ignored. It can be also considered that there is no short-range interaction between ions (those acting at the lowest distances of intermolecular separation). Finally, the diffusive and electric mobility of the ions are considered identical. In general, all the hypotheses presented above are reasonable for electrodialysis systems [40].

The transport of ions in the solutions and through the ion-exchange membranes placed between the two electrodes results in a transport of electric charges: cations move toward the cathode, while anions move toward the anode. The ion transfer in the membrane/solution system is strongly affected by the applied current density. At low current densities (i << limiting current density), ion transfer is governed mainly by diffusion-migration, following a quasi-ohmic behavior. At high current densities (i > limiting current density), ion transfer is mostly governed by complex convection phenomena.

For decades, electrodialysis has been mostly used for desalination of brackish water and seawater [13]. In recent years, it has been considered for several purposes, such as the recovery of sulfuric acid from acid mine drainage [41], concentration, purification

and demineralization of food products [42,43], deacidification of juices [44], purification of green tea [45], protein concentration [46], separation of organic acids [47,48], removal of potassium hydrogen tartrate from wine [49], treatment of solutions with molybdate [50], extraction of dissolved solids in the effluent from the shale gas production [51], remediation of contaminated soil with metals [52] and for extracting and recovering metals from the electroplating industry [12,53,62,54–61]. Regardless of the solution to be treated, the choice of membranes is the key factor in electrodialysis since they allow the passage or the retention of ions. For the separation efficiency, some of the membrane characteristics must be considered, such as ionic conductivity, mechanical resistance, chemical stability, and manufacturing cost [63,64].

Besides the characteristics provided by the manufacturer, it is important to perform studies on membrane characterization to determine properties that depend on the solution to be treated, such as the limiting current density, electrical resistance, and transport number of ions in the membrane. The energy consumption involved in changes of mass transfer mechanisms as electrodialysis is conducted must also be evaluated. It is also essential to know the apparent fraction of conductive area of the membrane and its deviation from ideality. Besides, the tendency of fouling and scaling occurrence must be evaluated; in these undesirable phenomena, the deposit of organic and inorganic material occurs at the surface of the membrane and blocks the ions passage due to the poisoning phenomenon, which leads to an increase in resistance [50]. Metal ions, for example, may precipitate at the membrane surface since electrodialysis operates under intense variations in concentration and pH especially at the membrane/electrolyte interface [65–67]. Besides, the presence of complexes in the solution to be treated can neutralize part of the fixed charges of the membranes [68], which increases their resistance. Therefore, evaluating the influence of the molar ratio between the complexes and free ions on the transport properties of the membrane/electrolyte system is crucial, as well as the influence of the species concentration and the solution pH. For performing these evaluations, methods of dynamic characterization of membranes may be used.

3. Chronopotentiometry: dynamic monitoring of ion transport

Among the methods of electrochemical characterization generally used in studies involving membranes, the use of chronopotentiometry stands out because it provides

direct access to the contribution of the total voltage of the cell in different states of the membrane/solution system [69]. This technique has been frequently used to evaluate membrane properties by assessing the chronopotentiograms (ChPs) and current-voltage curves (CVC), which can be constructed by means of chronopotentiometry [9,65,77–79,69–76].

3.1. Experimental setup and measurement procedures

Figure 8a shows a representation of an experimental setup for conducting chronopotentiometric measurements. It is composed of a three-compartment cell and two membranes; in general, one is an anion- and the other is a cation-exchange membrane. Two electrodes are introduced in the side compartments to apply a constant current density, and two reference electrodes immersed in Luggin capillaries on each side of the membrane under study are used to measure the membrane potential drop (membrane voltage) over time. Although the system presented in Figure 8a is often used in studies of chronopotentiometry, cells with more compartments may be employed to minimize the influence of electrode reactions on the membrane potential measurements [73,75,80]. Figure 8b presents a schematic representation of the six-compartment cell used by Balster et al. [81] and Długołecki et al. [82].

Chronopotentiometric curves (or chronopotentiograms) are used to evaluate the dynamic behavior of membranes and to determine some properties, such as the apparent fraction of conductive area, transport number of ions in the membrane, and transition time. The transition time corresponds to the moment at which the depletion of ions occurs at the membrane surface due to the intense occurrence of concentration polarization. This phenomenon will be discussed in detail in the next sections. Figure 9 presents a representation of typical chronopotentiometric curves obtained with monopolar membranes.

According to Figure 9, chronopotentiometric curves present well-defined regions and distinct shapes depending on the applied current density. In curve I, we can see that the membrane potential drop, U_m, presents a constant value. This occurs when the applied current density is lower than the limiting current density (i_{lim}), i.e. lower than the current density at which depletion of ions near the membrane surface occurs as a consequence of

intense concentration polarization. The potential difference recorded is mainly associated with the ohmic drop caused by the membrane/electrolyte system.

When the applied current density is slightly increased (curve II), the curve presents a subtle inflection related to the increase of the potential drop at a certain time, due to the formation of concentration gradients in the vicinity of the membrane. As the applied current density increases, this inflection point is also observed and becomes more evident (compare curve II with curve III).

For current densities higher than the limiting current density of a given system (curves III and IV), six different regions may be distinguished:

- Region 1: Before imposing a current density, the membrane potential drop is zero. When the current is switched-on, an immediate increase in the potential drop appears in the chronopotentiometric curve. This initial potential drop (U_{Ω}) is related to the ohmic contribution of the membrane/electrolyte system [67,83].

- Region 2: A slow increase of the potential drop takes place due to the development of small concentration gradients in the solution near the membrane surface. This is governed mainly by electro-diffusion mechanisms [73]. When an underlimiting current is applied (as shown for curve I), this region 2 extends even during a long time and, in this case, region 3 is not reached.

- Region 3: An inflection point at which the potential drop increase becomes more pronounced in a short time is registered due to the occurrence of intense concentration polarization. At this moment, the concentration of counter-ions in the solution near the membrane layer reaches values close to zero, causing a strong increase in the resistance faced by ions to be transferred through the membrane. This occurs only when the applied current density is greater than the corresponding limiting current density (compare curve I to curve IV). In region 3, it is possible to determine the time required for the ion depletion in the diffusion boundary layer, which is called transition time - τ, as shown in Figure 9 for curve III. Other methods may be used for determining transition times, such as the maximum of the time derivative of the potential drop. Differences between both methods will be discussed in the next section (3.2).

- Region 4: The system reaches a steady-state condition, where the potential drop ($U_{m,f}$) remains practically constant until the current ceases. The system develops another way to support itself with the emergence of overlimiting mechanisms of current transfer, such as electroconvection, gravitational convection, and dissociation of water molecules. In studies involving construction of current-voltage curves, this $U_{m,f}$ value is the one plotted against the applied current density.

- Region 5: When the current density is switched-off, the potential drop suddenly drops to a residual value that slowly disappears with time. The remaining potential difference across the membrane after interrupting the current represents the concentration overvoltage (U_c) [84]. This results from the differences in the concentration profiles created at both sides of the membrane while the current was imposed. For bipolar membranes, additional plateaus may be verified in region 5 [85].

- Region 6: This last region describes the diffusion relaxation of the system, in which the potential drop approaches zero over time.

3.2. Equations describing dynamic response of potential drop in membrane systems: The Sand's equation

When the concentration polarization phenomenon becomes intense due to operation at overlimiting current densities, it is possible to determine the time required for the electrolyte concentration to reach values close to zero. This property can be experimentally obtained from chronopotentiometric curves by using two methods. In the first one, the transition time is estimated by the point of intersection of the tangential lines of the regions before and after the increase in the potential drop [61,86], as shown for curve III in Figure 9. In the second method, the transition time is determined from the maximum of the derivative of the membrane potential drop with respect to time [76,79,87], as represented in Figure 10. In general, the transition times obtained by these two methods differ, which is more noticeable for heterogeneous membranes than for homogeneous ones [73]. Note that the intersection of the tangential lines (Figure 9) and

the inflection point considered in the derivative method (Figure 10) are different points. The first one corresponds to the end of region 2 and the beginning of region 3 of the chronopotentiogram. This is the point of the beginning of the rapid potential growth that occurs when intense concentration polarization takes place at the diffusion boundary layer and the ion concentration reaches values close to zero. At this moment, electro-diffusion is still the dominant mechanism of ion transfer because overlimiting mass transfer phenomena do not occur intensively yet. Conversely, when the transition time calculated by the derivative method is reached (see Figure 10), the membrane/electrolyte system already operates under intense concentration polarization. Thus, it may be suggested that the value obtained using the derivative method is more representative of the instant when the actual transition between different dominating mass transfer mechanisms in electromembrane systems occurs. The higher accuracy of the derivative method was demonstrated by Mareev et al. [76] because the transition times obtained by the authors using this method presented a very good agreement with those obtained using simulations based on a 3D ion transport model.

The transition time can also be obtained mathematically. In 1899, Sand [88] developed an equation that was adapted by Lerche and Wolf [89] and applied by Audinos and Pichelin [90] to homogeneous membranes. The latter authors evaluated the non-steady-state transport of counter-ions considering a homogeneous surface, in contact with univalent electrolytes, and without electroconvection.

The Sand equation was developed from Fick's second law [76], which presents the change in the electrolytic concentration as a function of distance and time (Equation 2), where x is the directional coordinate, t is time, and D is the electrolyte diffusion coefficient. In the case of binary electrolytes, $D = 2D_cD_a/(D_c + D_a)$, where D_c and D_a are the diffusion coefficients of the cationic and anionic species in the solution, respectively [91].

$$\frac{\partial \mathrm{C}(x,t)}{\partial \mathrm{t}} = D\frac{\partial^2 \mathrm{C}(x,t)}{\partial \mathrm{x}^2} \qquad \text{Equation 2}$$

Equation 2 has an analytical solution and requires two boundary conditions for its resolution. In the initial state ($t = 0$), concentration C is expressed by Equation 3.

$$C(x,0) = C_0 \qquad \text{Equation 3}$$

In positions sufficiently distant from the membrane, Equation 4 is also valid since we are evaluating the semi-infinite diffusion problem.

$$C(x \to \infty) = C_0 \qquad \text{Equation 4}$$

Equation 5 expresses the flow of counter-ions through the membrane (J_j^m), which principally occurs by migration, while Equation 6 expresses the flow in the solution (J_j^s), which occurs due to migration and diffusion [90]. In these equations, $\overline{t_j}$ and t_j represent the transport number of an ion *j* in the membrane and solution phase, respectively. In this case, *D*, $\overline{t_j}$ and t_j are assumed not to depend on the electrolytic concentration.

$$J_j^m = \frac{i\overline{t_j}}{zF} \qquad \text{Equation 5}$$

$$J_j^s = \frac{it_j}{zF} + D\left(\frac{\partial \mathrm{C}}{\partial \mathrm{x}}\right)_{x=0} \qquad \text{Equation 6}$$

Under constant current conditions, the flow of ions through the membrane and in the solution at the membrane surface ($x = 0$) are equal. Hence, combining Equation 5 and Equation 6, a boundary condition is obtained, which relates the concentration of the counter-ion at the membrane surface at a nonzero time (Equation 7).

$$\left(\frac{\partial \mathrm{C}}{\partial \mathrm{x}}\right)_{x=0} = -\frac{i}{zFD}\left(\overline{t_j} - t_j\right) \qquad \text{Equation 7}$$

Finally, the Fick's second law can be solved by applying Laplace transform (Equation 8) [80].

$$C(x,t) = C_0 - \frac{i\left(\overline{t_j} - t_j\right)}{zFD}\left[2\sqrt{\frac{Dt}{\pi}}exp\left(-\frac{x^2}{4Dt}\right) - x.erfc\left(\frac{x}{2\sqrt{Dt}}\right)\right] \qquad \text{Equation 8}$$

For $x = 0$, Equation 9 is obtained, which presents the concentration of ions at the surface of the membrane as a function of time.

$$C(0,t) = C_0 - \frac{i}{zFD}(\overline{t_j} - t_j)2\sqrt{\frac{Dt}{\pi}} \qquad \text{Equation 9}$$

Thus, by verifying that the ions concentration at the membrane decreases with time, Sand [88] developed the well-known Sand Equation (Equation 10) derived from the Nernst-Planck equation assuming a stagnant diffusion layer of infinite thickness near the membrane. This equation allows calculating the transition time.

$$\tau = \frac{\pi D}{4}\left(\frac{z_j F}{\overline{t_j} - t_j}\right)^2 \left(\frac{C_0}{i}\right)^2 \qquad \text{Equation 10}$$

As mentioned, the term of electrolyte diffusion coefficient (*D*) was considered to be independent of the concentration in the development of Sand equation. In 2016, Mareev et al. [92] evaluated the effect of including the concentration dependence of this term by introducing a function $D_{(c)}$, which considers the concentration variation in the diffusion boundary layer. The authors used NaCl solutions (0.002, 0.02 and 0.2 M) in the chronopotentiometric tests and verified that $D_{(c)}$ can be used in chronopotentiometric studies with any membrane or electrolyte.

3.3. Transition time and transport numbers

The transport number is a very important property considered in studies of electrodialysis since it measures the fraction of current density carried by each type of ions through the membrane and is an indicator of the current efficiency (thus, the membrane selectivity) [58]. In addition, the difference between the transport number in the solution and in the membrane is responsible for the occurrence of concentration polarization. In single salt solutions, the transport number of cations indicates the fraction of current that is associated with the cations transport through a membrane, whereas the transport number of anions indicates the fraction of current associated with the anions transport. In ideal conditions, this property presents a value close to 1 for counter-ions and close to zero for co-ions.

In the early 1990s, the transport number of counter-ions in membranes was often determined by radiotracer measurements [93–99]. However, it has been replaced with the

development of simpler and more modern techniques. The transport number began to be conventionally determined by two methods: the Hittorf [73,94,100–103] and, mainly, the emf method [77,86,111–115,100,104–110]. In the Hittorf method, a two-chamber electrodialysis cell separated by a membrane is filled with an electrolyte solution with the same concentration. A current density is applied for a period and the concentration variation in the diluted and concentrated compartments is evaluated as a function of time. In this method, Equation 11 and Equation 12 are used, where *V* is the volume of solution, C_i' and C_i^0 are the concentration of counter-ion when *t = t'* and *t = 0*, respectively, and *A* is the effective membrane area.

$$\overline{t_j} = \frac{z_j F J_j^m}{i} \qquad \text{Equation 11}$$

$$J_j^m = \frac{V(C_i' - C_i^0)}{At'} \qquad \text{Equation 12}$$

In the emf method, a two-chamber cell separated by a membrane is also used, but with two solutions of different concentrations. A current density is applied and the transport number of the counter-ion in the membrane is determined by measuring the cell potential (U_{cell}), according to Equation 13 [104], where C_{low} and C_{high} are the electrolyte concentration in the low and high concentration compartments, respectively.

$$\mathrm{U_{cell}} = \frac{RT}{F}\left(1 - 2\overline{t_j}\right) ln\left(\frac{C_{low}}{C_{high}}\right) \qquad \text{Equation 13}$$

In recent years, authors have frequently used chronopotentiometry, together with the Sand equation (Equation 10), to determine the transport number of ions in membranes. For this, a plot of experimental transition times (τ) vs. $(C_0/i)^2$ is constructed, as shown in Figure 11. In general, curves with a correlation coefficient close to a line are obtained. Therefore, the coefficient of the curve can be related to Equation 10, and $\overline{t_j}$ can be determined, since the other terms are generally known. The term of the transport number in the solution can be calculated by using the diffusion coefficients, according to Equation 14.

$$t_j = \frac{D_j}{(D_c + D_a)}$$ Equation 14

As showed by Mareev et al. [116], some care must be taken for the appropriate use of Sand equation because it is strongly dependent on the current density, the thickness of the diffusion boundary layer (δ), and the surface heterogeneity. The authors showed that the Sand equation is valid in two cases. The first one is when the membrane surface is homogeneous, and δ and *i* are sufficiently high; as shown in another work of Mareev et al. [76], the equation is only valid for current densities at least 1.5 times greater than the limiting current density of the membrane/electrolyte system. The second case in which the Sand equation is valid is when the membrane surface is inhomogeneous, but the typical size of surface heterogeneity is lower than δ. In this case, the concentration distribution at regions distant from the heterogeneous surface is similar as in the case of homogeneous surfaces, and the elongation of current lines caused by surface heterogeneity may be neglected.

Recently, results of transition time obtained by chronopotentiometry for anion- and cation-exchange membranes were compared to those obtained by X-ray computed microtomography [117]. The latter provides a detailed analysis of the membrane structure both on its surface and its inner parts. The authors verified that for homogeneous membranes, experimental transition times were in very good agreement with theoretical predictions based on Sand equation. In turn, transition times were not well predicted by the Sand equation in case of the heterogeneous ion-exchange membranes.

Table 1 presents a summary of some studies in the literature in which the authors determined the transport number of different ions and membranes using chronopotentiometry. Several authors reported in the table tested chronopotentiometry simultaneously with the Hittorf and emf methods.

Table 1 – Studies performed for determining transport number by using chronopotentiometry.

Ion	Solutions tested	Membrane	Producer	Reference
Cu^{2+}	0.1 – 2.0 g Cu^{2+}/L + H_2SO_4	HDX100/IONSEP-HC-C and PC-SK	HDX100: Hangzhou Iontech	[15]

			Environmental Technology Co. Ltd., China. PC-SK: PolymerChemie Altmeier GmbH, Germany	
Ni^{2+}, Mn^{2+}, Cu^{2+}, Co^{2+}, Zn^{2+}	0.025 M chloride solution	IONICS 67-HMR-412	Ionics Inc., USA	[65]
Na^{+}, Ca^{2+} and Mg^{2+}	0.02 M NaCl, $CaCl_2$ and $MgCl_2$	Modified CEM		[118]
Ni^{2+}	0.025 M $NiCl_2 + H_3BO_3$	IONICS 67-HMR-412	Ionics Inc., USA	[71]
Na^{+}	0.025 M NaCl	Neosepta CM-1, CMX, CMB and modified membranes	Tokuyama Co. Ltd., Japan.	[106]
Na^{+} and Cl^{-}	0.017 – 0.5 M NaCl	Neosepta AMX and CMX, Fumasep FAD and FKD	Neosepta Tokuyama Soda Co. Ltd., Japan. Fumasep: FuMA-TechGmbH, Germany	[119]
Cl^{-}	0.002, 0.02 and 0.2 M NaCl	Neosepta AMX	Astom Corp., Japan	[92]
Cl^{-}	NaCl	Prepared AEM		[120]
K^{+}	0.01 M KCl	Prepared membranes		[121]
K^{+}	0.5 M KCl	Modified CEM		[122]
K^{+} and Cl^{-}	0.001 M KCl	Suqing 201×4 Cl (AEM) and Suqing 001×4 Na (CEM)	Suqing Company, China.	[117]
Na^{+} and Cl^{-}	0.017 – 0.1 M NaCl. Temperature: 293 – 318K	Selemion CMV, Neosepta CMX, Selemion AMV, Neosepta AMX	Selemion: Asahi Glass, Japan. Neosepta: Astom Corp., Japan	[123]
Na^{+} and Cl^{-}	0.001 – 0.1 M NaCl	AEM and CEM prepared membranes		[124]
Na^{+}	0.01 M NaCl	CEM prepared membranes		[125]
Na^{+}	NaCl	Nafion 117 and CEM prepared membranes	Nafion: DuPont	[126]
Na^{+}	1 – 10 M NaCl	CEM prepared membrane		[127]
Na^{+} and Cl^{-}	0.025 M NaCl	Neosepta AM-1, AMX, AFN, Nafion 117 and modified membranes	Neosepta: Tokuyama Soda Co. Ltd., Japan. Nafion: DuPont, USA	[77]
Cl^{-}	0.025 M NaCl	Neosepta AMX and prepared membranes.	Tokuyama Co. Ltd., Japan.	[112]
Cl^{-}	0.01 M KCl, NaCl and LiCl	Prepared charged mosaic membranes and Selemion AMV	Selemion: Asahi Glass, Japan.	[37]
Cl^{-}	0.025 M NaCl	Neosepta AM-1, AMX, AFN and prepared membranes	Neosepta: Tokuyama Co. Ltd., Japan.	[128]
Na^{+}, H^{+}, Na^{+}, Cl^{-}, OH^{-}	0.001 and 0.01 M NaCl, HCl and NaOH solutions	Prepared membranes		[129]
Ni^{2+}	10^{-4} – 10^{-2} M $NiSO_4$ + 0 - 10^{-2} M CrO_3.	Nafion 117	DuPont, USA	[72]
Zn^{2+}	0.05 – 0.2 M $ZnSO_4.7H_2O$	IONICS 67-HMR-412	Ionics Inc., USA	[70]
NO_3^{-}, SO_4^{2-}, CH_3COO^{-} and Cl^{-}	0.01 M sodium salts: CH_3COONa, $NaNO_3$, NaCl and Na_2SO_4.	Prepared membranes		[130]

L-phenylalanine	0.02 M sodium phenylalanine	Fresh and fouled Neosepta AM-1 and AFX membranes	Neosepta: Tokuyama Co. Ltd., Japan.	[131]

3.4.The modified Sand equation: fraction of non-conducting regions in membranes

Choi and Moon [105] modified the Sand equation and included a term relative to the apparent fraction of conductive area (ε) (Equation 15). This equation is widely used in chronopotentiometric studies to determine the apparent fraction of conductive area or the transport number of counter-ions in heterogeneous membranes. The relationship between the transition times obtained by the equations of Sand and Choi and Moon is expressed as $\tau_{Choi-Moon} = \tau_{Sand}\varepsilon^2$. Thus, its use requires some care, as showed by Mareev et al. [116]. In the theory proposed by Choi and Moon, the electric current lines are assumed to be normal to the conductive surface, thus, the tangential component of ion transfer is neglected. In real membrane systems, this assumption may be considered acceptable when the typical size of surface heterogeneity is of the same order of magnitude as (or greater than) the thickness of the diffusion boundary layer. In addition to this, the equation proposed by Choi and Moon is valid only for current densities at least 1.5 times greater than the limiting current density of the membrane/electrolyte system [76]. Vobeckà et al. [117] also showed, using chronopotentiometry and X-ray computed microtomography, that the use of the modified Sand equation is limited for heterogeneous membranes.

The terms of Equation 15 are the same of those present in Equation 10. For the determination of ε, the same procedure described for determining the transport number by the Sand equation in homogeneous membranes (Equation 10) is performed. In this case, the coefficient of the curve of (τ) vs. $(C_0/i)^2$ is equal to the modified Sand equation and only ε is an unknown term, which can be finally determined. The solutions used for determining ε by chronopotentiometry are generally composed of single salts, such as NaCl or KCl. The value of transport number of ions in the membrane phase is generally given by manufacturers or it may be determined by the Hittorf or emf method. In the absence of $\overline{t_j}$ value, it may be calculated by using data of transport number of ions in the solution and the membrane permselectivity (Equation 16) [13]. The latter is related to the transport of electric charges by the counter-ions to the total electric current that cross the

membrane and is generally provided by manufactures [17]. In some cases, the permselectivity may also be calculated using Equation 17 [132,133], which considers the ε value equal to 1.

$$\tau = \frac{\varepsilon^2 \pi D}{4}\left(\frac{z_j F}{\overline{t_j} - t_j}\right)^2 \left(\frac{C_0}{i}\right)^2 \quad \text{Equation 15}$$

$$\overline{t_j} = Permselectivity \cdot \left(1 - t_j\right) + t_j \quad \text{Equation 16}$$

$$Permselectivity = \frac{z_j F C_0}{2\left(1 - t_j\right) i} \cdot \left(\frac{D\pi}{\tau}\right)^{0.5} \quad \text{Equation 17}$$

Table 2 presents a summary of some studies performed by chronopotentiometry for obtaining the apparent fraction of conductive area of the homogeneous and heterogeneous membranes most evaluated in the literature. The table presents the ε values and the solutions used in the experiments.

Table 2 - Summary of data of apparent fraction of conductive area of the membranes most evaluated in literature.

Membrane	Producer	Value of ε	Solution used for determining ε	Reference
Commercial homogeneous membranes				
Nafion 117	DuPont, USA	0.981	0.05M NaCl	[9]
Nafion 117	DuPont, USA	0.93	0.003 M KCl	[134]
Nafion 117	DuPont, USA	0.71	0.003 M KCl + 0.6 g/L Glucose	[134]
Nafion 117	DuPont, USA	0.63	0.003 M KCl + 0.96 g/L Glucose	[134]
Nafion 117	DuPont, USA	0.88	0.003 M NaCl	[134]
Nafion 117	DuPont, USA	0.76	0.003 M NaCl + 0.6 g/L Glucose	[134]
Nafion 117	DuPont, USA	0.62	0.003 M NaCl+ 0.96 g/L Glucose	[134]
Nafion 117	DuPont, USA	0.88	0.140 M KCl	[134]

Nafion 117	DuPont, USA	0.85	0.140 M KCl + 0.6 g/L Glucose	[134]
Nafion 117	DuPont, USA	0.87	0.140 M KCl + 0.96 g/L Glucose	[134]
Nafion 117	DuPont, USA	0.90	0.003 M KCl+0.140 M NaCl	[134]
Nafion 117	DuPont, USA	0.84	0.003 M KCl+0.140 M NaCl + 0.6 g/L Glucose	[134]
Nafion 117	DuPont, USA	0.89	0.003 M KCl+0.140 M NaCl + 0.96 g/L Glucose	[134]
PC-SK	PolymerChemie Altmeier GmbH, Germany	0.734	0.3 M KCl	[15]
IONICS 67-HMR-412	Ionics Inc., USA	0.935	0.025 M NaCl	[65]
Neosepta CMX	Tokuyama Co. Ltd., Japan.	0.97	0.02 M NH_4Cl	[104]
Neosepta CMX	Tokuyama Co. Ltd., Japan.	0.954	0.025 M NaCl	[135]
Neosepta CMX	Tokuyama Co. Ltd., Japan.	0.98	0.01 KCl	[136]
Neosepta AMX	Tokuyama Co. Ltd., Japan.	0.99	0.01 KCl	[136]
Neosepta CM-1	Tokuyama Co. Ltd., Japan.	0.973	0.025 M NaCl	[135]
Neosepta CMB	Tokuyama Co. Ltd., Japan.	0.916	0.025 M NaCl	[135]
Selemion CMV	Asahi Glass Co., Japan	0.98	0.02 M NH_4Cl	[104]
Selemion CMV	Asahi Glass Co., Japan	0.95	0.1 M NaCl	[137]
FKE	FuMA-Tech GmbH, Germany	0.988	0.025 M NaCl	[138]
Neosepta AFX	Astom Corp., Japan	0.969	0.025 M NaCl	[86]
Neosepta AFX	Astom Corp., Japan	0.985	0.025 M NaCl	[111]
Neosepta AFX	Astom Corp., Japan	0.916	0.025 M NaCl	[108]
Neosepta AMX	Astom Corp., Japan	0.98	0.025 M NaCl	[139]
204SZRA	Ionics Inc., USA	0.94	0.025 M NaCl	[139]

Commercial heterogeneous membranes				
HJC	Hanguk Jungsoo Co., Korea	0.93	0.02 M NH_4Cl	[104]
HJA	Haji, Korea	0.59	0.025 M NaCl	[139]
LNA	Lin'an, China	0.68	0.025 M NaCl	[139]
HQC	Hangzhou Qianqiu Chemical, China	0.827	0.025 M NaCl	[135]
HDX 100/IONSEP-HC-C	Hangzhou Iontech Environmental Technology Co., Ltd., China	0.804	0.05M NaCl	[9]
HDX 100/IONSEP-HC-C	Hangzhou Iontech Environmental Technology Co., Ltd., China	0.808	0.1 M KCl	[15]
Modified membranes				
PFAEM (VBC/St = 1/1)		0.972	0.025 M NaCl	[111]
PFAEM (VBC/St = 2/1)		0.985	0.025 M NaCl	[111]
PFAEM (VBC/St = 3/1)		0.974	0.025 M NaCl	[111]
PFAEM (VBC/St = 4/1)		0.979	0.025 M NaCl	[111]
PFAEM (VBC/St = 5/1)		0.957	0.025 M NaCl	[111]
PFAEM (VBC/St = 6/1)		0.96	0.025 M NaCl	[111]
20% S-PES		0.796	0.025 M NaCl	[135]
30% S-PES		0.826	0.025 M NaCl	[135]
40% S-PES		0.981	0.025 M NaCl	[135]
50% S-PES		0.983	0.025 M NaCl	[135]
S-PSU		0.921	0.025 M NaCl	[135]
0 SS		0.855	0.025 M NaCl	[138]
0.2SS-20nm		0.964	0.025 M NaCl	[138]
0.5SS-20nm		0.998	0.025 M NaCl	[138]
1SS-20nm		0.998	0.025 M NaCl	[138]
2SS-20nm		0.946	0.025 M NaCl	[138]
AFX/Py 100 vol.%		0.909	0.025 M NaCl	[86]

AFX/Py 80 vol.%		0.861	0.025 M NaCl	[86]
AFX/Py 60 vol.%		0.881	0.025 M NaCl	[86]
AFX/Py 40 vol.%		0.834	0.025 M NaCl	[86]
AFX/Py 20 vol.%		0.881	0.025 M NaCl	[86]
AFX/Py 10 vol.%		0.864	0.025 M NaCl	[86]
AFX/Py 5 vol.%		0.861	0.025 M NaCl	[86]
AFX/BPPO 1 wt%		0.903	0.025 M NaCl	[108]
AFX/BPPO 3 wt%		0.889	0.025 M NaCl	[108]
AFX/BPPO 5 wt%		0.860	0.025 M NaCl	[108]
AFX/BPPO 10 wt%		0.797	0.025 M NaCl	[108]
AFX/BPPO 15 wt%		0.833	0.025 M NaCl	[108]

3.5.Fouling and scaling phenomena

In recent years, several authors have verified that some monopolar membranes may show atypical behaviors in their chronopotentiometric curves. Depending on the ionic species present in the tested solution and the pH, insoluble species may be formed at the membrane surface during the electrodialysis process, which leads to the formation of additional inflection points in the ChPs [9,65,67,69,71,72]. This behavior is similar to those verified in bipolar membrane studies [85].

The formation of insoluble species on cation- and anion-exchange membranes occurs when current densities above the limiting one are applied, leading to water dissociation and the consequent formation of H^+ and OH^- at their surface. When water dissociates at a cation-exchange membrane, protons tend to pass through the membrane, while OH^- ions are retained on its surface, increasing the local pH. These OH^- ions may react with metal ions and form mainly hydroxides and oxides that adhere to the monopolar structure of the membrane [71]. At anion-exchange membranes, the opposite phenomenon occurs: OH^- ions pass through the membrane, whereas protons are retained on its surface, which causes a pH reduction. In general, the formation of insoluble species at the surface of anion-exchange membranes due to water dissociation is more difficult to occur than at cation-exchange ones. The evaluation of this phenomenon is very important for the electrodialysis efficiency since the formation of precipitates causes an increase in the potential drop and in the resistance of the membrane [65].

The formation of insoluble species on the surface of monopolar membranes can be verified in the chronopotentiometric curves obtained at $i > i_{lim}$ by some non-expected behaviors, which are represented in Figure 12. In the curve, an increase in the potential drop occurs when the system was expected to be at steady-state condition, after the achievement of the transition time [7,15,65,67,71,140–142]. The presence of additional plateaus during the system relaxation is also a typical behavior when a precipitate is formed at the membrane, as shown in Figure 12 [65,71,72,140,141]. In this case, the potential drop remains at non-zero values for long periods, which is a classical behavior for bipolar membranes. This is related to the hindered recombination of hydroxides and protons at the solution adjacent to the diffusion boundary layer (DBL), resulting from the dissociation of water in the bipolar membrane junction [143].

Using chronopotentiometry, Marder et al. [65] evaluated the transport properties of solutions with different metals: nickel, manganese, copper, cobalt, and zinc. The authors verified the formation of additional plateaus only with solutions of cobalt and nickel, due to the formation of the insoluble species $Ni(OH)_2$ and $Co(OH)_2$, respectively. Some years later, the effect of boric acid on the transport properties of nickel was evaluated by chronopotentiometry [71] and the deposition of $Ni(OH)_2$ was also verified at the surface of the cation-exchange membrane. Also using chronopotentiometry, Taky et al. [144] studied the transport properties of solutions containing Cr^{3+} and observed the formation of $Cr(OH)_3$ at the CEM. Barros et al. [7] evaluated transport properties of solutions from the effluent of the electroplating industry with EDTA as a complexing agent. The authors associated the occurrence of precipitate formation at the membrane surface with intense oscillations in the chronopotentiometric curves, besides an unexpected increase in the potential drop without achieving a constant value. An unexpected increase in the potential drop was also recently verified in the chronopotentiograms obtained by Barros et al. [67]; they evaluated the influence of a three-stage chemical cleaning using NaOH solutions in 0.1, 0.5 and 1.0 mol/L on electrochemical and structural properties of anion- and cation-exchange membranes previously used in the electrodialytic treatment of an effluent from the electroplating industry. The cleaning solution in 1.0 mol/L NaOH degraded the anion-exchange membrane and converted quaternary amines into tertiary ones. This led to intense water dissociation at the membrane surface during the chronopotentiometric tests, reducing the pH in the depleting diffusion boundary layer. This reduction in pH led

to the formation of precipitates at the membrane surface, which were responsible for the unexpected increase in the potential drop in the chronopotentiometric curves.

In some cases, the visual observation of precipitate formation is possible. Martí-Calatayud et al. [9] evaluated the transport of mixture solutions of $Fe_2(SO_4)_3$ and Na_2SO_4 emulating the composition of acid mine drainage through two different membranes, one homogeneous and the other heterogeneous. At the end of the experiments, the authors visually verified the presence of precipitates that were related to the shape of chronopotentiograms. Barros et al. [15] also compared two membranes, a homogeneous and a heterogeneous one, analyzing the evolution of the chronopotentiometric curves and the transport properties using solutions of copper in acid medium. In addition to the chronopotentiometric curves, the authors visually verified the formation of a blue precipitate only at the surface of the homogeneous membrane. This occurred due to the higher local concentration of Cu^{2+} ions near the conductive regions of the homogeneous membrane. The lower water content of the homogeneous membrane (9%) compared to the heterogeneous one (35%-50%) also favored the precipitate formation at the former; the lower the water content, the lower the membrane conductivity, which leads to smaller conducting interstices and lower ion mobility through the membrane [145].

Chronopotentiometry has been used not only to investigate the formation of precipitates and scaling in metallic solutions, but also to evaluate the influence of some substances on the fouling occurrence and on the fraction of conductive area of membranes. Freijanes et al. [134] evaluated the influence of glucose on membrane properties using NaCl and KCl solutions. The authors noted that at low electrolyte concentrations, the transition times were lower in the presence of glucose due to the reduction of the effective area of the membrane by this substance. Similar results were observed by Shahi et al. [129]. Also using chronopotentiometry, they verified that the presence of glycine in NaCl solutions reduced the ions migration due to the blockage of functional groups of the membrane matrix. Similarly, Park et al. [136] evaluated the influence of bovine serum albumin (BSA) on the transport properties of KCl solutions and noted that this substance altered the membrane heterogeneity. The authors verified the chemical adsorption of BSA on the cation-exchange membrane, and both chemical and electrostatic adsorption on the anion-exchange one, causing the reduction of its apparent fraction of conductive area. Kang et al. [146] studied the influence of lysine, a

large molecular amino acid, on the properties of two membranes and noted that they were strongly affected by molecules with a molar mass greater than 70 g/mol. Chronopotentiometry allowed the authors to verify that the apparent fraction of conductive area was reduced with the increase of the molar mass of the counter-ion.

Lee et al. [147] evaluated the influence of the presence of anionic surfactant foulant (sodium dodecylbenzenesulfonate) on the fouling potential of an anion-exchange membrane with NaCl solutions. By determining the transport properties and comparing the chronopotentiograms, the authors verified the occurrence of an intense fouling. Recently, Andreeva et al. [142] studied a mixed salt solution by chronopotentiometry to evaluate the mitigation of scaling at two cation-exchange membranes, being one commercial and the other one a modified membrane. The authors tested the application of constant and pulsed currents, in underlimiting and overlimiting conditions to reduce the tendency of precipitate formation on the surface of the membranes. For the commercial membrane, scaling occurred and the $CaCO_3$, $Ca(OH)_2$, and $Mg(OH)_2$ compounds were formed at its surface, whereas for the modified membrane, the amount of scaled species was considerably lower and only $CaCO_3$ was present. The use of pulsed electric field was also useful to reduce membrane scaling.

Choi and Moon [105] assessed the influence of pore size of three ion-exchange membranes, being two homogeneous and the other heterogeneous, on the shape of chronopotentiograms using some amine chloride solutions. Only ions smaller than the pore of the membrane can cross it; when the pore is smaller than the transporting ion, it behaves as a non-conductive area. From the curves obtained, it was clear that ions with greater molecular size were responsible for lower values of apparent fraction of membrane conductive area. For the determination of the apparent fraction of conductive area, the authors constructed curves showing the dependence of transition times on current densities represented in Sand's coordinates ($i\tau^{1/2}$ vs. i), as will be discussed below.

By rearranging the modified Sand equation (Equation 15), it can be represented as shown in Equation 18. The values of $i\tau^{1/2}$ are expected to be constant and independent of current density. As all the terms on the right side are usually known, the ε value can be finally determined. For the use of Equation 18, transition times may be experimentally obtained from the chronopotentiograms and transport number of ions in the membrane

can be determined by the emf or Hittorf method. This analysis of the dependence of transition time on current density represented in Sand's coordinates has been used by several authors for evaluating the influence of different ions and types of membranes on the apparent fraction of conductive area and fouling/scaling occurrence [79,83,105,125,130,148]. Recently, Barros et al. [61] evaluated the apparent fraction of conductive area of cation- and anion-exchange membranes after their use in electrodialysis operated at underlimiting and overlimiting current regimes; from the curves of $i\tau^{1/2}$ vs. i, the authors verified that fouling/scaling occurred more intensively in the ED conducted in underlimiting condition. Singh et al. [149] used this analysis to determine the permselectivity of modified anion-exchange membranes; for this purpose, the transport number of counter-ions in the membranes was determined using Equation 18 and applied in Equation 16. The invariability of $i\tau^{1/2}$ values presented as a function of i indicates that the counter-ion transfer runs with diffusion control. When the curves show a slope, the ion transfer across the membrane is accompanied by chemical reactions taking place in the membrane/electrolyte system [79,150]. Figure 13 shows the dependencies of transition time on current density represented in Sand's coordinates obtained by Pismenskaya et al. [151]. In the chronopotentiometric tests, the authors used the same ion-exchange membrane (CMX) and two different solutions: NaCl and LysHCl. As verified, the apparent fraction of conductive area was lower with LysHCl solution than with NaCl.

$$i\tau^{1/2} = \frac{\varepsilon C_0 z_j F (\pi D)^{1/2}}{2\left(\overline{t_j} - t_j\right)} \qquad \text{Equation 18}$$

4. Current-Voltage Curves

In addition to chronopotentiograms, chronopotentiometry allows obtaining curves of current versus voltage describing the steady-state behavior of membrane systems. Current-voltage curves, also known as polarization curves, are widely used in studies involving electrodialysis because they provide a general overview of the membrane resistance over a wide range of current densities. Moreover, relevant information about the system can be obtained from these curves, such as the limiting current density and the plateau length. The latter is related to the energy required to change the mechanism of ion transport from diffusion and migration to overlimiting phenomena. The curves also

provide qualitative information regarding the overlimiting mechanisms of current transfer and transport competition between different species.

4.1.General description of typical current-voltage curves of monopolar membranes

A typical current-voltage curve of a monopolar membrane is shown in Figure 14. The CVC can be divided into three regions based on the slopes of the curve: region I, II and III. In region I, also called quasi-ohmic region, the current and the voltage show a linear relationship. In this case, the flow of ions through the membrane increases proportionally with the electric field, following a quasi-ohmic behavior. From region I, it is possible to determine an important property of electrodialysis systems: the so-called ohmic resistance of the membrane system (R_1), which can be obtained by the inverse of the slope (α_1) of the tangential line of this region. This property is also often called "effective resistance" and it includes the ohmic resistance of the region between the measuring capillaries (membrane + solution), as well as the diffusion resistance of the depleted and enriched diffusion layers [152–154]. The ohmic resistance of the membrane/electrolyte system is an important property that indicates the contribution of the membrane and the adjacent diffusion layer to the cell voltage [72].

After the linear relationship of region I, the curve reaches region II, in which the current density remains practically constant with the membrane voltage increase. This region is also known as the plateau region. At the inflection of the curve, that is, at the intersection of the tangents of region I and II, the limiting current density is reached. As previously explained, in this condition, there is no substantial increase in the current flow across the membrane due to the scarcity of ions at the membrane surface (at the diluate side), even with an increase in the applied transmembrane voltage. From region II of the CVC, it is possible to determine the plateau length [72].

In region III, a new region of current increasing with membrane voltage appears due to the activation of overlimiting transport mechanisms, such as dissociation of water, gravitational convection and electroconvection, which allow the increase in ionic transfer through the membrane [65,69]. The electrical resistance of region III (R_3) can also be determined by the same methodology of the ohmic region, that is, by the inverse of the slope (α_3) of its tangential line.

The determination of each transport property by current-voltage curves will be discussed separately in the following sections.

4.2.Concentration polarization and limiting current density

Polarization is a well-known phenomenon involved in studies of electrodes and in all membrane processes [155]. In the case of ion-exchange membranes, it is associated with the preferential transport of counter-ions through the membrane phase and the consequent development of concentration gradients between the bulk solution and the vicinity of the membrane. In ion-exchange membrane studies, this phenomenon is often called as "concentration polarization". The reduction in the concentration of ions at the ion-exchange membrane surface facing the depleted compartment causes a sudden increase in the potential drop and in the electrical resistance. Therefore, the measurement of potential drop over time gives us valuable information about the formation of concentration gradients. The potential measurement is described in detail in the classical investigation of polarization by Cooke [156,157] and by Forgacs [158].

Concentration polarization is a phenomenon that occurs in electrodialysis due to the difference between the transport number of counter-ions in the solution and in the membrane phase [76]. The proposed model for a concentration profile from a membrane-electrolyte interface states that a mass balance of counter-ions inside the membrane and in the interface must exist. The mass balance considers ion transport by diffusion and electromigration in the DBL and in the membrane phase according to Equation 19. A scheme of the diffusion layer in a membrane/solution system is represented in Figure 15.

$$\frac{it_j}{F} + \frac{D_j\,(C_1 - C_2)}{\delta_1} = \frac{i\overline{t_j}}{F} - \frac{P(C_3 - C_2)}{\delta_m} \qquad \text{Equation 19}$$

In Equation 19, C_1 and C_2 are the ion concentration in the bulk solution and at the membrane surface, respectively, on the diluted side, δ_1 is the thickness of the diffusion layer on the diluted side, P is the electrolyte permeability coefficient of the membrane, C_3 is the ion concentration of the enriched solution at the membrane surface, and δ_m is the

membrane thickness. The first term on the left side of Equation 19 is related to the ion transport due to electromigration, whereas the second term is related to diffusion, both occurring in the solution layer next to the membrane interface. Since they have the same direction, the left side of the equation is a sum of both first and second terms. In turn, in the membrane phase (right side of Equation 19) the first term is related to the electromigration from the diluted side toward the concentrated one, whereas the second term shows an opposite sign and corresponds to the diffusion transport. Since ionic concentration C_3 is higher than C_2, the diffusion transport tends to occur in the opposite direction.

In the diluted compartment, where the diluted solution is in contact with a cation-exchange membrane, the transport number of cations in the solution is smaller than at the membrane surface. The same behavior is valid for anions in the bulk solution and at the surface of an anion-exchange membrane. At a certain moment, a concentration gradient between the surface adjacent to the membrane and the bulk solution is established. This gradient results in a diffusive transport of electrolytes; ions in the bulk solution move, by diffusion, to the membrane interface to minimize the concentration gradient established by the difference in the ionic transport rate. While diffusion is able to supply ions in the boundary layer, they are continuously transferred to the membrane interface. When the applied driving force (electric field) is such that the diffusion is no longer able to supply enough ions to compensate the migration flux through the membranes, ion depletion occurs on the surface of the membrane at the interface with the diluted solution. At this moment, the system leaves the previous condition, and an increase in the applied voltage does not lead to an increase of the current density, which is defined as limiting current density [42]. Hence, an increase in the energy consumption occurs without increasing the ion transport through the membranes.

Figure 16 presents a schematic drawing illustrating the evolution of concentration profiles of counter-ions in the diffusion boundary layer (DBL) at different current densities. The electric double layer (EDL) at each side of the membrane is also represented in the figure. This is an interfacial region with thickness typically in the order of several nanometers and it is located between the ion-exchange membrane and the adjacent solution [159,160]. The EDL is formed due to the generation of an electric field by the fixed charges on the surface of the membranes. The electric field generated is responsible for Coulomb forces that attract ions with opposite charge, which create the

EDL [17,161]. In Figure 16b, the different behaviors of ions supply as *i* increases are due to the change from diffusion and migration to overlimiting phenomena as the dominant mechanism of ion transport.

The concepts used so far in the studies of concentration polarization derived from the Nernst film model [18,162]. This model considers the existence of a "Nernst diffusion layer" region between the membrane/solution interface and the bulk solution, which is the diffusion boundary layer. During the development of this model, Nernst considered that, at this thin region, the electrolytic composition shows a linear profile and no convection phenomenon occurs, being the mass transport controlled by diffusion-migration [38]. The concept reported by Nernst was later improved by Levich [162] since he considered the occurrence of convective transport within the DBL [38].

When the limiting current density is exceeded and the concentration polarization phenomenon becomes intense, a mass transfer limitation occurs and any increase in the voltage that passes through the membrane does not increase the ionic transport. Generally, the extra energy supplied is spent in secondary reactions, such as the dissociation of water ($H_2O \rightarrow H^+ + OH^-$) [14]. The limiting current density, considering a solution of a single salt completely dissociated, can be calculated by the equation developed by Peers in 1956, represented by Equation 20 [163]. In this equation, under the local electroneutrality assumption, the limiting current density is reached when the concentration of counter-ions reaches zero at the surface of the membrane.

$$i_{lim} = \frac{DC_0F}{\delta(\overline{t_j} - t_j)} \qquad \text{Equation 20}$$

Equation 20 is a rearrangement of Equation 19, considering that the diffusion of ions in the membrane phase is negligible and that a limiting current density exists, above which intense concentration polarization may occur. In Equation 20, δ is the thickness of the diffusion boundary layer, defined as the distance from the membrane to the cross point of the tangents drawn to the concentration profile at the interface and bulk solution. This can be estimated using the Levich Equation represented by Equation 21 [164] and it is affected by the hydrodynamic conditions of the electrolyte solution, such as the stirring strength or flow rate of the solution.

$$\delta = \frac{L^{1/4}}{0.7(Sc^{1/4})\left(g\Delta C_g/4\nu^2\right)^{1/4}} \qquad \text{Equation 21}$$

In Equation 21, L is the effective radius of the membrane when it is circular, g is the gravitational acceleration, Sc is the Schmidt number, v is the kinematic viscosity of the solution, ΔCg is the concentration gradient between the boundary layer of the membrane interface and the bulk solution. In the condition of limiting current density, $\Delta Cg = C_0$ since the concentration of ions at the interface is zero.

The value of δ may also be determined from the potential drop evolution during the relaxation measurements of chronopotentiometry. When the current is switched-off, concentration polarization does not disappear immediately [165]. Sistat and Pourcelly [166] used chronopotentiometry together with a mathematical model to determine δ from the remaining potential drop. Theoretical and chronopotentiometric results showed a very good agreement. Some years later, Larchet et al. [75] evaluated the evolution of δ with time during chronopotentiometric measurements. The authors obtained a proportional relationship of δ with the difference between the electrolyte concentration in the solution bulk and at the interface ($\Delta c^{-0.2}$) different from that predicted by Levich ($\Delta c^{-0.25}$). This occurred because, in Levich's theory, the microscopic chaotic convection motion is not considered. It was also shown that when the current is switched-on, δ increases due to concentration changes in the current-induced DBL caused by ion diffusion. Then, gravitational convection takes place and causes a reduction of δ, which shows a maximum value and then achieves a steady-state value. When the current is switched-off, Δc decreases with time and δ increases, leading to a slower relaxation of the system.

Equation 20 provides the theoretical limiting current density. This equation requires the calculation of several unknown terms, including the transport number of ions in the membrane phase. Its use is especially complex when considering a solution that is not composed of a monovalent single salt. In this case, it may be very difficult to obtain the necessary parameters. The real limiting current density can be determined directly from the current-voltage curves obtained by chronopotentiometry [7,15,50,79,141,167], by determining the intersection point of the tangential lines of regions I and II of the CVC, as shown in Figure 14.

Membrane heterogeneity strongly influences the current-voltage curves and, according to Volodina et al. [168], the limiting current density is the property that presents greater differences between homogeneous and heterogeneous membranes. In their study performed by chronopotentiometry, the values of i_{lim} obtained were considerably smaller for the heterogeneous membranes than for the homogeneous ones. According to the authors, the non-uniform distribution of the local current density in the conductive areas (where the current lines are condensed) leads to an early ion depletion in these regions, which is responsible for the inflection point in the current-voltage curves. Then, the theoretical limiting current density was calculated by the Lévêque equation for the two types of membranes. For the homogeneous ones, the values calculated and those experimentally obtained by chronopotentiometry were very similar. However, for the heterogeneous membranes, the calculated values were considerably higher than the experimental ones. Therefore, Volodina et al. [168] verified that the tangential electrolytic diffusion toward the conducting regions is responsible for the high current density in the conducting regions of heterogeneous membranes.

Current-voltage curves of heterogeneous and homogeneous membranes were also evaluated, by chronopotentiometry, by Pismenskaya et al. [73]. The authors also verified a greater current density in the conductive areas of heterogeneous membranes and a lower electrolyte concentration in these regions, when compared to the homogeneous ones under the application of the same current density. The heterogeneous membranes showed a slower increase of the current density with the voltage due to the presence of non-conductive regions and the tangential electrolytic diffusions. Shortly thereafter, Volodina et al. [168] constructed current-voltage curves of homogeneous and heterogeneous membranes by chronopotentiometry, and verified that the local limiting current density across conducting regions of a heterogeneous membrane is several times higher than the average limiting current through a homogeneous membrane.

Barros et al. [15] also obtained current-voltage curves of homogeneous and heterogeneous membranes using chronopotentiometry. Although homogeneous membranes generally present greater apparent fractions of conductive area, the authors obtained $\varepsilon_{het} = 0.808$ and $\varepsilon_{hom} = 0.734$. Despite these atypical values of ε, the CVCs obtained by the authors showed similar shapes to those obtained by Volodina et al. [168] and Pismenskaya et al. [73]; the heterogeneous membrane showed lower values of limiting current density compared to the homogeneous one, in addition to a slower growth

of current density with the voltage in the ohmic region. This may be explained by the absence of tangential electrolyte diffusion toward conducting regions of the homogeneous membrane tested by Barros et al. [15], despite its considerably low apparent fraction of conductive area. Therefore, regardless of the value of ε, the irregular distribution of the conducting regions plays an important role in the shape of current-voltage curves.

Marder et al. [65] reduced the fraction of conductive area of a homogeneous membrane in 80%, 60% and 45%, and evaluated their CVCs by chronopotentiometry. The authors verified that the limiting current decreased in a linear relationship with the reduction of the fraction of conductive area. The relation of the limiting current density with the fouling occurrence was also studied; Lee et al. [147] verified that the occurrence of foulant deposition and chemical binding to the functional groups led to the decrease of the limiting current density as a consequence of the reduction in the fraction of membrane conductive area. In ref. [65], the authors also evaluated CVCs constructed for a homogeneous membrane and different metal chloride solutions to compare the limiting current density values obtained experimentally with those calculated by the classical Nernst diffusion layer theory. The values obtained using the two methods were very close and, in both cases, i_{lim} presented the same order: cobalt > zinc > nickel = copper > manganese. The difference between the values of i_{lim} for each evaluated metal was justified by the occurrence of gravitational convection.

The degree of cross-linking also influences the limiting current density, as shown by Singh et al. [149]. They modified an anion-exchange membrane with a cross-linking agent in three proportions and constructed chronopotentiograms and current-voltage curves for each membrane. The increase in the cross-linker content increased the limiting current density as a consequence of the higher mobility of counter-ions across the membranes. The cross-linking agent favored electro-migration of counter-ions and a higher applied current density was required to cause intense concentration polarization.

The relation between the equivalent charge of the species in solution with the transport properties obtained by chronopotentiograms and current-voltage curves is also very interesting, especially in systems with multicomponent electrolytes [7,69,72,79,169]. The equivalent charge is expressed in Equation 22, where z_j is the charge and C_j is the concentration of an ion j. According to the Peers equation (Equation 20), the limiting current density is known to be directly proportional to the salt

concentration. García-Gabaldón et al. [69] verified that the molar concentration of the species with the highest equivalent charge in solution also presents a linear relation with the limiting current density.

$$Q_{eq} = \sum |z_j| C_j \qquad \text{Equation 22}$$

The relation between the limiting current density and the liquid flow rate has also been investigated [119]. This effect is practically unnoticeable in solutions with high concentrations of salts, due to the low contribution of the thickness of the boundary layer in this condition. However, at low concentrations, changes in the hydrodynamic conditions influence the values of limiting current density. The thickness of the diffusion boundary layer at the membrane surface is reduced by the increase of the solution flow, which increases the limiting current density and enhances the performance of the separation. This is also in agreement with Peers equation (Equation 20).

The influence of the type of co-ions in the electrolyte to be treated by electrodialysis has also been evaluated via chronopotentiometry. Titorova et al. [170] and Benvenuti et al. [171] found that the presence of co-ions in the diffusion boundary layer of CEMs and AEMs, respectively, mitigates the concentration polarization phenomenon and increases the limiting current density of the membrane system.

The limiting current density can also be determined by the construction of the Cowan-Brown curve [172], especially when the plateau of the CVC is not well defined and the inflection after the ohmic region is very subtle, hindering the determination of the intersection of the two tangential lines of the curve [34,38,180–183,134,173–179]. In this case, a curve of membrane voltage/current density (V/i) vs. the inverse of current density ($1/i$) is constructed, which presents two well-defined sections. The limiting current density is determined from the intersection of the tangential lines of these sections. Figure 17 shows a representation of a Cowan-Brown curve.

4.3.Chronopotentiometry with weak electrolytes and complexes

Besides factors that influence any separation process by electrodialysis, the presence of weak electrolytes and complexes in the solution to be treated can modify ion transport

and affect the membrane properties [184]. The low mobility of complexes, for example, hinders their transport and causes a decrease in the current efficiency [185], which leads to an increase of the membrane resistance [68,184].

Some recent developments [33,35,186] showed the effectiveness of electrodialysis and bipolar electrodialysis batch systems for purifying fermentation broths and producing chemical precursors from biomass, which are weak organic electrolytes. Unlike strong electrolytes, which completely dissociate into their respective ions, weak electrolytes are characterized by forming ionic species with different valences, mobilities and ionic charges depending on the pH, the ionic strength of the solution or the molar concentration. Therefore, depending on the degree of dissociation of the weak electrolyte, ionic mobility of the prevailing counter-ion will influence the voltage drop through the ion-exchange membrane. The ionic charges of the species directly or indirectly affect which ion is preferentially transported, the electrical resistance of the electrodialysis cell, the mass transfer efficiency, and the energy efficiency of the overall process. Melnikov et al. [187] reported that existing models used for predicting the transport-structural parameters of ion-exchange membranes are not applicable to weak electrolytes and further studies are required for a comprehensive description of their transport through ion-exchange membranes.

The presence of weak electrolytes may also influence the shape of current-voltage curves and chronopotentiograms since some authors have verified the presence of two inflection points in the curves related to distinct limiting current densities. Pismenskaya et al. [188] constructed CVCs in galvanodynamic mode with solutions containing HPO_4^{2-} and PO_4^{3-} and a modified AEM selectively permeable to monovalent anions. The authors verified the presence of two waves in the CVCs and related them to the alteration of the diffusion layer resistance after the depletion of the first species and the intense changes of pH inside the membrane. This displacement of the equilibrium condition and the alteration of the species being transported through the membranes occurred because weak electrolytes undergo shifts in equilibrium due to concentration polarization. These shifts imply a change in the species present near the membrane. Gally et al. [189] also evaluated the transport of salts of phosphoric acid using chronopotentiometry and obtained chronopotentiograms with multiple transition times. The first transition time was associated with the depletion of $H_2PO_4^-$ at the DBL, whereas the second one appeared due to the depletion of HPO_4^{2-}. For a solution with chloride ions,

three transition times were obtained, which were related to the successive depletion of Cl^-, $H_2PO_4^-$, and HPO_4^{2-} species. Current-voltage curves with multiple waves were obtained for solutions presenting at least two species at similar concentrations, agreeing with the chronopotentiograms. The same behavior in current-voltage curves showing multiple waves was observed in other works in which NaH_2PO_4 [190–192], $KC_4H_5O_6$ [193], and EDTA [79] solutions were used.

Other authors verified the presence of two plateaus in CVCs using chronopotentiometry. Martí-Calatayud et al. [141] verified two plateaus using solutions of $Cr_2(SO_4)_3$. In this case, the CVCs obtained agreed with the chronopotentiograms because multiple transition times were also verified. Figure 18 shows the CVCs with two limiting current densities and ChPs with two transition times obtained by the authors. At low current densities, the transport of Cr^{3+} occurred preferentially, while the depletion of complex ions occurred more intensively at high current densities. A decrease in the resistance between the two limiting current densities was also observed, which may have occurred due to the dissociation of the Cr(III) complex within the membrane, and the subsequent enrichment of the membrane phase in multi-charged ions. Melnikova et al. [193] constructed CVCs with solutions of NaH_2PO_4 and also verified the presence of two limiting current densities. The first one appeared when the NaH_2PO_4 salt diffusion to the membrane surface was saturated and the second was related to the saturation of the H^+ flux when the membrane was almost completely converted into the HPO_4^{2-} form. Barros and Espinosa [7] constructed CVCs by chronopotentiometry, using solutions with zinc, copper and EDTA and verified two limiting current densities; the first inflection point was attributed to the depletion of $Zn(EDTA)^{2-}$ and the second to the depletion of $Cu(EDTA)^{2-}$. The ChP obtained by the authors also presented two inflections related to two transition times, thus confirming the ion transport competition between two species. The presence of two limiting current densities and two transition times was also verified in the CVCs and ChPs recently obtained by Barros et al. [79] with EDTA solutions; this was explained by chemical equilibrium shifts that occurred in the membrane/electrolyte system as OH^- ions were intensively transferred through the anion-exchange membrane, reducing the pH in the membrane phase and dissociating $HEDTA^{3-}$ into $EDTA^{4-}$ and H^+ ions. Scarazzato et al. [169] also verified the presence of two transition times in the ChP testing solutions with etidronic acid (HEDP) and copper ions. The authors justified it by the transport of different species after the equilibrium change in the membrane. The first and the second

transition times were attributed to the passage of $HHEDP^{3-}$ and $[CuHEDP]^{2-}$, respectively. However, the current-voltage curves showed typical features of monopolar membranes, without the presence of two limiting current densities. Benvenuti et al. [171] showed that the accumulation of co-ions in the DBL may also alter the chemical equilibrium of the species in this region, leading to the appearance of additional inflection points associated with transition times in the chronopotentiograms. Zook et al. [194] related the two transition times to the results of spectroelectrochemical microscopy and confirmed that the inflections in the ChP appeared exactly when the free ionophore and ion-ionophore complex concentrations approached zero at the membrane-solution interface.

Butylskii et al. [6] showed that besides ions competition, there may be another reason for the appearance of more than one transition time in chronopotentiograms, and this is related to the membrane heterogeneity. Two transition times were obtained by the authors by testing a commercial heterogeneous anion-exchange membrane and two prepared cation-exchange membranes in a 0.02 M NaCl solution. They verified that the first transition time appears in heterogeneous membranes when the concentration of ions at the conductive regions reaches a value very close to zero. In turn, the second transition time appears when the electrolyte concentration reaches a very small value at the whole surface of the membrane, including the conductive and non-conductive regions. Similar results were obtained by Mareev et al. [8]; the authors identified the nature of the two transition times present in chronopotentiograms of a heterogeneous membrane by using mathematical modeling. They verified that the first transition time (τ_1) appeared when the diffusive transport of ions from the solution to the conductive areas reached its limiting condition. From this moment, the electroconvective vortices appeared in the limit of the conductive/non-conductive regions. The second transition time (τ_2) appeared when the electroconvection-diffusion ion delivery to the overall membrane surface achieved its limiting value.

4.4. Resistance of ion-exchange membrane systems

The resistance that ions face when transported through the solution and the membranes in an electrodialysis system is one of the most important properties for the separation viability since the lower the resistance, the lower the energy consumption in the ED process. The total resistance involved in electrodialysis is the sum of different

resistances that ions face during their transport. Its value depends on some factors intrinsically related to the membrane, the type of solution and the cell configuration, such as the spacing between the membranes and electrodes [9,195]. In industries, the intermembrane distance tends to be the smallest for reducing the resistance, generally being between 0.5-2 mm [2].

Membranes with large thickness and those with reinforcing fibers present high electrical resistances. Heterogeneous membranes, in general, also present high electrical resistances due to the more tortuous counter-ion pathway. Membranes with high concentrations of fixed charged groups (ion-exchange capacity) in the matrix generally present low resistances due to the high attraction between membrane and ions [13,196,197]. Greater values of membrane water content also abruptly reduce its resistance; high values of water content lead to larger conducting channels, and ion mobility through the membrane is enhanced [145]. The crosslinking method is a common practice to improve the membrane materials by reducing an excessive swelling, but it tends to increase the resistance [109,198]. The type of solution also influences the resistance strongly: the presence of organic species, such as glucose, affects the water structure in the regions near the ions, and therefore, their hydration sphere and the corresponding Stokes radius. A decrease in the Stokes radius leads to a decrease in the resistance of the ion movement through the liquid since it increases the conductivity and the ions mobility [134].

For determining the electrical resistance in the ohmic region, several direct current methods can be used, and one of the simplest methods is by calculating the inverse of the slope of the tangential line of the current-voltage curve. The resistance behavior obtained by direct current methods is quite different at low and high solution concentrations [38]. Several authors have found that, in low concentrations condition, the decrease of the resistance with an increasing concentration is very pronounced, whereas at high concentrations, the resistance is independent from the concentration [15,82,161,199]. However, these methods do not allow distinguishing which type of resistance (the pure membrane resistance, the resistance of the DBL or the resistance of the interfacial ionic charge transfer through the double layer) is dominant in function of the electrolyte concentration.

Another possibility is determining the conductivity using, for example, a clip cell [86,97,106,107,109,139,200–202], which was proposed by Belaid et al. [203] and Lteif et al. [204]. In this methodology, the membrane conductance is often measured using a clip cell with platinum electrodes. With the results of the conductance of solution and solution+membrane, the electrical resistance is calculated using Equation 23, in which R_m is the electrical resistance of the membrane, R_{m+s} is the resistance of the membrane plus the reference solution, R_s the resistance of the reference solution, G_m is the membrane conductance, G_{m+s} is the combined conductance of the membrane and reference solution, and G_s is the conductance of the reference solution.

$$R_m = \frac{1}{G_m} = \frac{1}{G_{m+s}} - \frac{1}{G_s} = R_{m+s} - R_s \qquad \text{Equation 23}$$

Since direct current methods do not allow discriminating the individual resistances present in membrane/electrolyte systems, authors have studied the resistance using alternating current methods [119,161,205]. In these works, it was verified that at low concentrations, the main resistance that controls the system is that caused by the diffusion boundary layer, whereas at high concentrations, this resistance is no longer important. For identifying and differentiating each type of resistance, electrochemical impedance spectroscopy is generally used [199,206–208]. Although electrochemical impedance spectroscopy provides insightful results, this is one of the most complex methodologies, due to the need of knowing each phenomenon involved in the implemented model [38].

As already mentioned, chronopotentiometry has often been used to evaluate electrical resistances of systems operating in underlimiting and overlimiting conditions. Stodollick et al. [209] used chronopotentiometry to determine the resistance in overlimiting currents of a bipolar membrane by constructing current-voltage curves. The authors observed that the resistance in overlimiting conditions follows an exponential law and depends on the pH and ionic strength only with regard to the absolute level of the current. The relationship between the resistance of the overlimiting region and the ohmic resistance (R_3/R_1) obtained by chronopotentiometry has been evaluated [9,69,110,147,169,196,210], and as confirmed by Choi et al. [210], larger ions in solution reduce the R_3/R_1 ratio. This is explained by the decrease in the resistance of the overlimiting region with the increase in Péclet number since ions with larger Stokes radius enhance the mixing intensity.

In addition to the polarization curves, the chronopotentiograms also provide valuable information about the resistance. The ohmic potential drop in non-polarized state of a membrane after ceasing the application of current (i = 0) quantifies the resistance associated with the membrane and the solution [73,141]. Besides, the greater the final value of the potential drop registered for an applied current density, the greater its electrical resistance. Some authors have observed that after reaching the steady-state stage in chronopotentiograms, the potential drop may vary and, consequently, the resistance as well. As already mentioned, the increase in potential drop suggests the formation of some precipitate at the membrane when the limiting current density is exceeded, which can block the ions passage and increase the resistance [65,67,70,71]. Scarazzato et al. [169] observed an increase in the potential drop of chronopotentiograms, which may have occurred due to the formation of uncharged species after the reduction of the pH at the membrane surface. The reduction of the potential drop during the application of a current density above the limiting one has also been observed and is related to water dissociation and the change in the equilibrium of the species transported through the membrane. In this case, the generation of H^+ and OH^- intensifies the transport of these species through the membrane due to their high ionic mobility [85], leading to a change in the pH of the diffusion boundary layer, and the occurrence of the dissociation of species [9]. According to Kniaginicheva et al. [211], the total resistance begins to decrease due to the dominance of water dissociation when $i/i_{lim} > 2$.

Some authors [81,83,154,212–214] usually present chronopotentiograms and current-voltage curves with the "reduced potential drop" (U_m') by excluding the ohmic resistance contribution (U_Ω of Figure 9) from the measured voltage (U_m) (Equation 24). This is quite convenient especially when the purpose of the work is to compare electrochemical behavior of different membranes. Figure 19 shows the current-voltage curves obtained by Balster et al. [81] for the Nafion membrane (DuPont, USA) with and without subtracting the ohmic resistance.

$$U_m' = U_m - U_\Omega = U_m - iR_1 \qquad \text{Equation 24}$$

4.5. Plateau length

After the inflection point related to the limiting current density in the current-voltage curves, a plateau zone is reached, where the current density practically remains constant

with the membrane voltage increase (See Figure 14). This behavior occurs due to the depletion of ions in the diffusion boundary layer and the consequent increase of the resistance faced by ions to be transferred through the membrane. After exceeding a certain membrane voltage value, the water dissociation phenomenon takes place and new current carriers are supplied to the membrane surface (H^+ and OH^-). Besides, overlimiting mechanisms of ion transport take place, such as gravitational convection and/or electroconvection. From this condition, the system reaches the overlimiting regime and the delivery of ions to the membrane surface is improved. In the polarization curves, the plateau is a transition zone between the underlimiting region and the overlimiting one. Therefore, the plateau length indicates the membrane voltage that must be surpassed to change the main ionic transport mechanism from diffusion and migration to overlimiting mechanisms.

The plateau length depends on both the solution used in electrodialysis and on the membrane. In general, this property tends to decrease with the increase of electrolyte concentration [70,72,141,215]. However, in some cases, the inverse behavior may occur due to the size of the ions that preferentially pass through the membrane [15,169]. As already mentioned, Choi et al. [210] verified that ions with larger Stokes radius and, consequently, with higher Péclet number, tend to enhance the solution mixing, which reduces the resistance of the third region (R_3). These ions also facilitate an earlier transition to the overlimiting regime at lower transmembrane voltages by decreasing the plateau length. This behavior has already been verified by chronopotentiometry with anion- [7] and cation-exchange membranes [216].

The counter-ion hydration number also influences the plateau length, as verified by Gil et al. [118]. The authors obtained CVCs, from chronopotentiograms, for $MgCl_2$, $CaCl_2$ and NaCl solutions using a heterogeneous cation-exchange membrane. The plateau length decreased with cations in the following order: $Na^+ > Ca^{2+} > Mg^{2+}$. This was related to the degree of hydration of cations: hydrated ions, such as Mg^{2+}, engage larger volumes of water in their movement, favor electroconvection and reduce the plateau length. This implies that, when ions with a high degree of hydration are present in the solution, the onset of electroconvection occurs at lower voltage values [217]. Recently, Gil et al. [83] also constructed CVCs using solutions of $MgCl_2$, $CaCl_2$, NaCl and observed the same tendency of plateau length decrease in the presence of ions in the following order: $Na^+ > Ca^{2+} > Mg^{2+}$. The lowest plateau length obtained with $MgCl_2$ solution was justified by

the greatest Stokes radius of Mg^{2+}. As it was verified by Choi et al. [210], ions that present greater Stokes radius favor the activation of electroconvection at lower voltage values, which reduces the plateau length.

The structure of the membrane also influences the plateau length considerably. Choi and Moon [107] obtained CVCs of anion-exchange membranes after their use in electrodialysis under overlimiting conditions, for evaluating the shape of the curve in function of the changes in the membrane structure caused by water dissociation. Two CVCs were constructed for both sides of the membrane facing the diluate solution in the chronopotentiometric cell: for the front side, where ion depletion and water dissociation occurred during electrodialysis, and for the back side, where ions were concentrated in electrodialysis. The authors verified that one of the most remarkable changes observed after the alterations on the membrane structure due to water dissociation was in the plateau length. The OH^- ions generated as a consequence of water dissociation converted quaternary amines into tertiary amines. Also, part of these amines may have been converted into their neutral forms, resulting in a reduction of charged groups and leading to an increase of the plateau length. Therefore, the plateau length was observed to increase as the inhomogeneity degree of the membrane increases. A few years later, Ibañez et al. [218] performed a chronopotentiometric study on the relationship between membrane structures and plateau length. The authors constructed CVCs with membranes cast on a glass plate and dried in air; the results revealed significant differences in plateau length, especially when the orientation of the membrane toward the feed was changed. Then, Marder et al. [65] modified the fraction of conductive area of a cation-exchange membrane and also verified, by chronopotentiometry, that the plateau length increased with the reduction of this property. According to Verodina et al. [168], this is not only due to the non-uniformity of the distribution of the layer near the membrane, but also due to the non-uniformity of the distribution of the current lines passing through the membrane, as shown in Figure 20. Other authors found the same tendency of increase in plateau length when the heterogeneity is increased [218].

Fouling and scaling occurrence also affects the plateau length because the deposition of insoluble species on the membrane surface reduces this property [147,219,220]. In some cases, the reduction is so strong that the second and third regions of the CVC come together, making the determination of the third region of the CVC unfeasible [7,141]. This is in accordance with the works of refs. [67,221,222] since

they showed that fouled membranes lead to the onset of electroconvection at lower voltages, which means that the plateau length is reduced.

Several authors developed new membranes to reduce the plateau length and to promote the regime above the limiting current density operating at lower potential values [106,107,142,223–225]. Figure 21 shows current-voltage curves obtained by Roghmans et al. [226] for an unmodified cation-exchange membrane and for two coated membranes by a microgel with 25% and 31% of coverage. The plateau length of the unmodified membrane was approximately 1.0V, whereas for the modified membranes with 25% and 31% of coverage, the plateau length was approximately 0.6V and 0.55V, respectively.

5. Overlimiting phenomena

Electrodialysis is conventionally operated under underlimiting conditions, by applying 70%-80% of the limiting current density of the membrane/electrolyte system [61,227–229]. In this condition, the system operates at a quasi-ohmic regime and showcases predictable behaviors. Some years ago, the application of a current density above the limiting one was only related to operational inconveniences, such as the formation and deposition of precipitated salts on the surface of the membranes, which can lead to their degradation, increase its resistance, and imply an unnecessary energy consumption. In recent years, several authors have considered the operation of electrodialysis under overlimiting conditions since they have verified considerable advantages, such as the reduction of membrane area [107], reduction of apparatus dimensions [176], reduction of operating time and increase in ion transport [61,230].

5.1. Overview of overlimiting mass transfer mechanisms

The operation of electrodialysis at overlimiting condition is established from the occurrence of intense concentration polarization. When concentration polarization is intensified, the saturation of current density occurs due to the ion depletion at the membrane vicinity. When the limiting current density is reached, the voltage (and, consequently, the electrical resistance) over a membrane surrounded by two DBLs tends to infinity, theoretically. However, in practice, this does not occur because the system

adjusts itself to continue transporting electric current. The first explanation given for this transport of current in overlimiting condition was the generation of H^+ and OH^- ions during water dissociation, which was justified by the change in the solution pH on the membrane surface [39,231]. However, in 1956, Frilette [232] verified that besides there being no saturation of electric current, the saturation of Na^+ ions crossing a cation-exchange membrane did not occur, either, which was explained by the occurrence of the convection phenomenon. Therefore, from Frilette [232] and Peers [163], convection was also considered a justification for the current and ion transport under overlimiting condition.

With the aid of improved techniques and greater knowledge about the overlimiting condition, researchers began to discover other phenomena and mechanisms that occur simultaneously or as a result of water dissociation and convection, such as the Kharkats effect (or exaltation effect) and the current-induced membrane discharge (CIMD). In recent years, extensive efforts have been made to distinguish the effects of electroconvection and gravitational convection on the transfer of ions, in addition to understand the different types and mechanisms of electroconvection, such as stable/unstable, bulk electroconvection, electroosmosis of the first and second kind [223,233–235].

5.2.Electroconvection

Electroconvection is one of the major responsible phenomena for ion transport when the system operates in overlimiting conditions. However, its mechanisms are not completely understood yet, although some information in literature has been universally accepted. In theoretical studies about the types of convection, Rubinstein et al. [223,233,235–238] verified that, especially in homogeneous membranes, electroconvection results from the interaction between the electric field of the system and its respective space charge under conditions of deviation of the local electroneutrality condition. As a consequence, a nonpotential volume force grows strong enough to set in motion the fluid in the boundary layer adjacent to the membrane [69,107]. This occurs due to the formation of vortexes, which increase the counter-ions transfer in several times by mixing the depleted solution [39,239]. For heterogeneous membranes with curved or electrically heterogeneous surface, Dukhin and Mishchuk [240,241] showed that the

tangential component of electric current are necessary for the onset of electroconvection, since the curvature of the current lines toward the ion conducting regions causes the formation of vortices. In heterogeneous membranes, the accumulation of electric current lines leads to their distortion in the ion conductive pathways on the membrane surface, which is known as “funnel effect” [242]. This tangential component of ion fluxes in the diffusion boundary layer enables the emergence of electroconvection in heterogeneous membranes. When electroconvection emerges, hydrodynamic instabilities are produced, since a non-uniform electric field is formed as a result of the intense variation of fluid velocity and concentration of ions at the DBL [217]. Hence, vortexes are formed, and the system begins to be controlled by complex phenomena that will be mentioned below. Figure 22 shows a representation of electroconvection vortices formed near a heterogeneous surface containing well and poorly conducting areas.

Electroconvection (EC) can be classified as stable or unstable, also known as Dukhin-Mishchuk EC mode and Rubinstein-Zaltzman EC mode, respectively [39,243]. In the polarization curves, the registration of plateau regions with a moderate increase in current density is related to the stable EC, while the great increase in the final region of the curve is related to unstable EC or water dissociation [223,243]. In chronopotentiograms, the unstable EC causes intense oscillations of the potential drop and this is responsible for the increased delivery of ions, contributing to an enhanced mass transfer. This behavior of intense oscillations in chronopotentiometric curves because of electroconvection is shown in Figure 23, in the region between points 3-4. Moreover, large unstable vortices cause the suppression of the undesirable water dissociation phenomenon in comparison with stable vortices [145]. Druzgalski et al. [244] showed how electrohydrodynamics become chaotic by using some concepts from turbulence theory such as Reynolds-averaging. These intense oscillations related to the unstable EC may be associated with the breaking of large vortices into smaller ones, which may merge again and generate new large vortices.

It is known that electroconvection occurs more intensively in more diluted solutions due to the larger thickness of the space charge region near the membrane surface [39,168,243]. Diluted solutions exhibit stable electroconvection more intensively than concentrated solutions [222]. The properties of membranes are also important for the stability of electroconvection. Experimental studies have shown that when the depleted diffusion layer is immobilized by casting a thin layer of an agarose-gel on its

surface, the excess current noise cannot be observed after reaching the plateau, hindering the occurrence of electroconvection [245]. According to Andreeva et al. [142], the surface modification of the membrane by casting a conducting film on its surface allows an earlier onset of unstable electroconvection, which leads to a decrease of the plateau length. Pismenskaya et al. [246] used chronopotentiometry to evaluate electroconvection after modifying an anion-exchange membrane with a weakly crosslinked ion-exchange resin. The membrane modification enhanced the concentration of quaternary amines, whereas the secondary and tertiary ones were reduced. The fraction of membrane conductive areas increased, and they were redistributed because of the formation of agglomerations of conductive areas. This intensified electroconvection and enlarged the vortexes formed near the modified membrane in comparison with the unmodified one.

Some physical and mathematical models have been developed to explain the mechanisms involved in electroconvection. After Rubinstein and Shtilman [247], several works have been published to mathematically describe the overlimiting regime using the Nernst-Planck and Poisson equations [248,249]. These models are developed for 1D systems and consider the appearance of space charge region and the consequent reduction of DBL. Although 1D models may be useful to capture the experimentally observed pH fronts [250], they do not consider convection and are therefore unable to associate this variation of the DBL with the experimental results that show an increase of ion transfer in the overlimiting regime. Simulations show that, when the current density is equal or higher than the limiting current density, differences in the behavior of polarization curves constructed with models that do not consider electroconvection are visible [243]. Uzdenova et al. [251] proposed a 1D model based on the Nernst-Planck and Poisson equations for the galvanostatic mode, and compared the results with those obtained experimentally through chronopotentiometry; the calculated transition times were in good agreement with the experimental ones. However, the model was not able to simulate the chronopotentiometric curves beyond the inflection point related to additional transfer mechanisms at the overlimiting regime. In this case, the simulated potential drop continued to rise steeply, even when the extended space charge region was formed. This is the major limitation of 1D models. Therefore, 2D models, which are based on the Nernst-Planck-Poisson equation coupled with the Navier-Stokes equation, consider convection in addition to diffusion and migration as transfer mechanisms of ions, and were developed by Dukhin and Mishchuk [252] and Rubinstein et al. [253]. In recent

years, several 2D models have been developed in modeling studies on mass transfer phenomena because they allow, with good precision, evaluating the ion transfer through membranes in overlimiting current regimes [75,76,102,217,240,254–257]. In 2018, Nikonenko et al. [258] published a review on the existing mathematical models that describe ion transfer through electromembrane systems. The authors focused on the influence of the membrane heterogeneity (inside and at their surface) on the performance of separation processes. In several works reported by Nikonenko et al. [258], chronopotentiometry was used to evaluate the mathematical models, mainly to compare theoretical and experimental transition times.

The use of chronopotentiometry, together with mathematical assessments based mainly on 2D models, has generated very promising results in studies conducted in overlimiting current regimes. As mentioned in section 4.3, Mareev et al. [8] identified, mathematically, the nature of two transition times present in chronopotentiograms of a heterogeneous membrane. The first transition time (τ_1) appeared when the diffusive transport of ions from the solution to the conductive areas reached its limiting condition, whereas the second transition time (τ_2) appeared when the electroconvection-diffusion ion delivery to the overall membrane surface achieved its limiting value. This mathematical evaluation was possible because the authors developed a 2D model, which also consider electroconvection besides diffusion as mass transfer mechanism. Larchet et al. [75] treated experimental chronopotentiometric curves with numerical modelling using Kedem–Katchalsky equations. With the results, it was possible to assess the relationship between ion transfer effects, such as electroosmosis and streaming potential. Different mechanisms of streaming potential and their effects were discussed based on the shape of the ChPs and the numerical results. Mareev et al. [76] used a 2D model to simulate chronopotentiograms in underlimiting and overlimiting regime. The authors presented the diffusion layer thickness, δ, as a function of the Donnan potential drop at the interface between the membrane and the depleted solution. Simulated curves very close to the experimental ones were obtained, as shown in Figure 24. Roghmans et al. [226] modified cation-exchange membranes to assess the influence of geometrical and chemical membrane surface topology on the evolution of electroconvection. The study was performed by chronopotentiometry together with direct numerical simulations with a 2D model. The simulated results agreed with the experimental ones since they showed that the surface charge of the printed patterns influences the direction of the

electroconvective vortices, which is advantageous during ion transport toward the membrane. Uzdenova [259] developed a 2D model to obtain theoretical chronopotentiograms and current-voltage curves for the galvanodynamic mode. The model allowed the description of the formation of the extended space charge region and the development of electroconvection at a cation-exchange membrane. The increase in the electrolyte concentration, channel length and velocity of the forced flow showed to increase the intensity of electroconvection. The theoretical curves obtained were very similar to the experimental ones.

Mareev et al. [260] proposed a 2D non-stationary model of ion transport though a membrane using a new formulation of the boundary conditions at the conductive areas. By applying an electric current stream function, they showed the non-uniformity of the distribution of current lines over the conductive regions and its influence on chronopotentiograms and electrochemical impedance spectra. Mareev et al. [116] reported an approach for a three-dimensional (3D) modeling of transient ion transfer across a heterogeneous surface. Theorical transition times were compared to those experimentally obtained by chronopotentiometry and they were in a very good agreement. The authors also evaluated the assumption of the uniform current density distribution proposed by Rubinstein et al. [242] and verified that shorter transition times than the experimental ones were obtained for a 0.02 mol/L NaCl solution.

Druzgalski and Mani [261] developed a 3D model to solve the Poisson-Nernst-Planck and Navier-Stokes equations in order to compare the results with those obtained with a 2D model. Some qualitative similarities were verified by examining instantaneous snapshots from the models. In turn, significant differences were verified in quantitative predictions of mean quantities such as concentration, charge density, and current density. The authors showed the need of using 3D models since dimensionality significantly influences the quantitative evaluation of electroconvection, especially in the extended space charge region.

Experimental studies of electroconvection by evaluating ChPs and polarization curves without using a mathematical model are also often performed. Nebavskaya et al. [87] studied the influence of the ion exchange membrane surface charge and hydrophobicity in underlimiting and overlimiting regimes by chronopotentiometry. The authors noted that in underlimiting condition, the mass transfer

rate is mainly affected by the membrane surface charge, while in overlimiting conditions, the main factor is the degree of hydrophobicity. This may be explained by the difference in the convection types in the underlimiting (electroosmosis of the first kind) and overlimiting regimes (electroosmosis of the second kind). Electroosmosis of the first kind occurs by the action of the tangential electric field upon the diffuse part of the electric double layer, whereas in the electroosmosis of the second kind, the tangential electric field acts upon the extended space charge of the nonequilibrium double layer [235,262].

The influence of the hydrophobicity of the membrane on the overlimiting regime was also verified by Pismenskaya et al. [263]. They compared chronopotentiograms and current-voltage curves of virgin and used membranes after overlimiting experiments and suggested that intensive currents produced erosion of the ion-exchange polymer, which formed a continuous phase in the membrane. This erosion led to the exposure at the surface of small particles (about 100 nm) of relatively hydrophobic polyvinylchloride. The higher hydrophobicity of the surface was responsible for the increase in electroconvective vortices. Korzhova et al. [264] also evaluated chronopotentiograms and polarization curves as a function of the deposits of hydrophobic non-conducting spots of a fluoropolymer after modifying the membrane surface. The modified membranes showed larger amplitude of oscillations due to the greater hydrophobicity, lower voltage growth, and lower water dissociation rate. This occurred because the hydrophobic spots enhanced the intensity of the tangential electric force applied to the space charge region.

5.3.Gravitational convection

Another type of convection involved in the overlimiting regime is the gravitational one. Gravitational convection occurs by the non-uniform distribution of the solution density, which causes an Archimedes force. Together with the gravitational force, the fluid in the region near the membrane is set in motion [256,265]. The Archimedes force emerges due to the tendency of a body to be pushed out of the liquid's bulk onto its surface due to the lower body's density if compared to the liquid's density [266]. In an electrodialysis system, the rise of volume force is conditioned by gradients of concentration and/or temperature. Therefore, this phenomenon tends to occur more intensively in concentrated solutions, due to the higher Joule heating and higher concentration gradients. Theoretical [160,257,266,267] and experimental studies

[73,75,80,152,168,248,268,269] on gravitational convection are frequently published. Among the techniques employed in the experimental studies, the use of chronopotentiometry has shown special relevance.

Through chronopotentiometry, Pismenskaya et al. [73] verified that in a system with a 0.1 M NaCl solution, the main overlimiting mechanism is gravitational convection, whereas in a system with 0.01 M NaCl, the main mechanism is electroconvection. The authors verified a reduction of the potential drop in the ChPs after reaching a maximum point, which occurred due to the gravitational convection. This behavior of the ChP is represented in Figure 25 and is discussed in section 5.4, since this shape may also be caused by dissociation of water or by the current-induced co-ion transfer through the membranes. The reduction in potential drop observed by Pismenskaya et al. [73] was much greater with the heterogeneous membrane than with the homogeneous one. This was explained by the greater heat created by Joule effect at the heterogeneous membrane under application of a current density due to its greater resistance. In addition to this, the heat dissipation from the heterogeneous membrane was lower than from the homogeneous one, due to the greater thickness and resistance of the former. Therefore, the heat produced accumulated on the surface of the membrane and heated the depleted diffusion boundary layer.

Martí-Calatayud et al. [141] used chronopotentiometry to confirm that gravitational convection occurs even at current densities below the limiting current density. The authors noted that at currents below or slightly greater than the limiting one, gravitational convection is the main overlimiting mechanism, which causes a decrease in the thickness of the diffusion boundary layer and in the membrane potential drop. Krol et al. [80] evaluated chronopotentiometric and polarization curves obtained with the system in vertical and horizontal positions to evaluate the effects of gravitational convection. The authors verified that, in the horizontal position, without any forced convection, the steady-state condition was not achieved in the chronopotentiograms since the potential drop increased continuously with time. This occurred because concentration gradients in the depleted solution were established by gravitational force. Oscillations in potential drop caused by the gravitational convection were also verified. Hence, the work showed the importance of gravitational convection in a system under overlimiting regime. Pismenskaya et al. [268] also evaluated polarization curves by chronopotentiometry using systems in different positions. The authors verified that the differences between the curves

obtained with the system in horizontal and vertical positions did not exceed 6%. Therefore, gravitational convection could be neglected in their experiments.

The effects of gravitational convection are generally quite subtle. In addition to occurring only in solutions at high concentrations, gravitational convection is more intense in systems with greater intermembrane distances and in solutions with lower flow rates [269]. Hence, the effect of gravitational convection is greater in systems with high Grashof number [$Gr = (\Delta\rho_0/\rho_0).(gH^3/\nu^2)$] [248,257], in which $\Delta\rho_0$ is a characteristic variation in solution density in the system, ρ_0 is the initial solution density and H is intermembrane distance. Besides, whatever the nature of the bulk flow (laminar/turbulent, or natural/forced), the gravitational force is able to destroy the diffusion boundary layer only when the respective Rayleigh number is greater than 1000, which is a critical value for this mechanism [223,236].

5.4.Water dissociation

Water dissociation in membrane systems began to be intensively studied in the 1980s [270] and, in recent years, several works have been performed to understand its mechanisms and consequences. Studies focused on water dissociation performed by voltammetry, chronopotentiometry and electrochemical impedance spectroscopy are often performed, with the possibility of analyzing the evolution of the solution pH over the course of the experiments [142,152]. Water dissociation takes place in a thin layer at the membrane interface (~1 nm thick) and it occurs as proton-transfer reactions between molecules of water and the charged groups of the membrane [270,271]. When the applied current density approaches the limiting current density of the membrane system, the reaction rate rapidly increases [168]. Therefore, water dissociation becomes considerable when the concentration of salt ions on the surface of the membrane is comparable to the concentration of the H^+ and OH^- ions of the water [222].

The membrane type strongly influences water dissociation, and the range of the catalytic activity of ionogenic groups toward the reaction of water dissociation is presented as follows: $–N(CH_3)_3 < –SO_3H < =NH, –NH_2 < \equiv N$ [142,272]. For this reason, water tends to dissociate more intensively at anion- than at cation-exchange membranes. This can be justified by the different mechanisms of the phenomenon in both types of membranes, which can be proven by the different pH variations at the membranes and by

polarization curves [273]. Belova et al. [265] studied water dissociation on two anion-exchange membranes by chronopotentiometry. The authors noted that with one of the membranes (MA-40M), the intensity of water dissociation was low and electroconvection was more noticeable, whereas with the MA-40 membrane, electroconvection seemed to be suppressed by water dissociation. Kang et al. [135] assessed the influence of the surface charge density on the water dissociation behavior. They observed that the increase in the fixed charge density caused an increase in the water dissociation intensity, which is in accordance with the classical electric field-enhanced water dissociation theory. Kang et al. [77] used a Nafion membrane (DuPont, USA) with an iron hydroxide/oxide deposited layer for evaluating the influence of inorganic substances on water dissociation. The authors observed that the intensity of the phenomenon of the metal-embedded cation-exchange membranes was 10^4-10^5 times higher than those of the virgin membranes in the same conditions. They believed that the immobilized bipolar structure consisting of the H^+ and OH^- affinity groups increased the electric fields and the catalytic activity of the membrane.

The solution type also influences the rate of water dissociation, as observed by Rybalkina et al. [154] using chronopotentiometry with KCl and NH_4Cl electrolytes. They noted that the presence of NH_4^+ species in solution favors water dissociation at the AEM. This was explained by the intense transfer of OH^- ions through the membrane, toward the concentrate compartment, and the formation of NH_3 molecules at the enriched membrane boundary layer; a back diffusion of these NH_3 species occurred toward the depleted membrane boundary and water dissociation was catalyzed by these ions at the diluate side. It was also noted that, as water dissociation was intensified, secondary and tertiary fixed groups of the AEM were deprotonated, causing a reduction in the ion-exchange capacity of the membrane. The chronopotentiograms showed that the presence of NH_3 molecules at the membrane led to an increase in its resistance when the system was expected to be at steady-state condition. Current-voltage curves obtained for each solution also showed different shapes; lower limiting and over-limiting current densities at a given potential drop were obtained with the NH_4Cl solution.

Martí-Calatayud et al. [216] evaluated the relationship between current efficiency and plateau length by chronopotentiometry. They verified that water dissociation was more relevant in curves with long plateaus since greater values of membrane voltage are needed to reach the region of overlimiting currents. In contrast, in systems with lower

plateau lengths, the tendency of water dissociation occurrence is lower since electroconvection takes place more intensively. The authors observed that the transfer of nickel ions through the membrane was favored by electroconvection in conditions of low plateau length, while water dissociation considerably reduced the transfer efficiency.

The system configuration also affects the rate of water dissociation, which is negligible in systems with large distances between membranes, with or without agitation [274]. The reduction of water dissociation in pulsed-ED processes has also been evaluated in recent years, in addition to determining optimal conditions for pulse regimes, which consequently decreases fouling and scaling [182,275,276].

Another phenomenon, less evident, may occur associated with water dissociation: the exaltation effect, which was firstly studied by Kharkats [277]. This occurs by the generation of H^+ and OH^- ions and their presence in the region near the membrane since these ions may disturb the electric field and increase the exaltation of the transport of counter-ions. That is, OH^- ions generated in the depletion region attract cations from the salt and move them from the bulk solution to the interface, promoting their transport through the membrane, while H^+ ions promote the same mechanism with salt anions [160]. In general, the exaltation effect is neglected due to the greater relevance of electroconvection and the fact that the mobility of H^+ and OH^- is 5 to 10 times greater than the mobility of salt ions. However, Melnikova et al. [193] mathematically verified that this phenomenon is able to increase the transport of $H_2PO_4^-$ by 11%.

Water dissociation can also cause the current-induced membrane discharge (CIMD) [278]. In this case, the intense passage of OH^- ions through anion-exchange membranes, which have weak basic functional groups, can deprotonate their charges. Consequently, the membranes lose permselectivity, that is, the passage of co-ions through the anion-exchange membrane increases. Studies performed by IR-spectroscopy [107] show that after the intense passage of OH^- ions through commercial anion-exchange membranes with quaternary amines, these functional groups are rapidly converted into tertiary and secondary amines, by Hofmann reaction [43,264]. The process is intensified by the local Joule heating up to detachment of ionic groups.

Chronopotentiometric studies performed by Mikhaylin et al. [145] and Korzhova et al. [264] show that the presence of electroconvective unstable vortices lead to suppression of water dissociation, because of the competition that takes place between these two

phenomena. In this case, the vortices contribute to decrease the OH^- concentration in the depleted boundary solution. Belova et al. [152] and Slouka et al. [279] noted the opposite effect: a partial suppression of electroconvection by water dissociation at anion-exchange membranes. This may be related to the reduction of the space charge at the depleted interface by H^+ ions since they have opposite charges compared to the space charge at the membranes, being able to reduce it. The same phenomenon is valid for OH^- at cation-exchange membranes [39]. Finally, chronopotentiometric curves may also show a reduction in potential drop when water dissociation takes place [280]. This is explained by the formation of the conductive H^+ and OH^- ions and their intense transfer through the membranes. Recently, Titorova et al. [170] found that the type of co-ions in the solution to be treated by electrodialysis may also reduce the membrane potential drop. According to the authors, the current-induced co-ion transfer through the membranes reduces the electrical resistance of the diffusion boundary layer over time; this may lead to the appearance of a peak in the chronopotentiograms after reaching the transition time. A similar peak can also appear due to gravitational convection and/or water dissociation occurring at the membrane surface, as shown in Figure 25.

6. Conclusion and Future Directions

The present paper provides a review on the use of chronopotentiometry for determining transport properties of membrane/electrolyte systems and evaluating mass transfer phenomena involved in electromembrane processes operated in underlimiting and overlimiting current regimes.

The most relevant properties evaluated by chronopotentiometry are the limiting current density, electrical resistances, plateau length, transition times, transport number of counter-ions in the membrane phase and apparent fraction of conductive area. Moreover, the evolution of the potential of the membrane system over time also contains valuable qualitative information regarding the different mechanisms of mass transfer that arise when overlimiting currents are applied, such as gravitational convection, electroconvection or the dissociation of water. In recent years, great attention has been given to the use of chronopotentiometry in combination with mathematical models (1D, 2D, and recently also 3D), especially to understand the nature of overlimiting transfer phenomena. For instance, these studies have been used by electrochemists to explain the

phenomena involved in the registration of two transition times in chronopotentiometric curves, to determine the thickness of diffusion boundary layers, and to differentiate between stable and unstable modes of electroconvection.

The influence of the characteristics of ion-exchange membranes (heterogeneity, hydrophobicity, surface charge, type of fixed charge, and thickness), electrolytes (concentration, pH, and properties of counter-ions and co-ions) and system configurations (intermembrane distance, flow rate, and orientation of asymmetric membranes) on ion transport taking place in electrodialysis cells has been intensively assessed by means of chronopotentiometry. Most of such investigations are summarized in this review.

There is a great number of potential directions for future works on chronopotentiometry. One of them is the intensification of evaluations using membranes that have been developed recently, such as those presenting anti-fouling, anti-microbial, and monovalent-selective properties, in addition to profiled membranes, which present an integrated spacer functionality. Chronopotentiometry is also expected to be employed in investigations on membrane systems with solutions that will probably be treated intensively by electrodialysis in the coming years, such as municipal wastewaters. Chronopotentiometric evaluations with weak electrolytes are also expected to increase, such as solutions from fermentation broth; several authors have investigated the separation, by electrodialysis, of organic acids from this biological process, but the mechanisms of ion transfer across the membranes need to be better understood. Weak electrolytes contain species that dissociate at the membrane surface and inside it as a result of water dissociation and equilibrium shifts occurring simultaneously in the membrane/electrolyte system. Further studies are necessary to shed light on these phenomena, and methods able to measure the pH inside the membrane during the tests, for example, may be developed. Besides, in studies with weak electrolytes, the authors generally evaluate the ion transport using a commercial membrane and only one type of species in the electrolyte to facilitate the understanding of phenomena occurring in the membrane/electrolyte system. However, in industrial electrodialytic processes, the electrolytes have several types of competing species to be transported across the membranes. Therefore, to approximate the results to real membrane processes, further chronopotentiometric studies are expected to be conducted considering the transport of more complex mixtures across the membranes, at a greater range of electrolyte concentrations, and with different types of ion-exchange membranes.

Lastly, in recent years authors have developed robust models to simulate chronopotentiograms. In these models, solutions of single salts such as NaCl or weak electrolytes with phosphate anions have been used. The use of complex solutions in evaluations of mathematical models can be considered as a trend in chronopotentiometric studies. New models, especially 3D ones, are expected to be developed in the coming years; this is especially important considering the difficulty in simulating, with good precision, the region of the chronopotentiograms in which intense concentration polarization occurs, hindering the determination of transition times.

Acknowledgements

The authors gratefully acknowledge the financial support given by the Brazilian funding agencies CNPq (Process 141346/2016-7, 171241/2017-7, and 160320/2019-4), FAPESP (Process 2012/51871-9) and CAPES (Process 88881.190502/2018-01 and 88887.362657/2019-00). The financial support of Cyted (Network 318RT0551) and ERAMIN2 (FINEP, Brazil and AEI, Spain) is also acknowledged. This study was financed in part by the Coordenação de Aperfeiçoamento de Pessoal de Nível Superior - Brasil (CAPES) - Finance Code 001.

References

[1] E. Maigrot, J. Sabates, Apparat zur Lauterung von Zuckersaften mittels Elektrizitat, 50443, 1890.

[2] H. Strathmann, Ion-Exchange Membrane Processes in Water Treatment, in: Sustain. Sci. Eng., Elsevier, 2010: pp. 141–199. doi:10.1016/S1871-2711(09)00206-2.

[3] W. Zayani, S. Azizi, K.S. El-Nasser, Y. Ben Belgacem, I.O. Ali, N. Fenineche, H. Mathlouthi, New nanoparticles of (Sm,Zn)-codoped spinel ferrite as negative electrode in Ni/MH batteries with long-term and enhanced electrochemical performance, Int. J. Hydrogen Energy. 44 (2019) 11303–11310. doi:10.1016/j.ijhydene.2018.10.220.

[4] N.R. Chowdhury, R. Kumar, R. Kant, Theory for the chronopotentiometry on

rough and finite fractal electrode: Generalized Sand equation, J. Electroanal. Chem. 802 (2017) 64–77. doi:10.1016/j.jelechem.2017.08.039.

[5] J. Xue, M. Shao, Q. Shen, X. Liu, H. Jia, Electrodeposition of Cu2O nanocrystalline on TiO2 nanosheet arrays by chronopotentiometry for improvement of photoelectrochemical properties, Ceram. Int. 44 (2018) 11039–11047. doi:10.1016/j.ceramint.2018.03.078.

[6] D.Y. Butylskii, S.A. Mareev, N.D. Pismenskaya, P.Y. Apel, O.A. Polezhaeva, V.V. Nikonenko, Phenomenon of two transition times in chronopotentiometry of electrically inhomogeneous ion exchange membranes, Electrochim. Acta. 273 (2018) 289–299. doi:10.1016/j.electacta.2018.04.026.

[7] K.S. Barros, D.C.R. Espinosa, Chronopotentiometry of an anion-exchange membrane for treating a synthesized free-cyanide effluent from brass electrodeposition with EDTA as chelating agent, Sep. Purif. Technol. 201 (2018) 244–255. doi:10.1016/j.seppur.2018.03.013.

[8] S.A. Mareev, A. V. Nebavskiy, V.S. Nichka, M.K. Urtenov, V. V. Nikonenko, The nature of two transition times on chronopotentiograms of heterogeneous ion exchange membranes: 2D modelling, J. Memb. Sci. 575 (2019) 179–190. doi:10.1016/j.memsci.2018.12.087.

[9] M.C. Martí-Calatayud, D.C. Buzzi, M. García-Gabaldón, A.M. Bernardes, J.A.S. Tenório, V. Pérez-Herranz, Ion transport through homogeneous and heterogeneous ion-exchange membranes in single salt and multicomponent electrolyte solutions, J. Memb. Sci. 466 (2014) 45–57. doi:10.1016/j.memsci.2014.04.033.

[10] R.K. Jain, H.C. Gaur, B.J. Welch, Chronopotentiometry: A review of theoretical principles, J. Electroanal. Chem. 79 (1977) 211–236. doi:10.1016/S0022-0728(77)80444-0.

[11] P.J. Lingane, D.G. Peters, Chronopotentiometry, CRC Crit. Rev. Anal. Chem. 1 (1971) 587–634.

[12] S. Caprarescu, V. Purcar, D.-I. Vaireanu, Separation of Copper Ions from Synthetically Prepared Electroplating Wastewater at Different Operating Conditions using Electrodialysis, Sep. Sci. Technol. 47 (2012) 2273–2280.

doi:10.1080/01496395.2012.669444.

[13] R.K. Nagarale, G.S. Gohil, V.K. Shahi, Recent developments on ion-exchange membranes and electro-membrane processes, Adv. Colloid Interface Sci. 119 (2006) 97–130. doi:10.1016/j.cis.2005.09.005.

[14] R. Baker, Membrane Technology and Applications, 2nd ed., WILEY, California, 2004.

[15] K.S. Barros, T. Scarazzato, D.C.R. Espinosa, Evaluation of the effect of the solution concentration and membrane morphology on the transport properties of Cu(II) through two monopolar cation–exchange membranes, Sep. Purif. Technol. 193 (2018) 184–192. doi:10.1016/j.seppur.2017.10.067.

[16] Y. Mei, C.Y. Tang, Recent developments and future perspectives of reverse electrodialysis technology : A review, Desalination. 425 (2018) 156–174. doi:10.1016/j.desal.2017.10.021.

[17] H. Strathmann, Ion-exchange Membrane Separation Processes. Membrane Science Technology, 9th ed., Elsevier, Amsterdam, The Netherlands, 2004.

[18] F.G. Helfferich, Ion Exchange, McGraw-Hill, New York, NY, 1962.

[19] G.S. Ttivedi, B.G. Shah, S.K. Adhikary, V.K. Indusekhar, R. Rangarajan, Studies on Bipolar Membranes . Part II - Conversion of Sodium Acetate to Acetic Acid and Sodium Hydroxide, React. Funct. Polym. 32 (1997) 209–215.

[20] X. Zhang, C. Li, Y. Wang, J. Luo, T. Xu, Recovery of acetic acid from simulated acetaldehyde wastewaters: Bipolar membrane electrodialysis processes and membrane selection, J. Memb. Sci. 379 (2011) 184–190. doi:10.1016/j.memsci.2011.05.059.

[21] S. Novalic, T. Kongbangkerd, K.D. Kulbe, Separation of gluconate with conventional and bipolar electrodialysis, Desalination. 114 (1997) 45–50. doi:10.1016/S0011-9164(97)00153-7.

[22] S. Novalic, T. Kongbangkerd, K.D. Kulbe, Recovery of organic acids with high molecular weight using a combined electrodialytic process, J. Memb. Sci. 166 (2000) 99–104. doi:10.1016/S0376-7388(99)00247-1.

[23] X. Sun, H. Lu, J. Wang, Recovery of citric acid from fermented liquid by bipolar membrane electrodialysis, J. Clean. Prod. 143 (2017) 250–256. doi:10.1016/j.jclepro.2016.12.118.

[24] J.S. Jaime-Ferrer, E. Couallier, P. Viers, G. Durand, M. Rakib, Three-compartment bipolar membrane electrodialysis for splitting of sodium formate into formic acid and sodium hydroxide: Role of diffusion of molecular acid, J. Memb. Sci. 325 (2008) 528–536. doi:10.1016/j.memsci.2008.07.059.

[25] M. Szczygiełda, K. Prochaska, Alpha-ketoglutaric acid production using electrodialysis with bipolar membrane, J. Memb. Sci. 536 (2017) 37–43. doi:10.1016/j.memsci.2017.04.059.

[26] A. Achoh, V. Zabolotsky, S. Melnikov, Conversion of water-organic solution of sodium naphtenates into naphtenic acids and alkali by electrodialysis with bipolar membranes, Sep. Purif. Technol. 212 (2019) 929–940. doi:10.1016/j.seppur.2018.12.013.

[27] T. Rottiers, V. der B. Bruggen, L. Pinoy, Production of salicylic acid in a three compartment bipolar membrane electrodialysis configuration, J. Ind. Eng. Chem. 54 (2017) 190–199. doi:10.1016/j.jiec.2017.05.033.

[28] X. Liu, Q. Li, C. Jiang, X. Lin, T. Xu, Bipolar membrane electrodialysis in aqua-ethanol medium: Production of salicylic acid, J. Memb. Sci. 482 (2015) 76–82. doi:10.1016/j.memsci.2015.02.030.

[29] C. Jiang, Y. Zhang, H. Feng, Q. Wang, Y. Wang, T. Xu, Simultaneous CO2 capture and amino acid production using bipolar membrane electrodialysis (BMED), J. Memb. Sci. 542 (2017) 264–271. doi:10.1016/j.memsci.2017.08.004.

[30] L. Fu, X. Gao, Y. Yang, F. Aiyong, H. Hao, C. Gao, Preparation of succinic acid using bipolar membrane electrodialysis, Sep. Purif. Technol. 127 (2014) 212–218. doi:10.1016/j.seppur.2014.02.028.

[31] G. Liu, H. Luo, H. Wang, B. Wang, R. Zhang, S. Chen, Malic acid production using a biological electrodialysis with bipolar membrane, J. Memb. Sci. 471 (2014) 179–184. doi:10.1016/j.memsci.2014.08.014.

[32] F. Zhang, C. Huang, T. Xu, Production of sebacic acid using two-phase bipolar

membrane electrodialysis, Ind. Eng. Chem. Res. 48 (2009) 7482–7488. doi:10.1021/ie900485k.

[33] H. Ma, S. Yue, H. Li, Q. Wang, M. Tu, Recovery of lactic acid and other organic acids from food waste ethanol fermentation stillage: Feasibility and effects of substrates, Sep. Purif. Technol. 209 (2019) 223–228. doi:10.1016/j.seppur.2018.07.031.

[34] K. Prochaska, M.J. Woźniak-Budych, Recovery of fumaric acid from fermentation broth using bipolar electrodialysis, J. Memb. Sci. 469 (2014) 428–435. doi:10.1016/j.memsci.2014.07.008.

[35] M. Szczygiełda, J. Antczak, K. Prochaska, Separation and concentration of succinic acid from post-fermentation broth by bipolar membrane electrodialysis (EDBM), Sep. Purif. Technol. 181 (2017) 53–59. doi:10.1016/j.seppur.2017.03.018.

[36] B. Chen, C. Jiang, Y. Wang, R. Fu, Z. Liu, Selectrodialysis with bipolar membrane for the reclamation of concentrated brine from RO plant, Desalination. 442 (2018) 8–15. doi:10.1016/j.desal.2018.04.031.

[37] A. Yamauchi, A.M. EL Sayed, K. Mizuguchi, M. Kodama, Y. Sugito, Ion transport behavior in diffusion layer of new designed ion exchange-mosaic composite polymer membrane, J. Memb. Sci. 283 (2006) 301–309. doi:10.1016/j.memsci.2006.06.044.

[38] A. Campione, L. Gurreri, M. Ciofalo, G. Micale, A. Tamburini, A. Cipollina, Electrodialysis for water desalination: A critical assessment of recent developments on process fundamentals, models and applications, Desalination. 434 (2018) 121–160. doi:10.1016/j.desal.2017.12.044.

[39] V. V. Nikonenko, A. V. Kovalenko, M.K. Urtenov, N.D. Pismenskaya, J. Han, P. Sistat, G. Pourcelly, Desalination at overlimiting currents: State-of-the-art and perspectives, Desalination. 342 (2014) 85–106. doi:10.1016/j.desal.2014.01.008.

[40] K. Kontturi, L. Murtomäki, J.A. Manzanares, Ionic Transport Processes in Electrochemistry and Membrane Science, Oxford University Press, 2008. doi:10.1093/acprof:oso/9780199533817.001.0001.

[41] M.C. Martí-Calatayud, D.C. Buzzi, M. García-Gabaldón, E. Ortega, A.M. Bernardes, J.A.S. Tenório, V. Pérez-Herranz, Sulfuric acid recovery from acid mine drainage by means of electrodialysis, Desalination. 343 (2014) 120–127. doi:10.1016/j.desal.2013.11.031.

[42] H. Strathmann, Electrodialysis, a mature technology with a multitude of new applications, Desalination. 264 (2010) 268–288. doi:10.1016/j.desal.2010.04.069.

[43] W. Garcia-Vasquez, L. Dammak, C. Larchet, V. Nikonenko, D. Grande, Effects of acid-base cleaning procedure on structure and properties of anion-exchange membranes used in electrodialysis, J. Memb. Sci. 507 (2016) 12–23. doi:10.1016/j.memsci.2016.02.006.

[44] E. Vera, J. Ruales, M. Dornier, J. Sandeaux, R. Sandeaux, G. Pourcelly, Deacidification of clarified passion fruit juice using different configurations of electrodialysis, J. Chem. Technol. Biotechnol. 78 (2003) 918–925. doi:10.1002/jctb.827.

[45] D. Labbé, M. Araya-Farias, A. Tremblay, L. Bazinet, Electromigration feasibility of green tea catechins, J. Memb. Sci. 254 (2005) 101–109. doi:10.1016/j.memsci.2004.10.048.

[46] L. Bazinet, D. Ippersiel, B. Mahdavi, Fractionation of whey proteins by bipolar membrane electroacidification, Innov. Food Sci. Emerg. Technol. 5. 5 (2004) 17–25. doi:10.1016/j.ifset.2003.10.001.

[47] J. Kaláb, Z. Palatý, Electrodialysis of oxalic acid: batch process modeling Jiří, Chem. Pap. 66 (2012) 1118–1123. doi:10.2478/s11696-012-0232-5.

[48] J.S.J. Ferrer, S. Laborie, G. Durand, M. Rakib, Formic acid regeneration by electromembrane processes, J. Memb. Sci. 280 (2006) 509–516. doi:10.1016/j.memsci.2006.02.012.

[49] F. Gonçalves, C. Fernandes, P.C. dos. Santos, M.N. de. Pinho, Wine tartaric stabilization by electrodialysis and its assessment by the saturation temperature, J. Food Eng. 59 (2003) 229–235. doi:10.1016/S0260-8774(02)00462-4.

[50] L. Marder, S.D. Bittencourt, J. Zoppas Ferreira, A.M. Bernardes, Treatment of molybdate solutions by electrodialysis: The effect of pH and current density on

ions transport behavior, Sep. Purif. Technol. 167 (2016) 32–36. doi:10.1016/j.seppur.2016.04.047.

[51] M. Peraki, E. Ghazanfari, G.F. Pinder, T.L. Harrington, Electrodialysis: An application for the environmental protection in shale-gas extraction, Sep. Purif. Technol. 161 (2016) 96–103. doi:10.1016/j.seppur.2016.01.040.

[52] E. Velizarova, A.B. Ribeiro, L.M. Ottosen, A comparative study on Cu, Cr and As removal from CCA-treated wood waste by dialytic and electrodialytic processes, J. Hazard. Mater. 94 (2002) 147–160. doi:10.1016/S0304-3894(02)00063-8.

[53] L. Koene, L.J.J. Janssen, Removal of nickel from industrial process liquids, Electrochim. Acta. 47 (2001) 695–703. doi:10.1016/S0013-4686(01)00750-2.

[54] A. Smara, R. Delimi, E. Chainet, J. Sandeaux, Removal of heavy metals from diluted mixtures by a hybrid ion-exchange/electrodialysis process, Sep. Purif. Technol. 57 (2007) 103–110. doi:10.1016/j.seppur.2007.03.012.

[55] F.D.R. Amado, L.F. Rodrigues, M.A.S. Rodrigues, A.M. Bernardes, J.Z. Ferreira, C.A. Ferreira, Development of polyurethane/polyaniline membranes for zinc recovery through electrodialysis, Desalination. 186 (2005) 199–206. doi:10.1016/j.desal.2005.05.019.

[56] J. Carrillo-Abad, M. García-Gabaldón, V. Pérez-Herranz, Electrochemical recovery of zinc from the spent pickling solutions coming from hot dip galvanizing industries. Galvanostatic operation, Int. J. Electrochem. Sci. 7 (2012) 5442–5456. doi:10.1016/j.seppur.2011.07.029.

[57] L. Cifuentes, I. García, P. Arriagada, J.M. Casas, The use of electrodialysis for metal separation and water recovery from CuSO4-H2SO4-Fe solutions, Sep. Purif. Technol. 68 (2009) 105–108. doi:10.1016/j.seppur.2009.04.017.

[58] L. Cifuentes, G. Crisóstomo, J.P. Ibáñez, J.M. Casas, F. Alvarez, G. Cifuentes, On the electrodialysis of aqueous H2SO4-CuSO4 electrolytes with metallic impurities, J. Memb. Sci. 207 (2002) 1–16. doi:10.1016/S0376-7388(01)00733-5.

[59] J.H. Chang, A. V. Ellis, C.H. Tung, W.C. Huang, Copper cation transport and scaling of ionic exchange membranes using electrodialysis under

electroconvection conditions, J. Memb. Sci. 361 (2010) 56–62. doi:10.1016/j.memsci.2010.06.012.

[60] T. Scarazzato, Z. Panossian, J.A.S. Tenório, V. Pérez-Herranz, D.C.R. Espinosa, A review of cleaner production in electroplating industries using electrodialysis, J. Clean. Prod. 168 (2017) 1590–1602. doi:10.1016/j.jclepro.2017.03.152.

[61] K.S. Barros, T. Scarazzato, V. Pérez-Herranz, D.C.R. Espinosa, Treatment of Cyanide-Free Wastewater from Brass Electrodeposition with EDTA by Electrodialysis: Evaluation of Underlimiting and Overlimiting Operations, Membranes (Basel). 10 (2020) 69. doi:10.3390/membranes10040069.

[62] K.S. Barros, E.M. Ortega, V. Pérez-Herranz, D.C.R. Espinosa, Evaluation of brass electrodeposition at RDE from cyanide-free bath using EDTA as a complexing agent, J. Electroanal. Chem. 865 (2020) 114129. doi:10.1016/j.jelechem.2020.114129.

[63] G.M. Wu, S.J. Lin, C.C. Yang, Preparation and characterization of high ionic conducting alkaline non-woven membranes by sulfonation, J. Memb. Sci. 284 (2006) 120–127. doi:10.1016/j.memsci.2006.07.025.

[64] N.P. Berezina, N.A. Kononenko, O.A. Dyomina, N.P. Gnusin, Characterization of ion-exchange membrane materials: Properties vs structure, Adv. Colloid Interface Sci. 139 (2008) 3–28. doi:10.1016/j.cis.2008.01.002.

[65] L. Marder, E.M. Ortega Navarro, V. Perez-Herranz, A.M. Bernardes, J.Z. Ferreira, Evaluation of transition metals transport properties through a cation exchange membrane by chronopotentiometry, J. Memb. Sci. 284 (2006) 267–275. doi:10.1016/j.memsci.2006.07.039.

[66] N. Cifuentes-Araya, C. Astudillo-Castro, L. Bazinet, Mechanisms of mineral membrane fouling growth modulated by pulsed modes of current during electrodialysis: Evidences of water splitting implications in the appearance of the amorphous phases of magnesium hydroxide and calcium carbonate, J. Colloid Interface Sci. 426 (2014) 221–234. doi:10.1016/j.jcis.2014.03.054.

[67] K.S. Barros, M.C. Martí-Calatayud, V. Pérez-Herranz, D.C.R. Espinosa, A three-stage chemical cleaning of ion-exchange membranes used in the treatment by electrodialysis of wastewaters generated in brass electroplating industries,

Desalination. 492 (2020) 114628. doi:10.1016/j.desal.2020.114628.

[68] F. Aouad, A. Lindheimer, C. Gavach, Transport properties of electrodialysis membranes in the presence of Zn2+ complexes with Cl-, J. Memb. Sci. 123 (1997) 207–223. doi:10.1016/S0376-7388(96)00212-8.

[69] M. García-Gabaldón, V. Pérez-Herranz, E. Ortega, Evaluation of two ion-exchange membranes for the transport of tin in the presence of hydrochloric acid, J. Memb. Sci. 371 (2011) 65–74. doi:10.1016/j.memsci.2011.01.015.

[70] I. Herraiz-Cardona, E. Ortega, V. Pérez-Herranz, Evaluation of the Zn2+ transport properties through a cation-exchange membrane by chronopotentiometry, J. Colloid Interface Sci. 341 (2010) 380–385. doi:10.1016/j.jcis.2009.09.053.

[71] L. Marder, E.M. Ortega Navarro, V. Pérez-Herranz, A.M. Bernardes, J.Z. Ferreira, Chronopotentiometric study on the effect of boric acid in the nickel transport properties through a cation-exchange membrane, Desalination. 249 (2009) 348–352. doi:10.1016/j.desal.2009.06.040.

[72] M.C. Martí-Calatayud, M. García-Gabaldón, V. Pérez-Herranz, E. Ortega, Determination of transport properties of Ni(II) through a Nafion cation-exchange membrane in chromic acid solutions, J. Memb. Sci. 379 (2011) 449–458. doi:10.1016/j.memsci.2011.06.014.

[73] N. Pismenskaia, P. Sistat, P. Huguet, V. Nikonenko, G. Pourcelly, Chronopotentiometry applied to the study of ion transfer through anion exchange membranes, J. Memb. Sci. 228 (2004) 65–76. doi:10.1016/j.memsci.2003.09.012.

[74] C. Larchet, S. Nouri, V. Nikonenko, Application of chronopotentiometry to study the diffusion layer thickness adjacent to an ion-exchange membrane under natural convection, Desalination. 200 (2006) 146–148. doi:10.1016/j.desal.2006.03.276.

[75] C. Larchet, S. Nouri, B. Auclair, L. Dammak, V. Nikonenko, Application of chronopotentiometry to determine the thickness of diffusion layer adjacent to an ion-exchange membrane under natural convection, Adv. Colloid Interface Sci. 139 (2008) 45–61. doi:10.1016/j.cis.2008.01.007.

[76] S.A. Mareev, D.Y. Butylskii, N.D. Pismenskaya, V. V. Nikonenko, Chronopotentiometry of ion-exchange membranes in the overlimiting current range. Transition time for a finite-length diffusion layer: Modeling and experiment, J. Memb. Sci. 500 (2016) 171–179. doi:10.1016/j.memsci.2015.11.026.

[77] M.S. Kang, Y.J. Choi, H.J. Lee, S.H. Moon, Effects of inorganic substances on water splitting in ion-exchange membranes: I. Electrochemical characteristics of ion-exchange membranes coated with iron hydroxide/oxide and silica sol, J. Colloid Interface Sci. 273 (2004) 523–532. doi:10.1016/j.jcis.2004.01.050.

[78] T. Scarazzato, K.S. Barros, T. Benvenuti, M.A. Siqueira Rodrigues, D.C. Romano Espinosa, A. Moura Bernardes, V. Pérez-Herranz, Achievements in electrodialysis processes for wastewater and water treatment, Elsevier Inc., 2020. doi:10.1016/B978-0-12-817378-7.00005-7.

[79] K.S. Barros, M.C. Martí-Calatayud, E.M. Ortega, V. Pérez-Herranz, D.C.R. Espinosa, Chronopotentiometric study on the simultaneous transport of EDTA ionic species and hydroxyl ions through an anion-exchange membrane for electrodialysis applications, J. Electroanal. Chem. 879 (2020) 114782. doi:10.1016/j.jelechem.2020.114782.

[80] J.J. Krol, M. Wessling, H. Strathmann, Chronopotentiometry and overlimiting ion transport through monopolar ion exchange membranes, J. Memb. Sci. 162 (1999) 155–164. doi:10.1016/S0376-7388(99)00134-9.

[81] J. Balster, M.H. Yildirim, D.F. Stamatialis, R. Ibanez, R.G.H. Lammertink, V. Jordan, M. Wessling, Morphology and microtopology of cation-exchange polymers and the origin of the overlimiting current, J. Phys. Chem. B. 111 (2007) 2152–2165. doi:10.1021/jp068474t.

[82] P. Długołecki, B. Anet, S.J. Metz, K. Nijmeijer, M. Wessling, Transport limitations in ion exchange membranes at low salt concentrations, J. Memb. Sci. 346 (2010) 163–171. doi:10.1016/j.memsci.2009.09.033.

[83] V.V. Gil, M.A. Andreeva, L. Jansezian, J. Han, N.D. Pismenskaya, V.V. Nikonenko, C. Larchet, L. Dammak, Impact of heterogeneous cation-exchange membrane surface modification on chronopotentiometric and current–voltage

characteristics in NaCl, CaCl2 and MgCl2 solutions, Electrochim. Acta. 281 (2018) 472–485. doi:10.1016/j.electacta.2018.05.195.

[84] P. Sistat, G. Pourcelly, Chronopotentiometric response of an ion-exchange membrane in the underlimiting current-range. Transport phenomena within the diffusion layers, J. Memb. Sci. 123 (1997) 121–131.

[85] F.G. Wilhelm, N.F.A. Van der Vegt, M. Wessling, H. Strathmann, Chronopotentiometry for the advanced current-voltage characterisation of bipolar membranes, J. Electroanal. Chem. 502 (2001) 152–166. doi:10.1016/S0022-0728(01)00348-5.

[86] D. Kim, H.-S. Park, S. Seo, J. Park, S. Moon, Y. Choi, Y.S. Jiong, D.H. Kim, M. Kang, Facile surface modification of anion-exchange membranes for improvement of diffusion dialysis performance, J. Colloid Interface Sci. 416 (2014) 19–24. doi:10.1016/j.jcis.2013.10.013.

[87] K.A. Nebavskaya, V. V. Sarapulova, K.G. Sabbatovskiy, V.D. Sobolev, N.D. Pismenskaya, P. Sistat, M. Cretin, V. V. Nikonenko, Impact of ion exchange membrane surface charge and hydrophobicity on electroconvection at underlimiting and overlimiting currents, J. Memb. Sci. 523 (2017) 36–44. doi:10.1016/j.memsci.2016.09.038.

[88] H.J.S. Sand, On the Concentration at the Electrodes in a Solution , with special reference to the Liberation of Hydrogen by Electrolysis of a Mixture of Copper Sulphate and Sulphuric Acid, J. London, Edinburgh, Dublin Philos. Mag. J. Sci. 17 (1899). doi:10.1016/0302-4598(75)85003-3.

[89] D. Lerche, H. Wolf, Quantitative Characterisation of current-induced diffusion layers at cation-exchange membranes. I. investigations of temporal and local behaviour of concentration profile at constant current density, Bioelectrochemistry Bioenerg. 2 (1975) 293–302. doi:10.1016/0302-4598(75)85003-3.

[90] R. Audinos, G. Pichelin, Characterization of electrodialysis membranes by chronopotentiometry, Desalination. 68 (1988) 251–263. doi:10.1016/0011-9164(88)80059-6.

[91] D.R. Lide, Handbook of Chemistry and Physics, CRC Press, New York, 1997.

[92] S.A. Mareev, D.Y. Butyl'skii, A. V. Kovalenko, N.D. Pis'menskaya, L. Dammak, C. Larchet, V. V. Nikonenko, Inclusion of the concentration dependence of the diffusion coefficient in the sand equation, Russ. J. Electrochem. 52 (2016) 996–1000. doi:10.1134/S1023193516100098.

[93] G. Pourcelly, Conductivity and selectivity of ion exchange membranes: Structure-correlations, Desalination. 147 (2002) 359–361. doi:10.1016/S0011-9164(02)00609-4.

[94] M. Boucher, N. Turcotte, V. Guillemette, G. Lantagne, A. Chapotot, G. Pourcelly, R. Sandeaux, C. Gavach, Recovery of spent acid by electrodialysis in the zinc hydrometallurgy industry: Performance study of different cation-exchange membranes, Hydrometallurgy. 45 (1997) 137–160. doi:10.1016/S0304-386X(96)00069-2.

[95] G. Suresh, Y.M. Scindia, A.K. Pandey, A. Goswami, Self-diffusion coefficient of water in Nafion-117 membrane with different monovalent counterions: A radiotracer study, J. Memb. Sci. 250 (2005) 39–45. doi:10.1016/j.memsci.2004.10.013.

[96] I. Tugas, G. Pourcelly, C. Gavach, Electrotransport of protons and chloride ions in anion exchange membranes for the recovery of acids. Part I. Equilibrium properties, J. Memb. Sci. 85 (1993) 183–194. doi:10.1016/0376-7388(93)85167-U.

[97] I. Tugas, J.M. Lambert, J. Maillols, J.L. Bribes, G. Pourcelly, C. Gavach, Identification of the ionic species in anion exchange membranes equilibrated with sulphuric acid solutions by means of Raman spectroscopy and radiotracers, J. Memb. Sci. 78 (1993) 25–33. doi:10.1016/0376-7388(93)85244-Q.

[98] A. Chapotot, G. Pourcelly, C. Gavach, Transport competition between monovalent and divalent cations through cation-exchange membranes. Exchange isotherms and kinetic concepts, J. Memb. Sci. 96 (1994) 167–181. doi:10.1016/0376-7388(94)00107-3.

[99] E.W. Schneider, M.W. Verbrugge, Radiotracer method for simultaneous measurement of cation, anion and water transport through ion-exchange membranes, Appl. Radiat. Isot. 44 (1993) 1399–1408. doi:10.1016/0969-

8043(93)90091-N.

[100] C. Larchet, B. Auclair, V. Nikonenko, Approximate evaluation of water transport number in ion-exchange membranes, Electrochim. Acta. 49 (2004) 1711–1717. doi:10.1016/j.electacta.2003.11.030.

[101] B. Auclair, V. Nikonenko, C. Larchet, M. Métayer, L. Dammak, Correlation between transport parameters of ion-exchange membranes, J. Memb. Sci. 195 (2001) 89–102. doi:10.1016/S0376-7388(01)00556-7.

[102] V.I. Zabolotsky, L. Novak, A. V. Kovalenko, V. V. Nikonenko, M.H. Urtenov, K.A. Lebedev, A.Y. But, Electroconvection in systems with heterogeneous ion-exchange membranes, Pet. Chem. 57 (2017) 779–789. doi:10.1134/S0965544117090109.

[103] E. Stránská, Relationships between transport and physical–mechanical properties of ion exchange membranes, Desalin. Water Treat. 56 (2015) 3220–3227. doi:10.1080/19443994.2014.981413.

[104] J.-H. Choi, S.-H. Kim, S.-H. Moon, Heterogeneity of Ion-Exchange Membranes: The Effects of Membrane Heterogeneity on Transport Properties., J. Colloid Interface Sci. 241 (2001) 120–126. doi:10.1006/jcis.2001.7710.

[105] J.-H. Choi, S.-H. Moon, Pore size characterization of cation-exchange membranes by chronopotentiometry using homologous amine ions, J. Memb. Sci. 191 (2001) 225–236. doi:10.1016/S0376-7388(01)00513-0.

[106] M.S. Kang, Y.J. Choi, I.J. Choi, T.H. Yoon, S.H. Moon, Electrochemical characterization of sulfonated poly(arylene ether sulfone) (S-PES) cation-exchange membranes, J. Memb. Sci. 216 (2003) 39–53. doi:10.1016/S0376-7388(03)00045-0.

[107] J.H. Choi, S.H. Moon, Structural change of ion-exchange membrane surfaces under high electric fields and its effects on membrane properties, J. Colloid Interface Sci. 265 (2003) 93–100. doi:10.1016/S0021-9797(03)00136-X.

[108] H.S. Park, D.H. Kim, J.S. Park, S.H. Moon, Y. Lee, K.H. Yeon, M.S. Kang, Surface modification and use of polymer complex agents to mitigate metal crossover of anion-exchange membranes, J. Colloid Interface Sci. 430 (2014) 24–

30. doi:10.1016/j.jcis.2014.05.024.

[109] Y.J. Choi, J.H. Song, M.S. Kang, B.K. Seo, Preparation and electrochemical characterizations of anion-permselective membranes with structurally stable ion-exchange sites, Electrochim. Acta. 180 (2015) 71–77. doi:10.1016/j.electacta.2015.08.105.

[110] Y.J. Choi, J.M. Park, K.H. Yeon, S.H. Moon, Electrochemical characterization of poly(vinyl alcohol)/formyl methyl pyridinium (PVA-FP) anion-exchange membranes, J. Memb. Sci. 250 (2005) 295–304. doi:10.1016/j.memsci.2004.10.034.

[111] D.H. Kim, J.H. Park, S.J. Seo, J.S. Park, S. Jung, Y.S. Kang, J.H. Choi, M.S. Kang, Development of thin anion-exchange pore-filled membranes for high diffusion dialysis performance, J. Memb. Sci. 447 (2013) 80–86. doi:10.1016/j.memsci.2013.07.017.

[112] Y.J. Choi, M.S. Kang, J. Cho, S.H. Moon, Preparation and characterization of LDPE/polyvinylbenzyl trimethyl ammonium salts anion-exchange membrane, J. Memb. Sci. 221 (2003) 219–231. doi:10.1016/S0376-7388(03)00265-5.

[113] Y.S. Kang, S.-H. Moon, J.-S. Park, S.-J. Seo, M.-J. Lee, Y.-W. Choi, M.-S. Kang, D.-H. Kim, Pore-filled anion-exchange membranes for non-aqueous redox flow batteries with dual-metal-complex redox shuttles, J. Memb. Sci. 454 (2013) 44–50. doi:10.1016/j.memsci.2013.11.051.

[114] M. Wang, X. liang Wang, Y. xiang Jia, X. Liu, An attempt for improving electrodialytic transport properties of a heterogeneous anion exchange membrane, Desalination. 351 (2014) 163–170. doi:10.1016/j.desal.2014.07.039.

[115] R.K. Nagarale, V.K. Shahi, R. Rangarajan, Preparation of polyvinyl alcohol-silica hybrid heterogeneous anion-exchange membranes by sol-gel method and their characterization, J. Memb. Sci. 248 (2005) 37–44. doi:10.1016/j.memsci.2004.09.025.

[116] S.A. Mareev, V.S. Nichka, D.Y. Butylskii, M.K. Urtenov, N.D. Pismenskaya, P.Y. Apel, V.V. Nikonenko, Chronopotentiometric Response of an Electrically Heterogeneous Permselective Surface: 3D Modeling of Transition Time and Experiment, J. Phys. Chem. C. 120 (2016) 13113–13119.

doi:10.1021/acs.jpcc.6b03629.

[117] L. Vobeckà, M. Svoboda, J. Beneš, T. Belloň, Z. Slouka, Heterogeneity of heterogeneous ion-exchange membranes investigated by chronopotentiometry and X-ray computed microtomography, J. Memb. Sci. 559 (2018) 127–137. doi:10.1016/j.memsci.2018.04.049.

[118] V. V. Gil, M.A. Andreeva, N.D. Pismenskaya, V. V. Nikonenko, C. Larchet, L. Dammak, Effect of counterion hydration numbers on the development of Electroconvection at the surface of heterogeneous cation-exchange membrane modified with an MF-4SK film, Pet. Chem. 56 (2016) 440–449. doi:10.1134/S0965544116050066.

[119] P. Długołęcki, B. Anet, S.J. Metz, K. Nijmeijer, M. Wessling, Transport limitations in ion exchange membranes at low salt concentrations, J. Memb. Sci. 346 (2010) 163–171. doi:10.1016/j.memsci.2009.09.033.

[120] A. Jasti, S. Prakash, V.K. Shahi, Stable and hydroxide ion conductive membranes for fuel cell applications: Chloromethyaltion and amination of poly(ether ether ketone), J. Memb. Sci. 428 (2013) 470–479. doi:10.1016/j.memsci.2012.11.016.

[121] P. V. Vyas, B.G. Shah, G.S. Trivedi, P. Ray, S.K. Adhikary, R. Rangarajan, Studies on heterogeneous cation-exchange membranes, React. Funct. Polym. 44 (2000) 101–110. doi:10.1016/S1381-5148(99)00084-X.

[122] A. Yamauchi, A.M. El Sayed, New approach to a collodion membrane composite via fluorocarbon polymer (Nafion) blending in terms of a diffusion coefficient of redox substances and transport properties, Desalination. 192 (2006) 364–373. doi:10.1016/j.desal.2005.06.053.

[123] F.Q. Mir, A. Shukla, Sharp decline in counter-ion transport number of electrodialysis ion exchange membrane on moderate increase in temperature, Desalination. 372 (2015) 1–6. doi:10.1016/j.desal.2015.06.009.

[124] P. V Vyas, P. Ray, S.K. Adhikary, B.G. Shah, R. Rangarajan, Studies of the effect of variation of blend ratio on permselectivity and heterogeneity of ion-exchange membranes, J. OfColloid Interface Sci. 257 (2003) 127–134.

[125] R.K. Nagarale, V.K. Shahi, S.K. Thampy, R. Rangarajan, Studies on

electrochemical characterization of polycarbonate and polysulfone based heterogeneous cation-exchange membranes, React. Funct. Polym. 61 (2004) 131–138. doi:10.1016/j.reactfunctpolym.2004.04.007.

[126] Y. Choi, M. Kang, S. Moon, A new preparation method for cation-exchange membrane using monomer sorption into reinforcing materials, Desalination. 146 (2002) 287–291.

[127] G. Ramachandraiah, V.K. Shahi, R. Rangarajan, R. Prakash, D. Vasudevan, Solution–Membrane Equilibrium at Metal-Deposited Cation-Exchange Membranes: Chronopotentiometric Characterization of Metal-Modified Membranes, J. Colloid Interface Sci. 216 (2002) 179–184. doi:10.1006/jcis.1999.6292.

[128] M.-S. Kang, Y.-J. Choi, S.-H. Moon, Characterization of anion-exchange membranes containing pyridinium groups, AIChE J. 49 (2003) 3213–3220. doi:10.1002/aic.690491220.

[129] V.K. Shahi, S.K. Thampy, R. Rangarajan, Chronopotentiometric studies on dialytic properties of glycine across ion-exchange membranes, J. Memb. Sci. 203 (2002) 43–51. doi:10.1016/S0376-7388(01)00745-1.

[130] P. Ray, V.K. Shahi, T. V. Pathak, G. Ramachandraiah, Transport phenomenon as a function of counter and co-ions in solution: Chronopotentiometric behavior of anion exchange membrane in different aqueous electrolyte solutions, J. Memb. Sci. 160 (1999) 243–254. doi:10.1016/S0376-7388(99)00088-5.

[131] J.-H. Choi, S.-J. Oh, S.-H. Moon, Structural effects of ion-exchange membrane on the separation ofL-phenylalanine (L-Phe) from fermentation broth using electrodialysis, J. Chem. Technol. Biotechnol. 77 (2002) 785–792. doi:10.1002/jctb.638.

[132] A. Alabi, L. Cseri, A. Al Hajaj, G. Szekely, P. Budd, L. Zou, Electrostatically-coupled graphene oxide nanocomposite cation exchange membrane, J. Memb. Sci. 594 (2020) 117457. doi:10.1016/j.memsci.2019.117457.

[133] L. Cseri, J. Baugh, A. Alabi, A. AlHajaj, L. Zou, R.A.W. Dryfe, P.M. Budd, G. Szekely, Graphene oxide-polybenzimidazolium nanocomposite anion exchange membranes for electrodialysis, J. Mater. Chem. A. 6 (2018) 24728–24739.

doi:10.1039/C8TA09160A.

[134] Y. Freijanes, V.M. Barragán, S. Muñoz, Chronopotentiometric study of a Nafion membrane in presence of glucose, J. Memb. Sci. 510 (2016) 79–90. doi:10.1016/j.memsci.2016.02.054.

[135] M.-S. Kang, Y.-J. Choi, S.-H. Moon, Effects of charge density on water splitting at cation-exchange membrane surface in the over-limiting current region, Korean J. Chem. Eng. 21 (2004) 221–229. doi:10.1007/BF02705402.

[136] J.S. Park, J.H. Choi, K.H. Yeon, S.H. Moon, An approach to fouling characterization of an ion-exchange membrane using current-voltage relation and electrical impedance spectroscopy, J. Colloid Interface Sci. 294 (2006) 129–138. doi:10.1016/j.jcis.2005.07.016.

[137] X.T. Le, P. Viel, D.P. Tran, F. Grisotto, S. Palacin, Surface Homogeneity of Anion Exchange Membranes : A Chronopotentiometric Study in the Overlimiting Current Range, J. Phys. Chem. Biophys. 113 (2009) 5829–5836.

[138] C. Klaysom, S. Moon, B.P. Ladewig, G.Q.M. Lu, L. Wang, The Influence of Inorganic Filler Particle Size on Composite Ion-Exchange Membranes for Desalination, J. Phys. Chem. C. 115 (2011) 15124–15132. doi:dx.doi.org/10.1021/jp112157z.

[139] H. Lee, M. Hong, Influence of the heterogeneous structure on the electrochemical properties of anion exchange membranes, J. Memb. Sci. 320 (2008) 549–555. doi:10.1016/j.memsci.2008.04.052.

[140] M.C. Martí-Calatayud, M. García-Gabaldón, V. Pérez-Herranz, Mass Transfer Phenomena during Electrodialysis of Multivalent Ions: Chemical Equilibria and Overlimiting Currents, Appl. Sci. 8 (2018) 1566. doi:10.3390/app8091566.

[141] M.C. Martí-Calatayud, M. García-Gabaldón, V. Pérez-Herranz, Effect of the equilibria of multivalent metal sulfates on the transport through cation-exchange membranes at different current regimes, J. Memb. Sci. 443 (2013) 181–192. doi:10.1016/j.memsci.2013.04.058.

[142] M.A. Andreeva, V.V. Gil, N.D. Pismenskaya, L. Dammak, N.A. Kononenko, C. Larchet, D. Grande, V.V. Nikonenko, Mitigation of membrane scaling in

electrodialysis by electroconvection enhancement, pH adjustment and pulsed electric field application, J. Memb. Sci. 549 (2018) 129–140. doi:10.1016/j.memsci.2017.12.005.

[143] F.G. Wilhelm, N.F.A. Van Der Vegt, H. Strathmann, M. Wessling, Comparison of bipolar membranes by means of chronopotentiometry, J. Memb. Sci. 199 (2002) 177–190. doi:10.1016/S0376-7388(01)00696-2.

[144] M. Taky, G. Pourcelly, C. Gavach, A. Elmidaoui, Chronopotentiometric response of a cation exchange membrane in contact with chromiumIII solutions, Desalination. 105 (1996) 219–228. doi:10.1016/0011-9164(96)00079-3.

[145] S. Mikhaylin, V. Nikonenko, N. Pismenskaya, G. Pourcelly, S. Choi, H.J. Kwon, J. Han, L. Bazinet, How physico-chemical and surface properties of cation-exchange membrane affect membrane scaling and electroconvective vortices: Influence on performance of electrodialysis with pulsed electric field, Desalination. 393 (2015) 102–114. doi:10.1016/j.desal.2015.09.011.

[146] M.-S. Kang, S.-H. Cho, S.-H. Kim, Y.-J. Choi, S.-H. Moon, Electrodialytic separation characteristics of large molecular organic acid in highly water-swollen cation-exchange membranes, J. Memb. Sci. 222 (2003) 149–161. doi:10.1016/S0376-7388(03)00267-9.

[147] H.J. Lee, M.K. Hong, S.D. Han, J. Shim, S.H. Moon, Analysis of fouling potential in the electrodialysis process in the presence of an anionic surfactant foulant, J. Memb. Sci. 325 (2008) 719–726. doi:10.1016/j.memsci.2008.08.045.

[148] N. Pismenskaya, K. Igritskaya, E. Belova, V. Nikonenko, G. Pourcelly, Transport properties of ion-exchange membrane systems in LysHCl solutions, Desalination. 200 (2006) 149–151. doi:10.1016/j.desal.2006.03.277.

[149] A.K. Singh, S. Kumar, M. Bhushan, V.K. Shahi, High performance cross-linked dehydro-halogenated poly (vinylidene fluoride-co-hexafluoro propylene) based anion-exchange membrane for water desalination by electrodialysis, Sep. Purif. Technol. 234 (2020) 116078. doi:10.1016/j.seppur.2019.116078.

[150] K.J. Vetter, Electrochemical kinetics: theoretical and experimental aspects., Acad. Press. New York. (1967).

[151] N. Pismenskaya, K. Igritskaya, E. Belova, V. Nikonenko, G. Pourcelly, Transport properties of ion-exchange membrane systems in LysHCl solutions, Desalination. 200 (2006) 149–151. doi:10.1016/j.desal.2006.03.277.

[152] E.I. Belova, G.Y. Lopatkova, N.D. Pismenskaya, V. V. Nikonenko, C. Larchet, G. Pourcelly, Effect of anion-exchange membrane surface properties on mechanisms of overlimiting mass transfer, J. Phys. Chem. B. 110 (2006) 13458–13469. doi:10.1021/jp062433f.

[153] N.D. Pismenskaya, O.A. Rybalkina, A.E. Kozmai, K.A. Tsygurina, E.D. Melnikova, V. V. Nikonenko, Generation of H+ and OH− ions in anion-exchange membrane/ampholyte-containing solution systems: A study using electrochemical impedance spectroscopy, J. Memb. Sci. 601 (2020) 117920. doi:10.1016/j.memsci.2020.117920.

[154] O.A. Rybalkina, K.A. Tsygurina, E.D. Melnikova, G. Pourcelly, V. V. Nikonenko, N.D. Pismenskaya, Catalytic effect of ammonia-containing species on water splitting during electrodialysis with ion-exchange membranes, Electrochim. Acta. 299 (2019) 946–962. doi:10.1016/j.electacta.2019.01.068.

[155] S.P. Nunes, K.-V. Peinemann, Membrane Technology in the Chemical Industry, Second, WILEY-VCH Verlag GmbH & Co. KGaA, Weinheim, Germany, 2006. doi:10.1002/3527608796.

[156] B.A. Cooke, Concentration polarization in electrodialysis-I. The electrometric measurement of interfacial concentration, Electrochim. Acta. 3 (1961) 307–317. doi:10.1016/0013-4686(61)85007-X.

[157] B.A. Cooke, S.J. Van der Walt, Concentration polarization in electrodialysis-III. Practical electrodialysis systems, Electrochim. Acta. 5 (1961) 216–228. doi:10.1016/0013-4686(61)85016-0.

[158] C. Forgacs, Theoretical and practical aspects of scale control in electrodialysics desalination apparatus, Dechema Monograph, 1962.

[159] P. Długołecki, P. Ogonowski, S.J. Metz, M. Saakes, K. Nijmeijer, M. Wessling, On the resistances of membrane, diffusion boundary layer and double layer in ion exchange membrane transport, J. Memb. Sci. 349 (2010) 369–379. doi:10.1016/j.memsci.2009.11.069.

[160] V. V. Nikonenko, N.D. Pismenskaya, E.I. Belova, P. Sistat, P. Huguet, G. Pourcelly, C. Larchet, Intensive current transfer in membrane systems: Modelling, mechanisms and application in electrodialysis, Adv. Colloid Interface Sci. 160 (2010) 101–123. doi:10.1016/j.cis.2010.08.001.

[161] S. Sang, Q. Wu, K. Huang, A discussion on ion conductivity at cation exchange membrane/solution interface, Colloids Surfaces A Physicochem. Eng. Asp. 320 (2008) 43–48. doi:10.1016/j.colsurfa.2008.01.010.

[162] V.G. Levich, Physicochemical Hydrodynamics, Englewood Cliffs, New Jersey, 1962.

[163] A.M. Peers, Membrane Phenomena, Discuss. Faraday Soc. 21 (1956) 124.

[164] V. Levich, Physicochemical Hydrodynamics, Prentice Hall, NJ, 1962.

[165] A. Yaroshchuk, L. Karpenko, V. Ribitsch, Measurements of transient membrane potential after current switch-off as a tool to study the electrochemical properties of supported thin nanoporous layers, J. Phys. Chem. B. 109 (2005) 7834–7842. doi:10.1021/jp040599f.

[166] P. Sistat, G. Pourcelly, Chronopotentiometric response of an ion-exchange membrane in the underlimiting current-range. Transport phenomena within the diffusion layers, J. Memb. Sci. 123 (1997) 121–131. doi:10.1016/S0376-7388(96)00210-4.

[167] A.M. Ashrafi, N. Gupta, D. Neděla, An investigation through the validation of the electrochemical methods used for bipolar membranes characterization, J. Memb. Sci. 544 (2017) 195–207. doi:10.1016/j.memsci.2017.09.026.

[168] E. Volodina, N. Pismenskaya, V. Nikonenko, C. Larchet, G. Pourcelly, Ion transfer across ion-exchange membranes with homogeneous and heterogeneous surfaces, J. Colloid Interface Sci. 285 (2005) 247–258. doi:10.1016/j.jcis.2004.11.017.

[169] T. Scarazzato, Z. Panossian, M. García-Gabaldón, E.M. Ortega, J.A.S. Tenório, V. Pérez-Herranz, D.C.R. Espinosa, Evaluation of the transport properties of copper ions through a heterogeneous ion-exchange membrane in etidronic acid solutions by chronopotentiometry, J. Memb. Sci. 535 (2017) 268–278.

doi:10.1016/j.memsci.2017.04.048.

[170] V.D. Titorova, S.A. Mareev, A.D. Gorobchenko, V.V. Gil, V.V. Nikonenko, K.G. Sabbatovskii, N.D. Pismenskaya, Effect of current-induced coion transfer on the shape of chronopotentiograms of cation-exchange membranes, J. Memb. Sci. (2021) 119036. doi:10.1016/j.memsci.2020.119036.

[171] T. Benvenuti, M. García-Gabaldón, E.M. Ortega, M.A.S. Rodrigues, A.M. Bernardes, V. Pérez-Herranz, J. Zoppas-Ferreira, Influence of the co-ions on the transport of sulfate through anion exchange membranes, J. Memb. Sci. 542 (2017) 320–328. doi:10.1016/j.memsci.2017.08.021.

[172] D.A. Cowan, J.H. Brown, Effect of Turbulence on Limiting Current in Electrodialysis Cells, Ind. Eng. Chem. 51 (1959) 1445–1448. doi:10.1021/ie50600a026.

[173] D.A. Cowan, J.H. Brown, Effect of Turbulence on Limiting Current in Electrodialysis Cells, Ind. Eng. Chem. 51 (1959) 1445–1448. doi:10.1021/ie50600a026.

[174] S.K. Nataraj, K.M. Hosamani, T.M. Aminabhavi, Potential application of an electrodialysis pilot plant containing ion-exchange membranes in chromium removal, Desalination. 217 (2007) 181–190. doi:10.1016/j.desal.2007.02.012.

[175] N. Tzanetakis, W.M. Taama, K. Scott, R.J.J. Jachuck, R.S. Slade, J. Varcoe, Comparative performance of ion exchange membranes for electrodialysis of nickel and cobalt, Sep. Purif. Technol. 30 (2003) 113–127. doi:10.1016/S1383-5866(02)00139-9.

[176] A. Bukhovets, T. Eliseeva, N. Dalthrope, Y. Oren, The influence of current density on the electrochemical properties of anion-exchange membranes in electrodialysis of phenylalanine solution, Electrochim. Acta. 56 (2011) 10283–10287. doi:10.1016/j.electacta.2011.09.025.

[177] C. Casademont, P. Sistat, B. Ruiz, G. Pourcelly, L. Bazinet, Electrodialysis of model salt solution containing whey proteins: Enhancement by pulsed electric field and modified cell configuration, J. Memb. Sci. 328 (2009) 238–345. doi:10.1016/j.memsci.2008.12.013.

[178] V. Geraldes, M.D. Afonso, Limiting current density in the electrodialysis of multi-ionic solutions, J. Memb. Sci. 360 (2010) 499–508. doi:10.1016/j.memsci.2010.05.054.

[179] J. Balster, D.F. Stamatialis, M. Wessling, Towards spacer free electrodialysis, J. Memb. Sci. 341 (2009) 131–138. doi:10.1016/j.memsci.2009.05.048.

[180] J. Balster, I. Pünt, D.F. Stamatialis, M. Wessling, Multi-layer spacer geometries with improved mass transport, J. Memb. Sci. 282 (2006) 351–361. doi:10.1016/j.memsci.2006.05.039.

[181] H.J. Lee, H. Strathmann, S.H. Moon, Determination of the limiting current density in electrodialysis desalination as an empirical function of linear velocity, Desalination. 190 (2006) 43–50. doi:10.1016/j.desal.2005.08.004.

[182] P. Malek, J.M. Ortiz, B.S. Richards, A.I. Schäfer, Electrodialytic removal of NaCl from water: Impacts of using pulsed electric potential on ion transport and water dissociation phenomena, J. Memb. Sci. 435 (2013) 99–109. doi:10.1016/j.memsci.2013.01.060.

[183] J.G.D. Tadimeti, S. Chattopadhyay, Uninterrupted swirling motion facilitating ion transport in electrodialysis, Desalination. 392 (2016) 54–62. doi:10.1016/j.desal.2016.04.007.

[184] F. Aouad, A. Lindheimer, M. Chaouki, C. Gavach, Loss of permselectivity of anion exchange membranes in contact with zinc chloride complexes, Desalination. 121 (1999) 13–22. doi:10.1016/S0011-9164(99)00003-X.

[185] A.T. Cherif, A. Elmidaoui, C. Gavach, Separation of Ag+, Zn2+ and Cu2+ ions by electrodialysis with monovalent cation specific membrane and EDTA, J. Memb. Sci. 76 (1993) 39–49. doi:10.1016/0376-7388(93)87003-T.

[186] K. Prochaska, J. Antczak, M. Regel-Rosocka, M. Szczygiełda, Removal of succinic acid from fermentation broth by multistage process (membrane separation and reactive extraction), Sep. Purif. Technol. 192 (2018) 360–368. doi:10.1016/j.seppur.2017.10.043.

[187] S. Melnikov, D. Kolot, E. Nosova, V. Zabolotskiy, Peculiarities of transport-structural parameters of ion-exchange membranes in solutions containing anions

of carboxylic acids, J. Memb. Sci. 557 (2018) 1–12. doi:10.1016/j.memsci.2018.04.017.

[188] N. Pismenskaya, V. Nikonenko, B. Auclair, G. Pourcelly, Transport of weak-electrolyte anions through anion exchange membranes - Current-voltage characteristics, J. Memb. Sci. 189 (2001) 129–140. doi:10.1016/S0376-7388(01)00405-7.

[189] C. Gally, M. García-Gabaldón, E.M. Ortega, A.M. Bernardes, V. Pérez-Herranz, Chronopotentiometric study of the transport of phosphoric acid anions through an anion-exchange membrane under different pH values, Sep. Purif. Technol. 238 (2020) 116421. doi:10.1016/j.seppur.2019.116421.

[190] E.D. Belashova, N.D. Pismenskaya, V. V. Nikonenko, P. Sistat, G. Pourcelly, Current-voltage characteristic of anion-exchange membrane in monosodium phosphate solution. Modelling and experiment, J. Memb. Sci. 542 (2017) 177–185. doi:10.1016/j.memsci.2017.08.002.

[191] E.D. Belashova, O.A. Kharchenko, V. V. Sarapulova, V. V. Nikonenko, N.D. Pismenskaya, Effect of Protolysis Reactions on the Shape of Chronopotentiograms of a Homogeneous Anion-Exchange Membrane in NaH2PO4 Solution, Pet. Chem. 57 (2017) 1207–1218. doi:10.1134/S0965544117130035.

[192] E.H. Rotta, C.S. Bitencourt, L. Marder, A.M. Bernardes, Phosphorus recovery from low phosphate-containing solution by electrodialysis, J. Memb. Sci. 573 (2019) 293–300. doi:10.1016/j.memsci.2018.12.020.

[193] E.D. Melnikova, N.D. Pismenskaya, L. Bazinet, S. Mikhaylin, V. V. Nikonenko, Effect of ampholyte nature on current-voltage characteristic of anion-exchange membrane, Electrochim. Acta. 285 (2018) 185–191. doi:10.1016/j.electacta.2018.07.186.

[194] J.M. Zook, S. Bodor, R.E. Gyurcsányi, E. Lindner, Interpretation of chronopotentiometric transients of ion-selective membranes with two transition times, J. Electroanal. Chem. 638 (2010) 254–261. doi:10.1016/j.jelechem.2009.11.007.

[195] R.F. Dalla Costa, C.W. Klein, A.M. Bernardes, J.Z. Ferreira, Evaluation of the

electrodialysis process for the treatment of metal finishing wastewater, J. Braz. Chem. Soc. 13 (2002) 540–547. doi:10.1590/S0103-50532002000400021.

[196] E.Y. Choi, H. Strathmann, J.M. Park, S.H. Moon, Characterization of non-uniformly charged ion-exchange membranes prepared by plasma-induced graft polymerization, J. Memb. Sci. 268 (2006) 165–174. doi:10.1016/j.memsci.2005.06.052.

[197] R. Simons, Preparation of a high performance bipolar membrane, J. Memb. Sci. 78 (1993) 13–23. doi:10.1016/0376-7388(93)85243-P.

[198] S. Glabman, N. Uzal, X. Dou, X. Wei, Y. Chen, J.G. Hong, B. Zhang, H. Zhang, Potential ion exchange membranes and system performance in reverse electrodialysis for power generation: A review, J. Memb. Sci. 486 (2015) 71–88. doi:10.1016/j.memsci.2015.02.039.

[199] P. Długołecki, P. Ogonowski, S.J. Metz, M. Saakes, K. Nijmeijer, M. Wessling, On the resistances of membrane, diffusion boundary layer and double layer in ion exchange membrane transport, J. Memb. Sci. 349 (2010) 369–379. doi:10.1016/j.memsci.2009.11.069.

[200] L. Dammak, C. Larchet, D. Grande, Ageing of ion-exchange membranes in oxidant solutions, Sep. Purif. Technol. 69 (2009) 43–47. doi:10.1016/j.seppur.2009.06.016.

[201] G.S. Gohil, V.K. Shahi, R. Rangarajan, Comparative studies on electrochemical characterization of homogeneous and heterogeneous type of ion-exchange membranes, J. Memb. Sci. 240 (2004) 211–219. doi:10.1016/j.memsci.2004.04.022.

[202] T.W. Xu, Y. Li, L. Wu, W.H. Yang, A simple evaluation of microstructure and transport parameters of ion-exchange membranes from conductivity measurements, Sep. Purif. Technol. 60 (2008) 73–80. doi:10.1016/j.seppur.2007.07.049.

[203] N.N. Belaid, B. Ngom, L. Dammak, C. Larchet, B. Auclair, Â membranaire : interpre Â tation et exploitation Conductivite Á le a Á solution interstitielle he Â te Â roge Á ne selon le mode, Eur. Polym. J. 35. 35 (1999) 879–897.

[204] R. Lteif, L. Dammak, C. Larchet, B. Auclair, Conductivité électrique membranaire: Étude de l'effet de la concentration, de la nature de l'electrolyte et de la structure membranaire, Eur. Polym. J. 35 (1999) 1187–1195. doi:10.1016/S0014-3057(98)00213-4.

[205] S. Nouri, L. Dammak, G. Bulvestre, B. Auclair, Comparison of three methods for the determination of the electrical conductivity of ion-exchange polymers, Eur. Polym. J. 38 (2002) 1907–1913. doi:10.1016/S0014-3057(02)00057-5.

[206] J.W. Post, M. Saakes, H.H.M. Rijnaarts, A.H. Galama, J. Veerman, D.A. Vermaas, K. Nijmeijer, Membrane resistance: The effect of salinity gradients over a cation exchange membrane, J. Memb. Sci. 467 (2014) 279–291. doi:10.1016/j.memsci.2014.05.046.

[207] A.H. Galama, N.A. Hoog, D.R. Yntema, Method for determining ion exchange membrane resistance for electrodialysis systems, Desalination. 380 (2016) 1–11. doi:10.1016/j.desal.2015.11.018.

[208] R.F. Silva, M. De Francesco, A. Pozio, Tangential and normal conductivities of Nafion® membranes used in polymer electrolyte fuel cells, J. Power Sources. 134 (2004) 18–26. doi:10.1016/j.jpowsour.2004.03.028.

[209] J. Stodollick, R. Femmer, M. Gloede, T. Melin, M. Wessling, Electrodialysis of itaconic acid: A short-cut model quantifying the electrical resistance in the overlimiting current density region, J. Memb. Sci. 453 (2014) 275–281. doi:10.1016/j.memsci.2013.11.008.

[210] J.-H. Choi, H.-J. Lee, S.-H. Moon, Effects of Electrolytes on the Transport Phenomena in a Cation-Exchange Membrane., J. Colloid Interface Sci. 238 (2001) 188–195. doi:10.1006/jcis.2001.7510.

[211] E. Kniaginicheva, N. Pismenskaya, S. Melnikov, E. Belashova, P. Sistat, M. Cretin, V. Nikonenko, Water splitting at an anion-exchange membrane as studied by impedance spectroscopy, J. Memb. Sci. 496 (2015) 78–83. doi:10.1016/j.memsci.2015.07.050.

[212] M. Wessling, L.G. Morcillo, S. Abdu, Nanometer-thick lateral polyelectrolyte micropatterns induce macrosopic electro-osmotic chaotic fluid instabilities, Sci. Rep. 4 (2014) 1–5. doi:10.1038/srep04294.

[213] E. Korzhova, N. Pismenskaya, D. Lopatin, O. Baranov, L. Dammak, V. Nikonenko, Effect of surface hydrophobization on chronopotentiometric behavior of an AMX anion-exchange membrane at overlimiting currents, J. Memb. Sci. 500 (2016) 161–170. doi:10.1016/j.memsci.2015.11.018.

[214] H.-W. Rösler, F. Maletzki, E. Staude, Ion transfer across electrodialysis membranes in the overlimiting current range: chronopotentiometric studies, J. Memb. Sci. 72 (1992) 171–179. doi:10.1016/0376-7388(92)80197-R.

[215] V.M.B.C. Ruíz-Bauzá, Current–Voltage Curves for Ion-Exchange Membranes: A Method for Determining the Limiting Current Density, J. Colloid Interface Sci. 205 (1998) 365–373.

[216] M.C. Martí-Calatayud, M. García-Gabaldón, V. Pérez-Herranz, Study of the effects of the applied current regime and the concentration of chromic acid on the transport of Ni2+ ions through Nafion 117 membranes, J. Memb. Sci. 392–393 (2012) 137–149. doi:10.1016/j.memsci.2011.12.012.

[217] V. V. Nikonenko, A.M. Uzdenova, A. V. Kovalenko, M.K. Urtenov, S.A. Mareev, N.D. Pis'menskaya, G. Pourcelly, Effect of electroconvection and its use in intensifying the mass transfer in electrodialysis (Review), Russ. J. Electrochem. 53 (2017) 1122–1144. doi:10.1134/s1023193517090099.

[218] R. Ibanez, D.F. Stamatialis, M. Wessling, Role of membrane surface in concentration polarization at cation exchange membranes, J. Memb. Sci. 239 (2004) 119–128. doi:10.1016/j.memsci.2003.12.032.

[219] S. Mikhaylin, L. Bazinet, Fouling on ion-exchange membranes : Classification , characterization and strategies of prevention and control, Adv. Colloid Interface Sci. 229 (2016) 34–56. doi:10.1016/j.cis.2015.12.006.

[220] T. Scarazzato, Z. Panossian, J.A.S. Tenório, V. Pérez-Herranz, D.C.R. Espinosa, Water reclamation and chemicals recovery from a novel cyanide-free copper plating bath using electrodialysis membrane process, Desalination. 436 (2018) 114–124. doi:10.1016/j.desal.2018.01.005.

[221] V. Sarapulova, E. Nevakshenova, X. Nebavskaya, A. Kozmai, D. Aleshkina, G. Pourcelly, V. Nikonenko, N. Pismenskaya, Characterization of bulk and surface properties of anion-exchange membranes in initial stages of fouling by red wine,

J. Memb. Sci. 559 (2018) 170–182. doi:10.1016/j.memsci.2018.04.047.

[222] M.A. Andreeva, V.V. Gil, N.D. Pismenskaya, V.V. Nikonenko, L. Dammak, C. Larchet, D. Grande, N.A. Kononenko, Effect of homogenization and hydrophobization of a cation-exchange membrane surface on its scaling in the presence of calcium and magnesium chlorides during electrodialysis, J. Memb. Sci. 540 (2017) 183–191. doi:10.1016/j.memsci.2017.06.030.

[223] I. Rubinstein, B. Zaltzman, Electro-osmotically induced convection at a permselective membrane, Phys. Rev. E. 62 (2000) 2238–2251. doi:10.1103/PhysRevE.62.2238.

[224] J. Balster, M.H. Yildirim, D.F. Stamatialis, R. Ibanez, R.G.H. Lammertink, V. Jordan, M. Wessling, Morphology and Microtopology of Cation-Exchange Polymers and the Origin of the Overlimiting Current, J. Phys. Chem. B. 111 (2007) 2152–2165. doi:10.1021/jp068474t.

[225] E.M. Akberova, V.I. Vasil'eva, V.I. Zabolotsky, L. Novak, Effect of the sulfocation-exchanger dispersity on the surface morphology, microrelief of heterogeneous membranes and development of electroconvection in intense current modes, J. Memb. Sci. 566 (2018) 317–328. doi:10.1016/j.memsci.2018.08.042.

[226] F. Roghmans, E. Evdochenko, F. Stockmeier, S. Schneider, A. Smailji, R. Tiwari, A. Mikosch, E. Karatay, A. Kühne, A. Walther, A. Mani, M. Wessling, 2D Patterned Ion-Exchange Membranes Induce Electroconvection, Adv. Mater. Interfaces. 6 (2019) 1–11. doi:10.1002/admi.201801309.

[227] D. Cardoso, L. Stéphano, M. Antônio, S. Rodrigues, A. Moura, J. Alberto, S. Tenório, Water recovery from acid mine drainage by electrodialysis, Miner. Eng. 40 (2013) 82–89. doi:10.1016/j.mineng.2012.08.005.

[228] T. Scarazzato, D.C. Buzzi, A.M. Bernardes, D.C. Romano Espinosa, Treatment of wastewaters from cyanide-free plating process by electrodialysis, J. Clean. Prod. 91 (2015) 241–250. doi:10.1016/j.jclepro.2014.12.046.

[229] H. Meng, D. Deng, S. Chen, G. Zhang, A new method to determine the optimal operating current (Ilim′) in the electrodialysis process, Desalination. 181 (2005) 101–108. doi:10.1016/j.desal.2005.01.014.

[230] S.D. Bittencourt, L. Marder, T. Benvenuti, J.Z. Ferreira, A.M. Bernardes, Analysis of different current density conditions in the electrodialysis of zinc electroplating process solution, Sep. Sci. Technol. 52 (2017) 2079–2089. doi:10.1080/01496395.2017.1310896.

[231] R. Simons, Strong electric field effects on proton transfer between membrane-bound amines and water, Nature. 30 (1979) 824–826. doi:10.1038/280824a0.

[232] V.J. Frilette, Electrogravitational transport at synthetic ion exchange membrane surfaces, J. Phys. Chem. 61 (1957) 168–174. doi:10.1021/j150548a010.

[233] I. Rubinshtein, B. Zaltzman, J. Pretz, C. Linder, Experimental verification of the electroosmotic mechanism of overlimiting conductance through a cation exchange electrodialysis membrane, Russ. J. Electrochem. 38 (2002) 853–863. doi:10.1023/A:1016861711744.

[234] I. Rubinstein, B. Zaltzman, Electro-Osmotic Slip of the Second Kind and Instability in Concentration Polarization At Electrodialysis Membranes, Math. Model. Methods Appl. Sci. 11 (2001) 263–300. doi:10.1142/S0218202501000866.

[235] T. Pundik, I. Rubinstein, B. Zaltzman, Bulk electroconvection in electrolyte, Phys. Rev. E - Stat. Nonlinear, Soft Matter Phys. 72 (2005) 1–8. doi:10.1103/PhysRevE.72.061502.

[236] I. Rubinstein, B. Kedem, Zaltzman O., Electric fields in and around ion-exchange membranes, J. Memb. Sci. 125 (1997) 17–21.

[237] I. Rubinstein, Electroconvection at an electrically inhomogeneous permselective interface, Phys. Fluids A. 3 (1991) 2301–2309. doi:10.1063/1.857869.

[238] S.M. Rubinstein, G. Manukyan, A. Staicu, I. Rubinstein, B. Zaltzman, R.G.H. Lammertink, F. Mugele, M. Wessling, Direct observation of a nonequilibrium electro-osmotic instability, Phys. Rev. Lett. 101 (2008) 1–4. doi:10.1103/PhysRevLett.101.236101.

[239] R. Kwak, G. Guan, W.K. Peng, J. Han, Microscale electrodialysis: Concentration profiling and vortex visualization, Desalination. 308 (2013) 138–146. doi:10.1016/j.desal.2012.07.017.

[240] S.S. Dukhin, Electrokinetic phenomena of the second kind and their applications, Adv. Colloid Interface Sci. 35 (1991) 173–196. doi:10.1016/0001-8686(91)80022-C.

[241] N.A. Mishchuk, Electro-osmosis of the second kind near the heterogeneous ion-exchange membrane, Colloids Surfaces A Physicochem. Eng. Asp. 140 (1998) 75–89.

[242] I. Rubinstein, B. Zaltzman, T. Pundik, Ion-exchange funneling in thin-film coating modification of heterogeneous electrodialysis membranes, Phys. Rev. E - Stat. Physics, Plasmas, Fluids, Relat. Interdiscip. Top. 65 (2002) 10. doi:10.1103/PhysRevE.65.041507.

[243] M.K. Urtenov, A.M. Uzdenova, A. V. Kovalenko, V. V. Nikonenko, N.D. Pismenskaya, V.I. Vasil'eva, P. Sistat, G. Pourcelly, Basic mathematical model of overlimiting transfer enhanced by electroconvection in flow-through electrodialysis membrane cells, J. Memb. Sci. 447 (2013) 190–202. doi:10.1016/j.memsci.2013.07.033.

[244] C.L. Druzgalski, M.B. Andersen, A. Mani, Direct numerical simulation of electroconvective instability and hydrodynamic chaos near an ion-selective surface, Phys. Fluids. 25 (2013) 110804. doi:10.1063/1.4818995.

[245] F. Maletzki, H.W. Rösler, E. Staude, Ion transfer across electrodialysis membranes in the overlimiting current range: stationary voltage current characteristics and current noise power spectra under different conditions of free convection, J. Memb. Sci. 71 (1992) 105–116. doi:10.1016/0376-7388(92)85010-G.

[246] N.D. Pismenskaya, S.A. Mareev, E. V. Pokhidnya, C. Larchet, L. Dammak, V. V. Nikonenko, Effect of Surface Modification of Heterogeneous Anion-Exchange Membranes on the Intensity of Electroconvection at Their Surfaces, Russ. J. Electrochem. 55 (2019) 1203–1220. doi:10.1134/S1023193519120139.

[247] I. Rubinstein, L. Shtilman, Voltage against current curves of cation exchange membranes, J. Chem. Soc. Faraday Trans. 2 Mol. Chem. Phys. 75 (1979) 231–246. doi:10.1039/F29797500231.

[248] V.I. Zabolotsky, V. V Nikonenko, N.D. Pismenskaya, E. V Laktionov, M.K.

Urtenov, H. Strathmann, M. Wessling, G.H. Koops, Coupled transport phenomena in overlimiting current electrodialysis, Sep. Purif. Technol. 14 (1998) 255–267.

[249] M.A.K. Urtenov, E. V. Kirillova, N.M. Seidova, V. V. Nikonenko, Decoupling of the Nernst-Planck and Poisson equations. Application to a membrane system at overlimiting currents, J. Phys. Chem. B. 111 (2007) 14208–14222. doi:10.1021/jp073103d.

[250] M.B. Andersen, D.M. Rogers, J. Mai, B. Schudel, A. V. Hatch, S.B. Rempe, A. Mani, Spatiotemporal pH dynamics in concentration polarization near ion-selective membranes, Langmuir. 30 (2014) 7902–7912. doi:10.1021/la5014297.

[251] A. Uzdenova, A. Kovalenko, M. Urtenov, V. Nikonenko, 1D Mathematical Modelling of Non-Stationary Ion Transfer in the Diffusion Layer Adjacent to an Ion-Exchange Membrane in Galvanostatic Mode, Membranes (Basel). 8 (2018) 84. doi:10.3390/membranes8030084.

[252] S.S. Dukhin, N.A. Mishchuk, Unlimited increase in the current through an ionite granule, Kolloid. Zh. 49 (1987) 1197.

[253] I. Rubinstein, E. Staude, O. Kedem, Role of the membrane surface in concentration polarization at ion-exchange membrane, Desalination. 69 (1988) 101–114. doi:10.1016/0011-9164(88)80013-4.

[254] V. Nikonenko, V. Zabolotsky, C. Larchet, B. Auclair, G. Pourcelly, Mathematical description of ion transport in membrane systems, Desalination. 147 (2002) 369–374. doi:10.1016/S0011-9164(02)00611-2.

[255] S.M. Davidson, M. Wessling, A. Mani, On the Dynamical Regimes of Pattern-Accelerated Electroconvection, Sci. Rep. 6 (2016) 1–10. doi:10.1038/srep22505.

[256] N.A. Mishchuk, S.S. Dukhin, Chapter 10, in: A. Delgado (Ed.), Interfacial Electrokinet. Electrophor., Marcel Dekker, New York, 2002: p. 241.

[257] A. Pismenskiy, V. Nikonenko, M. Urtenov, G. Pourcelly, Mathematical modelling of gravitational convection in electrodialysis processes, Desalination. 192 (2006) 374–379. doi:10.1016/j.desal.2005.06.054.

[258] V. Nikonenko, A. Nebavsky, S. Mareev, A. Kovalenko, M. Urtenov, G.

Pourcelly, Modelling of ion transport in electromembrane systems: Impacts of membrane bulk and surface heterogeneity, Appl. Sci. 9 (2018). doi:10.3390/app9010025.

[259] A. Uzdenova, 2D mathematical modelling of overlimiting transfer enhanced by electroconvection in flow-through electrodialysis membrane cells in galvanodynamic mode, Membranes (Basel). 9 (2019). doi:10.3390/membranes9030039.

[260] S. Mareev, A. Kozmai, V. Nikonenko, E. Belashova, G. Pourcelly, P. Sistat, Chronopotentiometry and impedancemetry of homogeneous and heterogeneous ion-exchange membranes, Desalin. Water Treat. 56 (2015) 3207–3210. doi:10.1080/19443994.2014.981930.

[261] C. Druzgalski, A. Mani, Statistical analysis of electroconvection near an ion-selective membrane in the highly chaotic regime, Phys. Rev. Fluids. 1 (2016). doi:10.1103/PhysRevFluids.1.073601.

[262] E.D. Belashova, N.A. Melnik, N.D. Pismenskaya, K.A. Shevtsova, A. V. Nebavsky, K.A. Lebedev, V. V. Nikonenko, Overlimiting mass transfer through cation-exchange membranes modified by Nafion film and carbon nanotubes, Electrochim. Acta. 59 (2012) 412–423. doi:10.1016/j.electacta.2011.10.077.

[263] N.D. Pismenskaya, V. V. Nikonenko, N.A. Melnik, K.A. Shevtsova, E.I. Belova, G. Pourcelly, D. Cot, L. Dammak, C. Larchet, Evolution with time of hydrophobicity and microrelief of a cation-exchange membrane surface and its impact on overlimiting mass transfer, J. Phys. Chem. B. 116 (2012) 2145–2161. doi:10.1021/jp2101896.

[264] E. Korzhova, N. Pismenskaya, D. Lopatin, O. Baranov, L. Dammak, V. Nikonenko, Effect of surface hydrophobization on chronopotentiometric behavior of an AMX anion-exchange membrane at overlimiting currents, J. Memb. Sci. 500 (2015) 161–170. doi:10.1016/j.memsci.2015.11.018.

[265] E. Belova, G. Lopatkova, N. Pismenskaya, V. Nikonenko, C. Larchet, Role of water splitting in development of electroconvection in ion-exchange membrane systems, Desalination. 199 (2006) 59–61. doi:10.1016/j.desal.2006.03.142.

[266] V.M. Volgin, A.D. Davydov, Natural-Convective Instability of Electrochemical

Systems: A Review*, Elektrokhimiya. 42 (2006) 567–608. doi:10.1134/S1023193506060012.

[267] V.M. Volgin, O. V. Volgina, D.A. Bograchev, A.D. Davydov, Simulation of ion transfer under conditions of natural convection by the finite difference method, J. Electroanal. Chem. 546 (2003) 15–22. doi:10.1016/S0022-0728(03)00103-7.

[268] N.D. Pismenskaya, V. V Nikonenko, E.I. Belova, G.Y. Lopatkova, P. Sistat, G. Pourcelly, K. Larshe, Coupled convection of solution near the surface of ion-exchange membranes in intensive current regimes, Russ. J. Electrochem. 43 (2007) 307–327. doi:10.1134/S102319350703010X.

[269] V.I. Zabolotsky, V. V. Nikonenko, N.D. Pismenskaya, On the role of gravitational convection in the transfer enhancement of salt ions in the course of dilute solution electrodialysis, J. Memb. Sci. 119 (1996) 171–181. doi:10.1016/0376-7388(96)00121-4.

[270] R. Simons, Water splitting in ion exchange membranes, Electrochim. Acta. 30 (1985) 275–282. doi:10.1016/0013-4686(85)80184-5.

[271] R. Simons, Electric field effects on proton transfer between ionizable groups and water in ion exchange membranes, Electrochim. Acta. 29 (1984) 151–158. doi:10.1016/0013-4686(84)87040-1.

[272] V.I. Zabolotskii, N. V Shel'deshov, N.P. Gnusin, Dissociation of Water Molecules in Systems with Ion-exchange Membranes, Russ. Chem. Rev. 57 (1988) 801–808. doi:10.1070/rc1988v057n08abeh003389.

[273] J.J. Krol, M. Wessling, H. Strathmann, Concentration polarization with monopolar ion exchange membranes: Current-voltage curves and water dissociation, J. Memb. Sci. 162 (1999) 145–154. doi:10.1016/S0376-7388(99)00133-7.

[274] A. Elattar, A. Elmidaoui, N. Pismenskaia, C. Gavach, G. Pourcelly, Comparison of transport properties of monovalent anions through anion-exchange membranes, J. Memb. Sci. 143 (1998) 249–261. doi:10.1016/S0376-7388(98)00013-1.

[275] S. Mikhaylin, V. Nikonenko, G. Pourcelly, L. Bazinet, Intensification of

demineralization process and decrease in scaling by application of pulsed electric field with short pulse/pause conditions, J. Memb. Sci. 468 (2014) 389–399. doi:10.1016/j.memsci.2014.05.045.

[276] N.A. Mishchuk, S. V. Verbich, F. Gonzalez-Caballero, Concentration Polarization and Specific Selectivity of Membranes in Pulse Mode, Colloid J. 63 (2001) 586–594. doi:10.1023/A:1012399018946.

[277] Y.I. Kharkats, The mechanism of "supralimiting" currents at ion-exchange membrane/electrolyte interfaces, Sov. Electrochem. 21 (1985) 917–920.

[278] M.B. Andersen, M. Van Soestbergen, A. Mani, H. Bruus, P.M. Biesheuvel, M.Z. Bazant, Current-induced membrane discharge, Phys. Rev. Lett. 109 (2012) 1–5. doi:10.1103/PhysRevLett.109.108301.

[279] Z. Slouka, S. Senapati, Y. Yan, H.C. Chang, Charge inversion, water splitting, and vortex suppression due to DNA sorption on ion-selective membranes and their ion-current signatures, Langmuir. 29 (2013) 8275–8283. doi:10.1021/la4007179.

[280] M. Martí-Calatayud, M. García-Gabaldón, V. Pérez-Herranz, Mass Transfer Phenomena during Electrodialysis of Multivalent Ions: Chemical Equilibria and Overlimiting Currents, Appl. Sci. 8 (2018) 1566. doi:10.3390/app8091566.

[281] T. Sata, Ion Exchange Membranes: Preparation, Characterization, Modification and Application, Royal Society of Chemistry, Cambridge, 2004.

[282] N.A. Mishchuk, Polarization of systems with complex geometry, Curr. Opin. Colloid Interface Sci. 18 (2013) 137–148. doi:10.1016/j.cocis.2013.02.005.

Figure Captions

Figure 1 - Classification of membranes according to their heterogeneity and polarity.

Figure 2 – Schematic drawing illustrating a counter-ion pathway through homogeneous and heterogeneous ion-exchange membranes (Adapted from ref. [9]).

Figure 3 - SEM images of a (a) heterogeneous and (b) homogeneous cation-exchange membrane. Red arrows indicate dispersed agglomerates of ion-exchange particles. Blue arrows indicate the polymer binder (Adapted from ref. [15]).

Figure 4 - Schematic representation of a polymer matrix of a cation-exchange membrane equilibrated in an electrolyte (Adapted from ref. [2]).

Figure 5 - A schematic diagram of a typical monopolar electrodialysis system.

Figure 6 - Schematic diagram of the function of a bipolar membrane.

Figure 7 - Representation of a typical repeating unit within a bipolar membrane electrodialysis system.

Figure 8 - Schematic representation of a chronopotentiometric setup with a) the typical three-compartment cell and b) the six-compartment cell used in refs. [81,82].

Figure 9 - Representation of typical chronopotentiometric curves of monopolar membranes.

Figure 10 - Determination of transition time using the derivative method (Adapted from ref. [65]).

Figure 11 - Representation of the (τ) vs. $(C_0/i)^2$ curve for determining the counter-ion transport number.

Figure 12 - Representation of a chronopotentiometric curve with precipitate formation (full line). Dashed line corresponds to a classical shape of a chronopotentiometric curve for a monopolar membrane (Adapted from ref. [71]).

Figure 13 - Dependencies of transition time on current density represented in Sand's coordinates obtained by ref. [151] using one membrane and two different solutions: NaCl and LysHCl (Adapted from [151]).

Figure 14 - Typical current-voltage curve of an ion-exchange membrane.

Figure 15 - Concentration profile at the membrane-solution interface during electrodialysis (Adapted from ref. [281]).

Figure 16 - a) and b) Schematic drawing illustrating the evolution of concentration profiles of counter-ions in the diffusion boundary layer at different current densities (Adapted from ref. [160]).

Figure 17 - Representation of a Cowan-Brown curve.

Figure 18 – a) CVCs with two limiting current densities and b) ChP with two transition times (Adapted from ref. [141]).

Figure 19 - Current-voltage curves obtained with and without discounting the ohmic resistance (Adapted from ref. [81]).

Figure 20 - Representation of the current lines distribution close to the surface of (a) homogeneous and (b) heterogeneous ion-exchange membranes.

Figure 21 – CVC of an unmodified membrane and of two coated membranes with 25% and 31% of surface coverage degree with a microgel (adapted from ref. [226]).

Figure 22 – A scheme of electroconvection vortices formed near a heterogeneous surface containing well and poorly conducting areas (Adapted from ref. [282]).

Figure 23 - Representation of a chronopotentiometric curve with the typical oscillations due to the occurrence of electroconvection (adapted from ref. [268]).

Figure 24 - Theoretical (solid) and experimental (dashed) chronopotentiometric curves of a cation-exchange membrane at different current densities in 0.02 M NaCl solution (Adapted from ref. [76]).

Figure 25 - Representation of a chronopotentiometric curve with the typical decrease in potential drop due to gravitational convection, dissociation of water and/or current-induced co-ion transfer (adapted from ref. [73]).

Figures

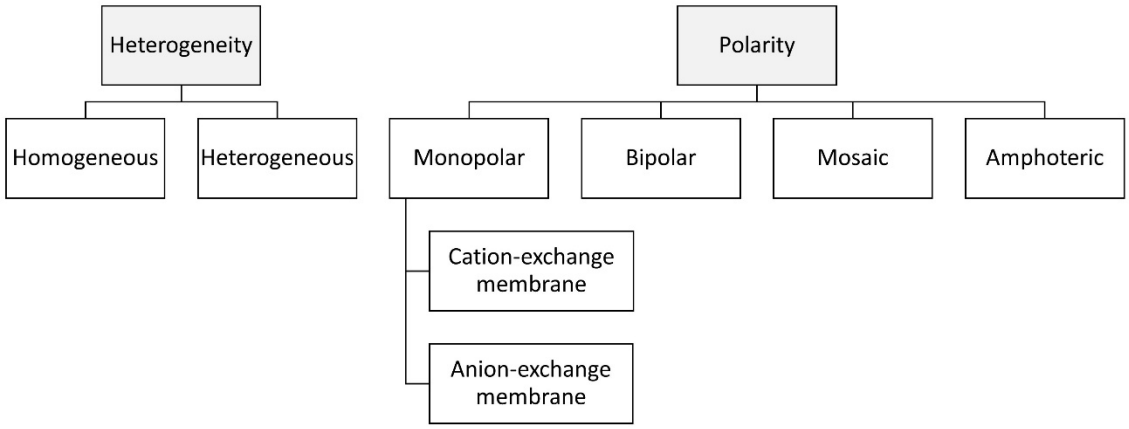

Figure 1

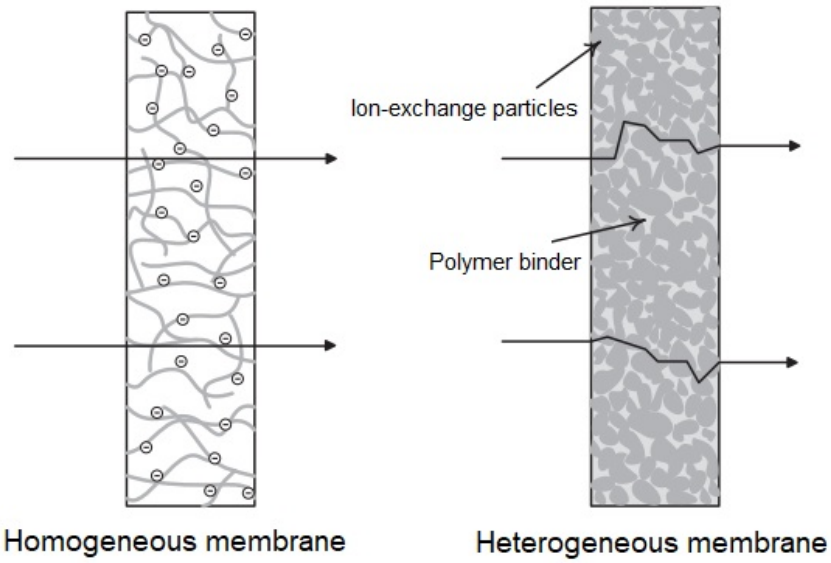

Figure 2

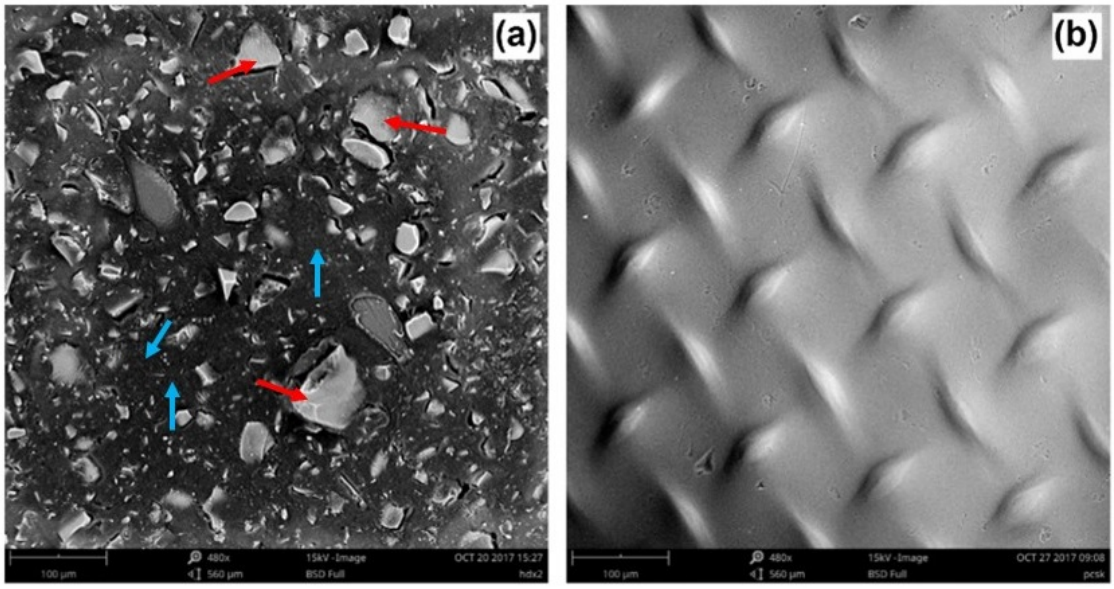

Figure 3

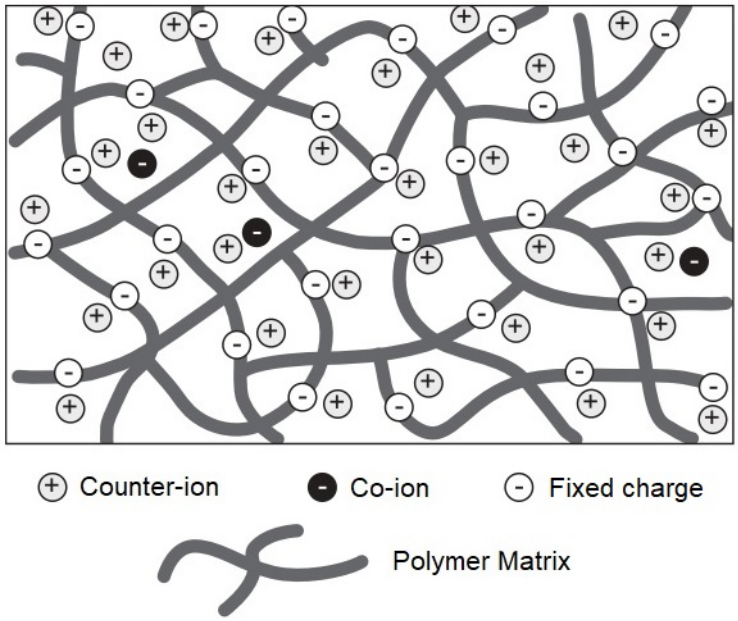

Figure 4

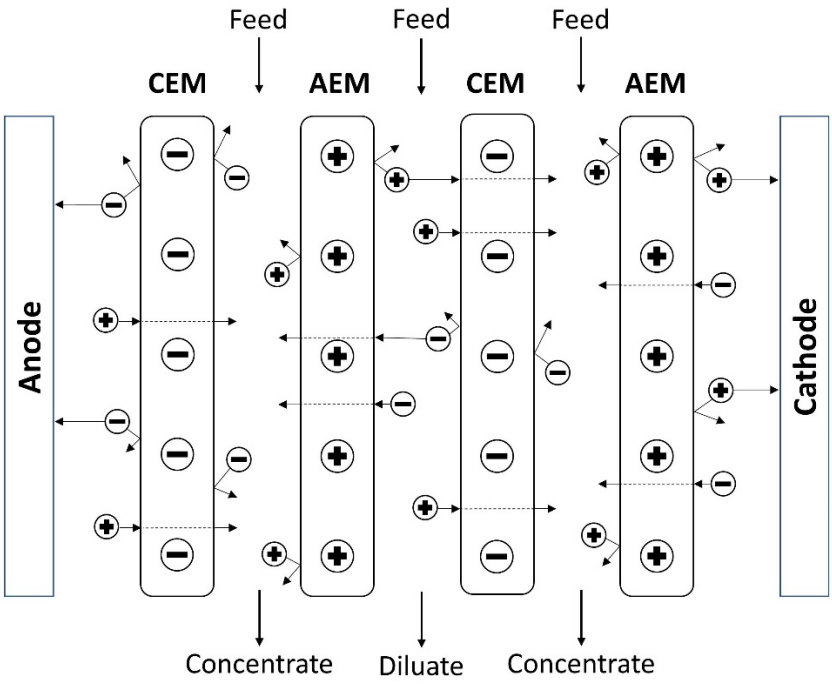

Figure 5

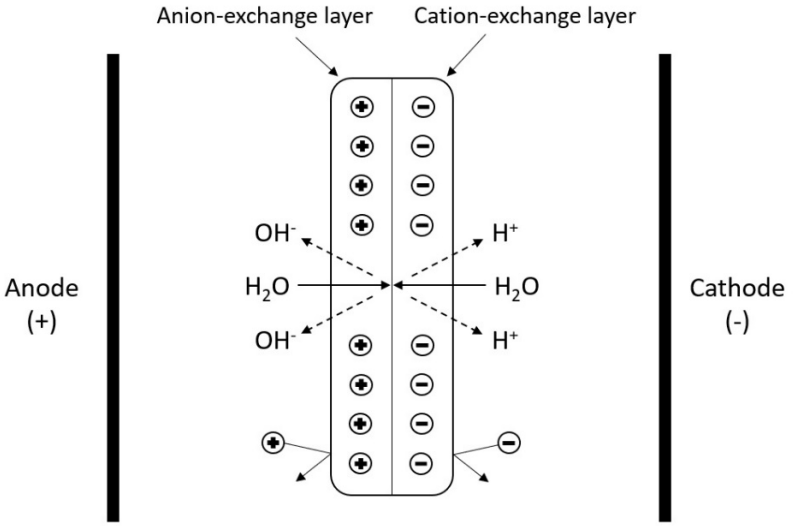

Figure 6

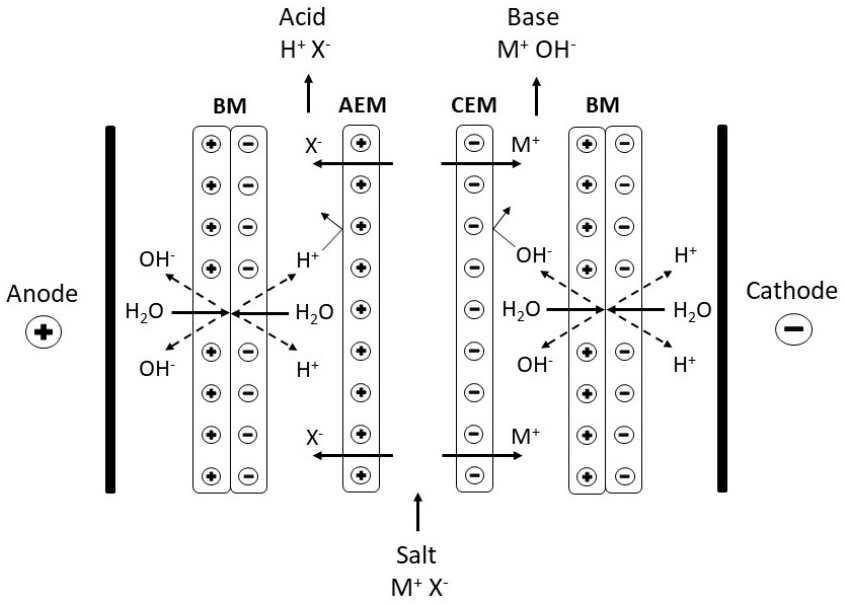

Figure 7

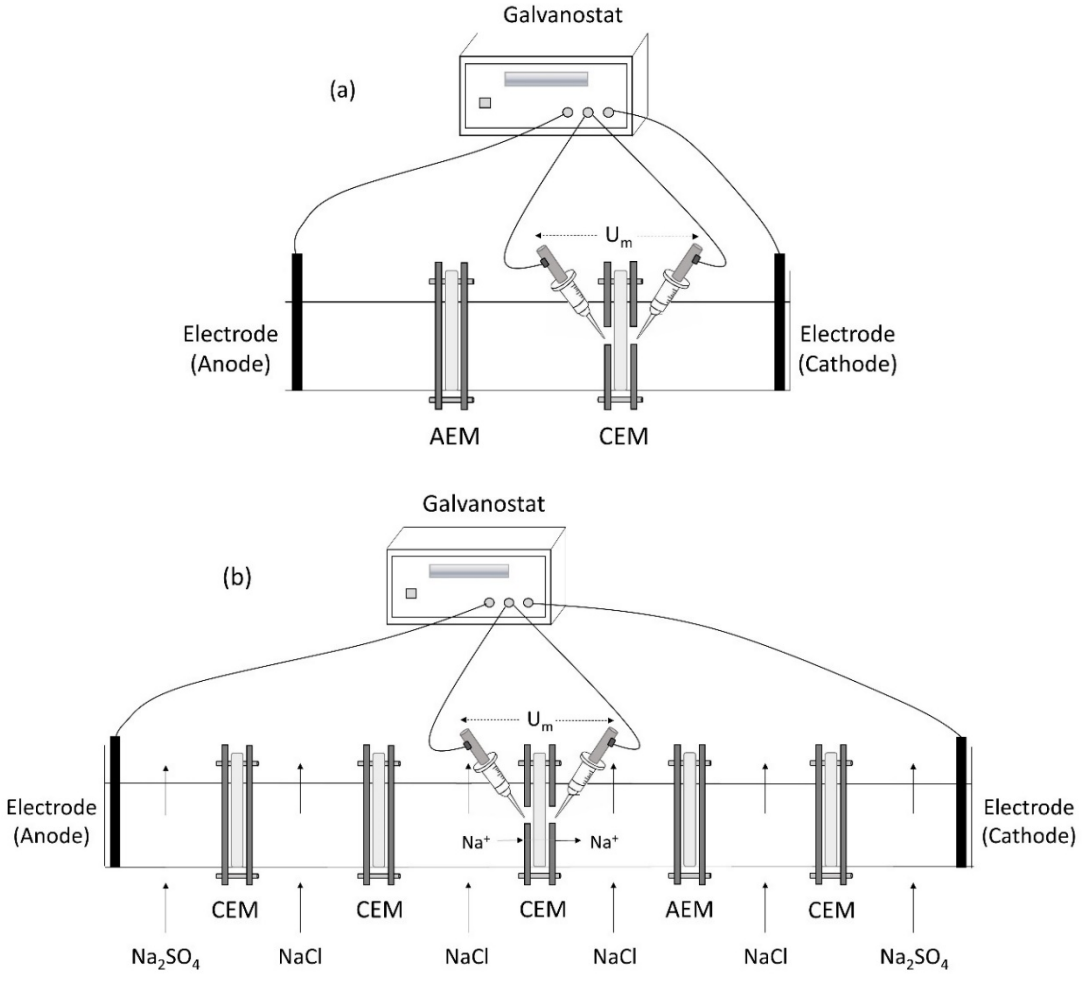

Figure 8

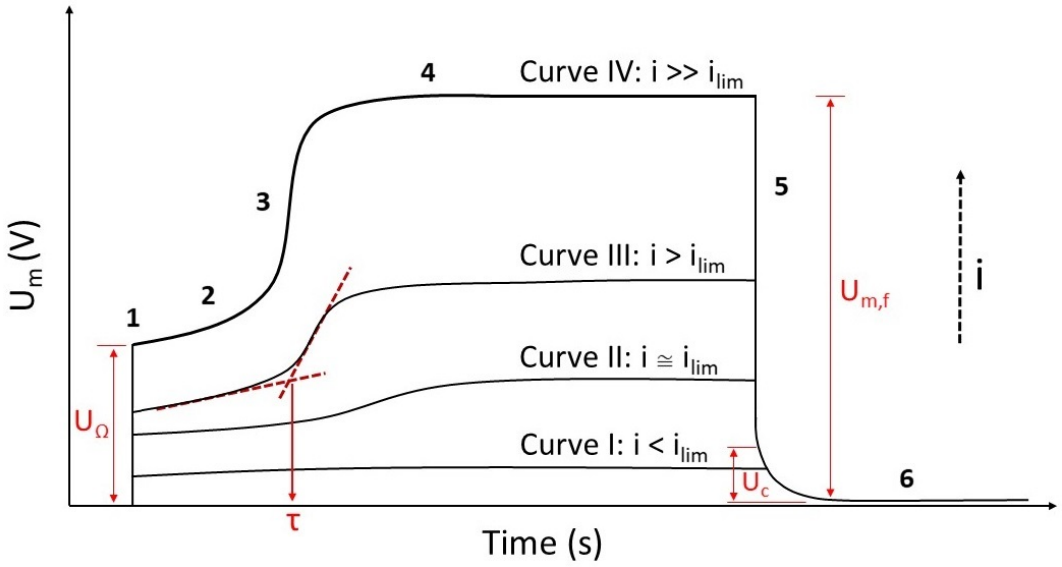

Figure 9

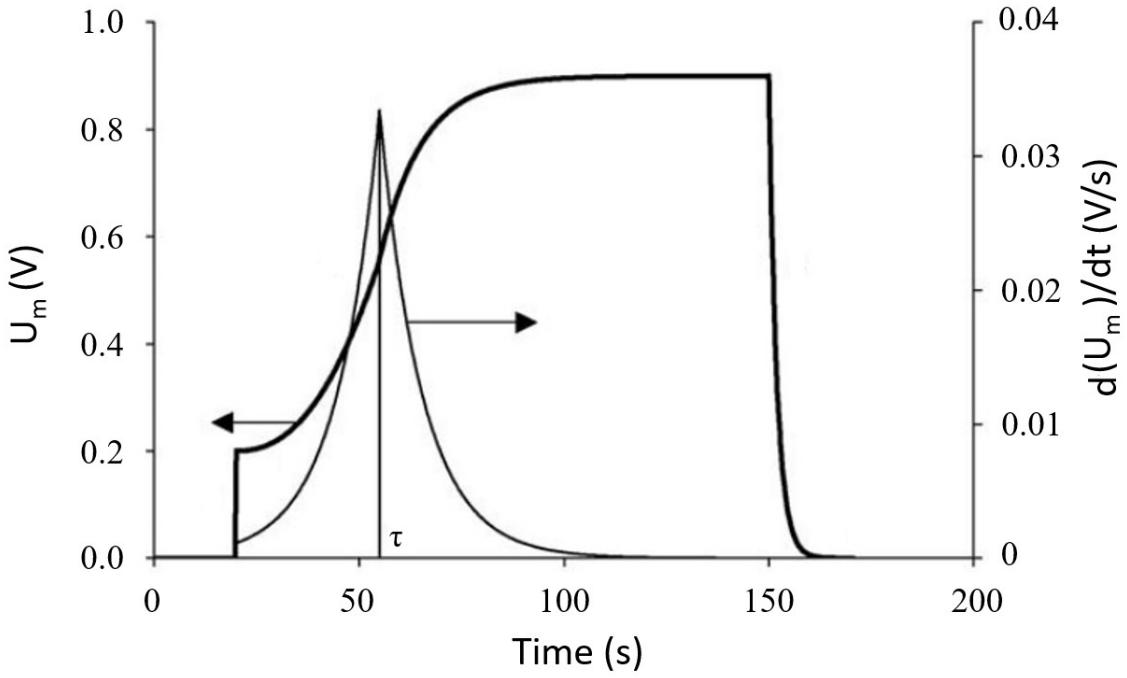

Figure 10

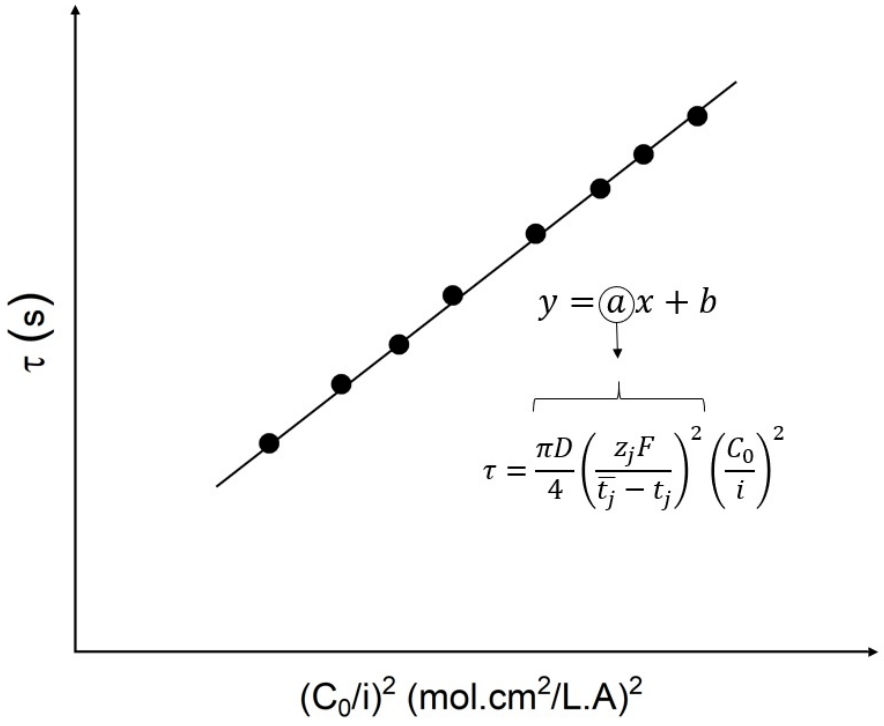

Figure 11

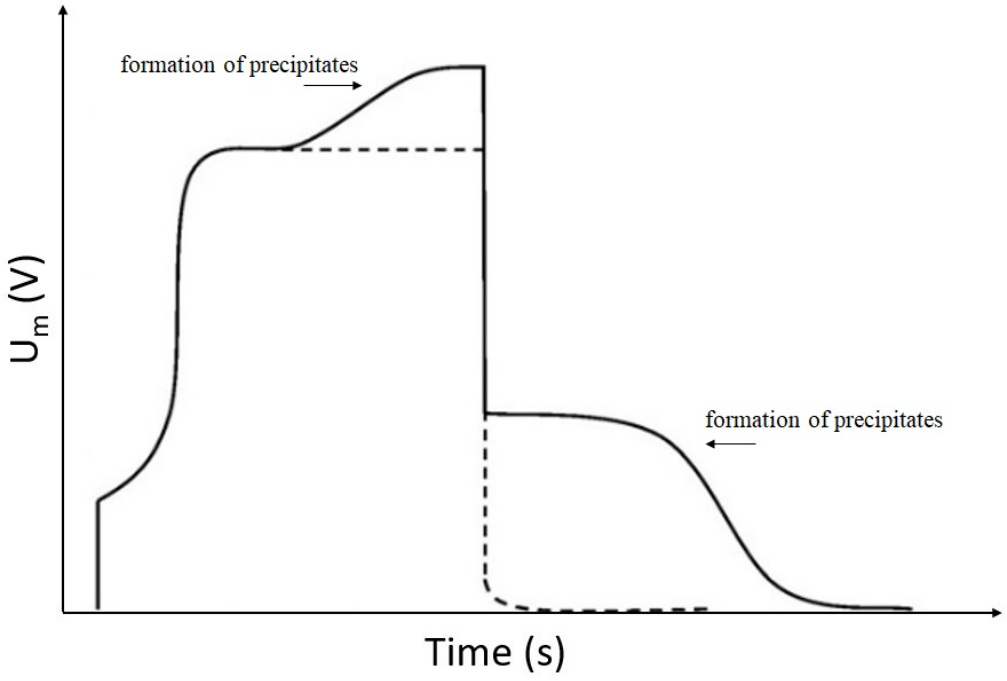

Figure 12

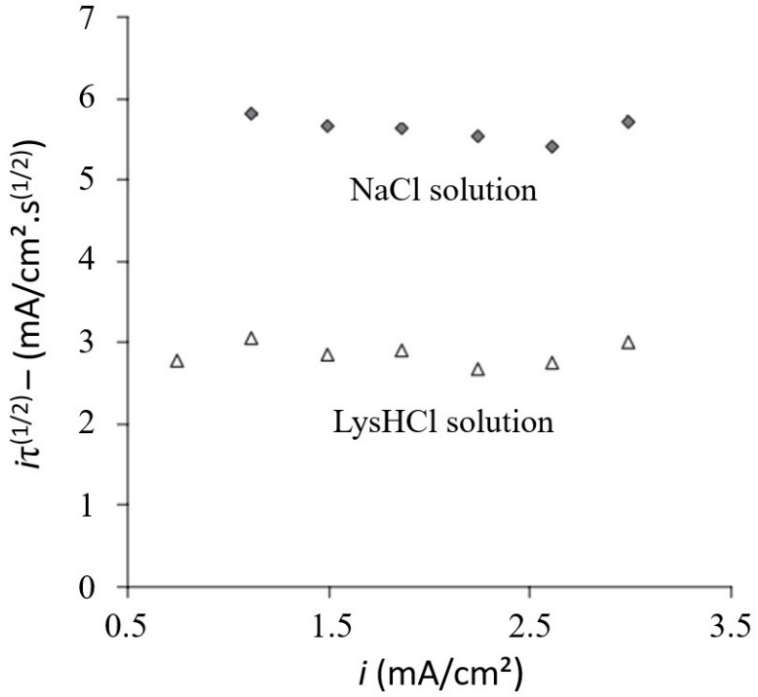

Figure 13

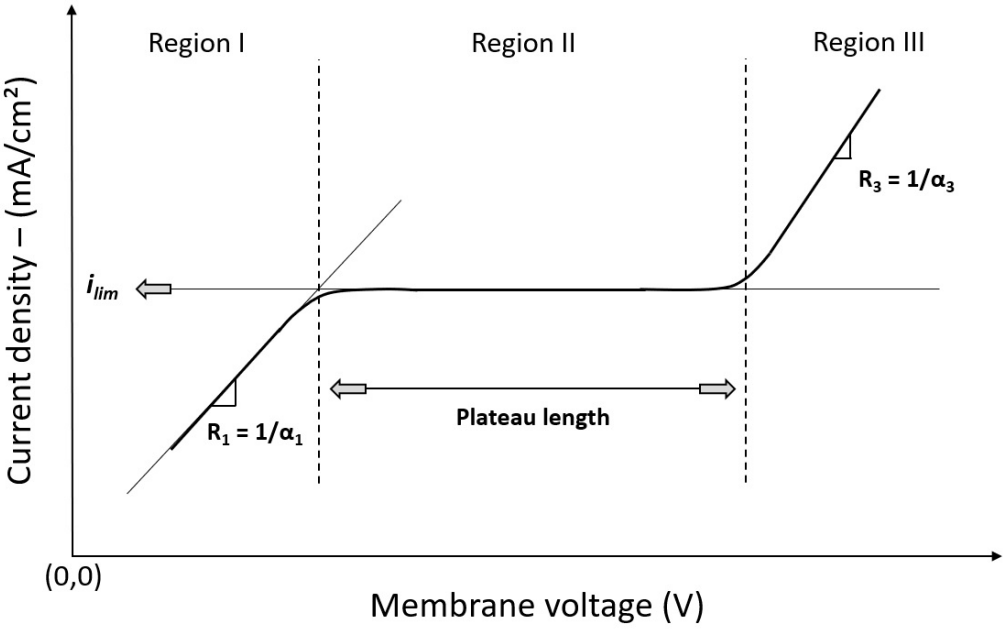

Figure 14

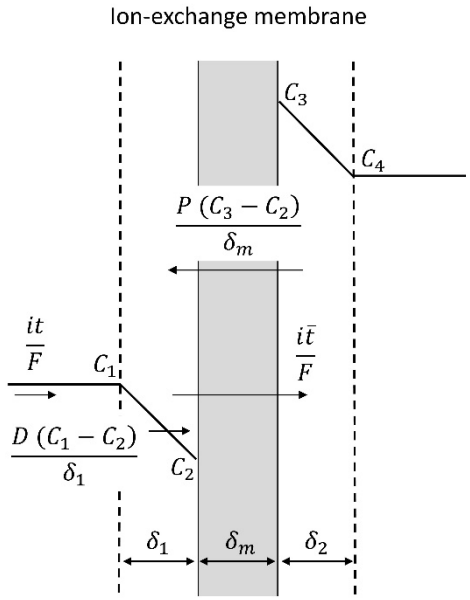

Figure 15

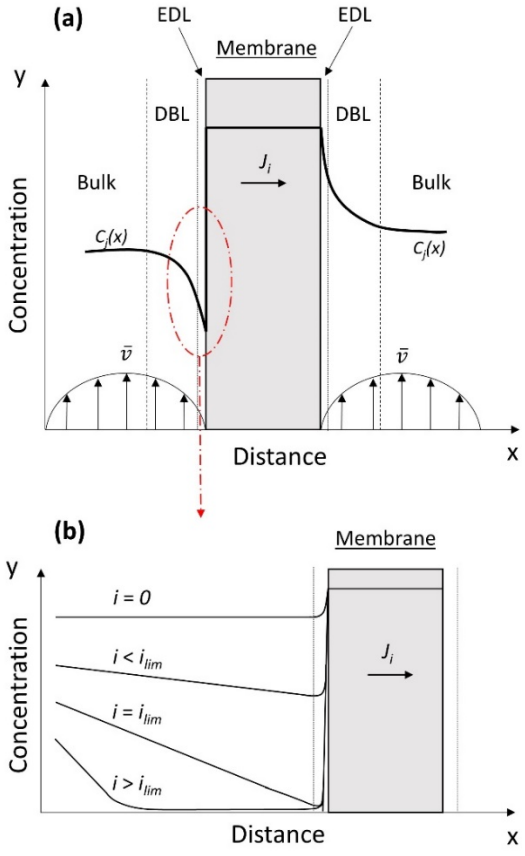

Figure 16

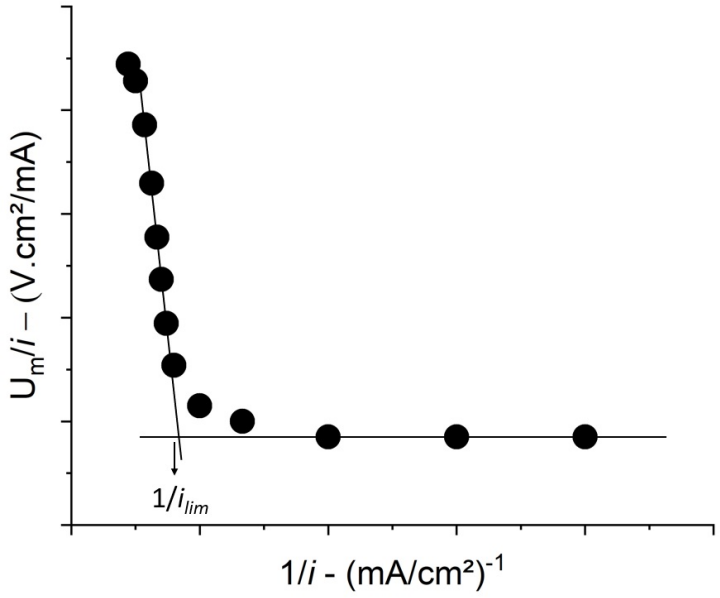

Figure 17

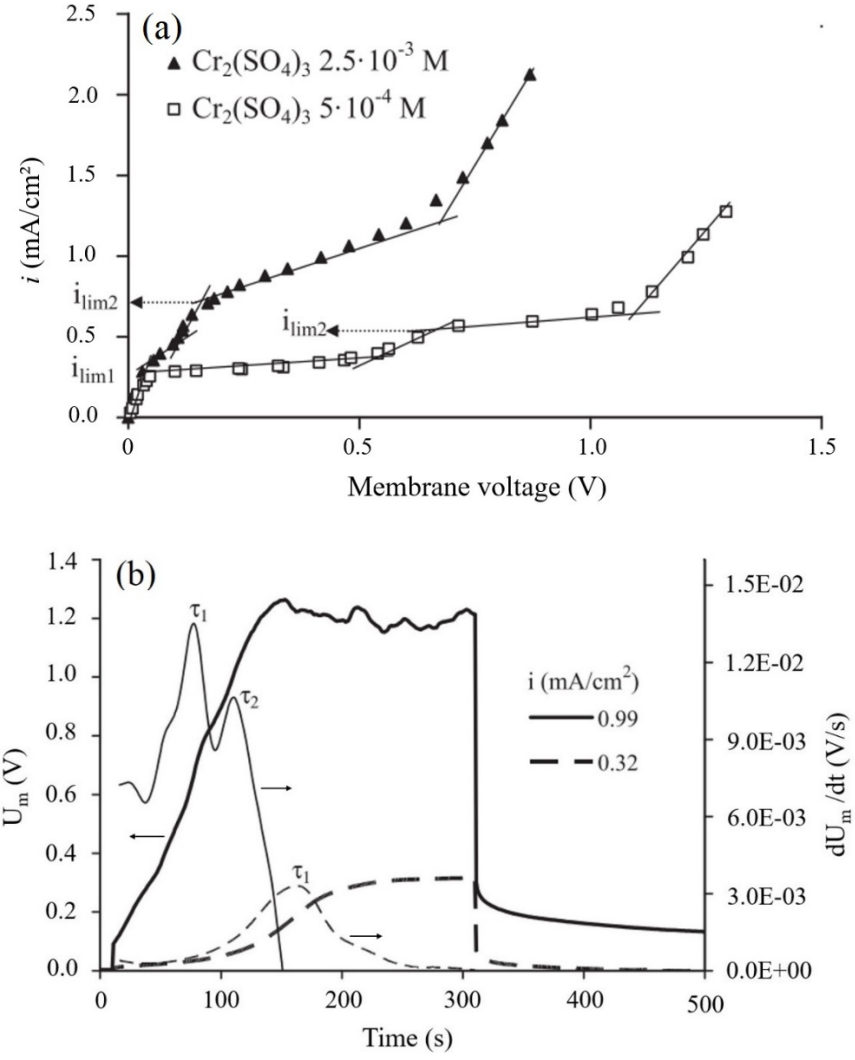

Figure 18

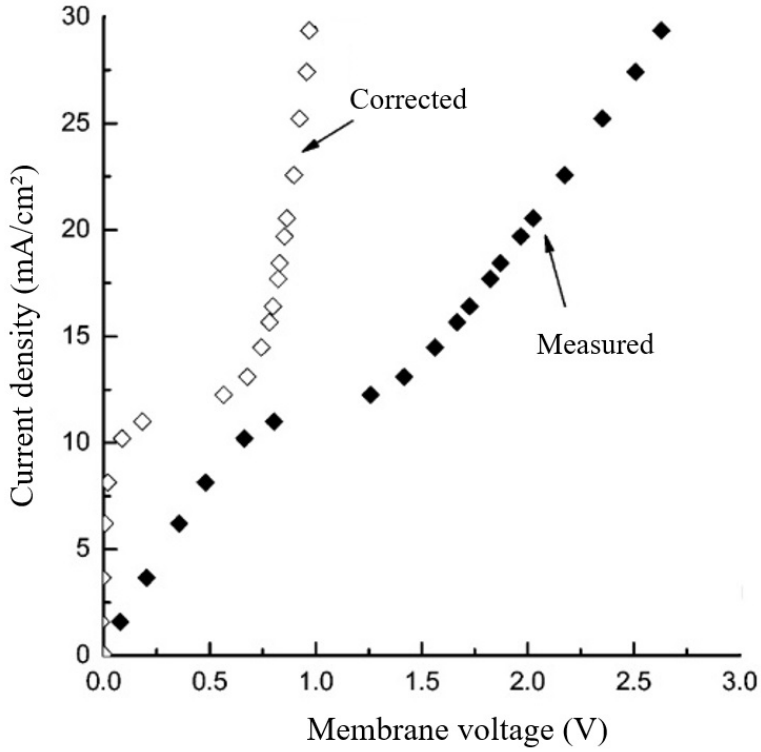

Figure 19

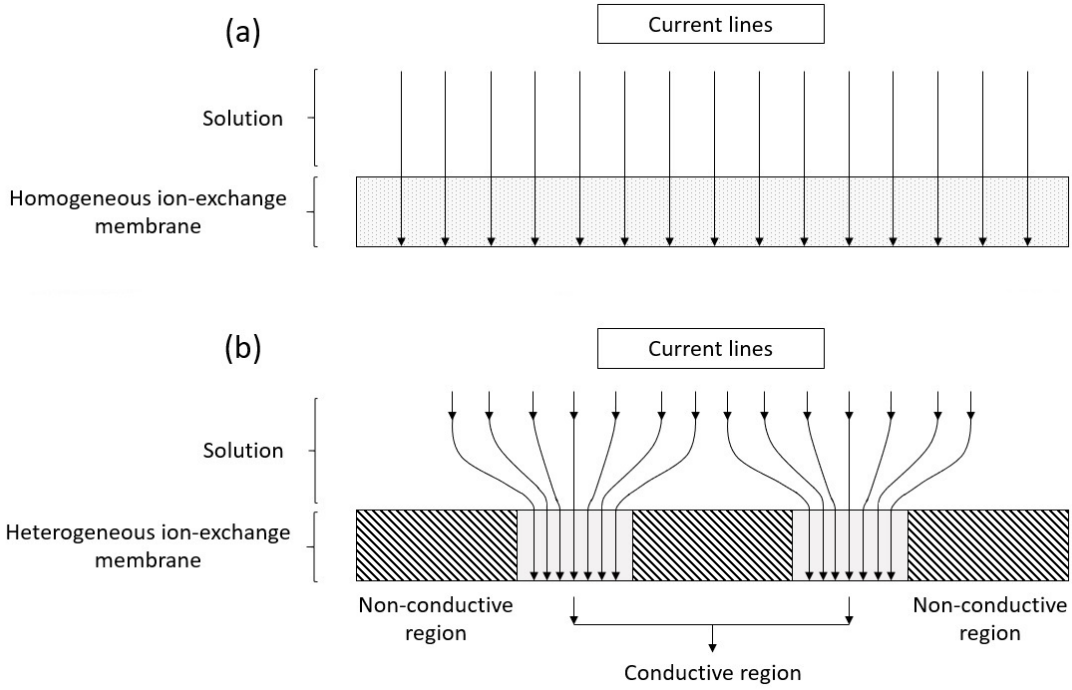

Figure 20

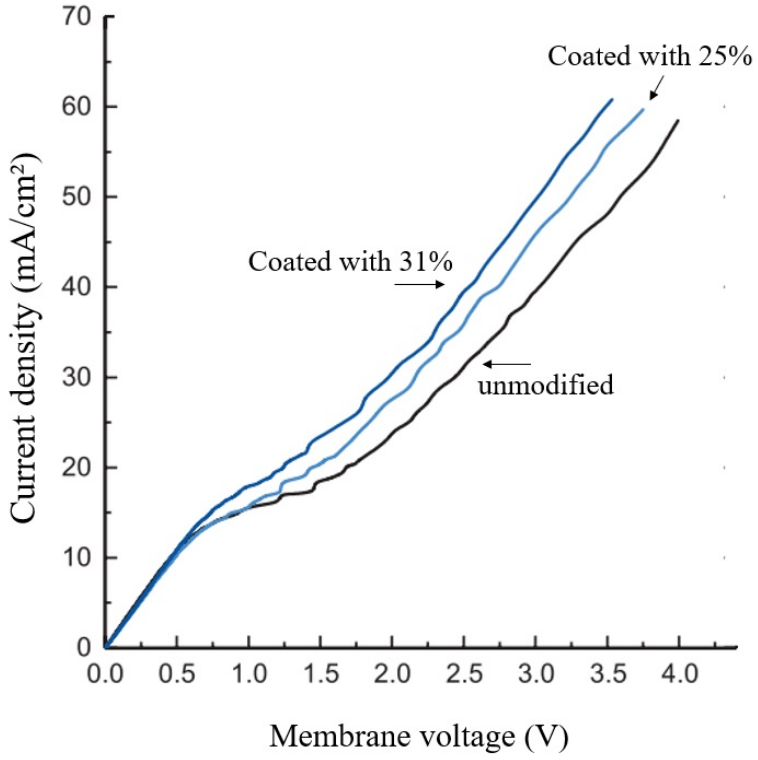

Figure 21

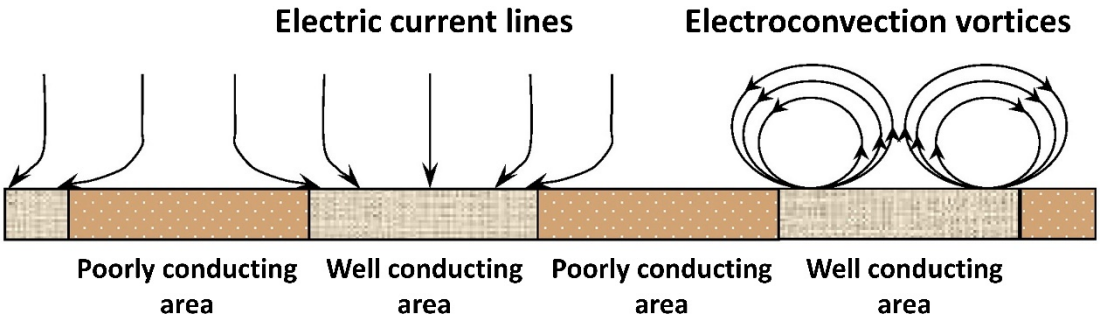

Figure 22

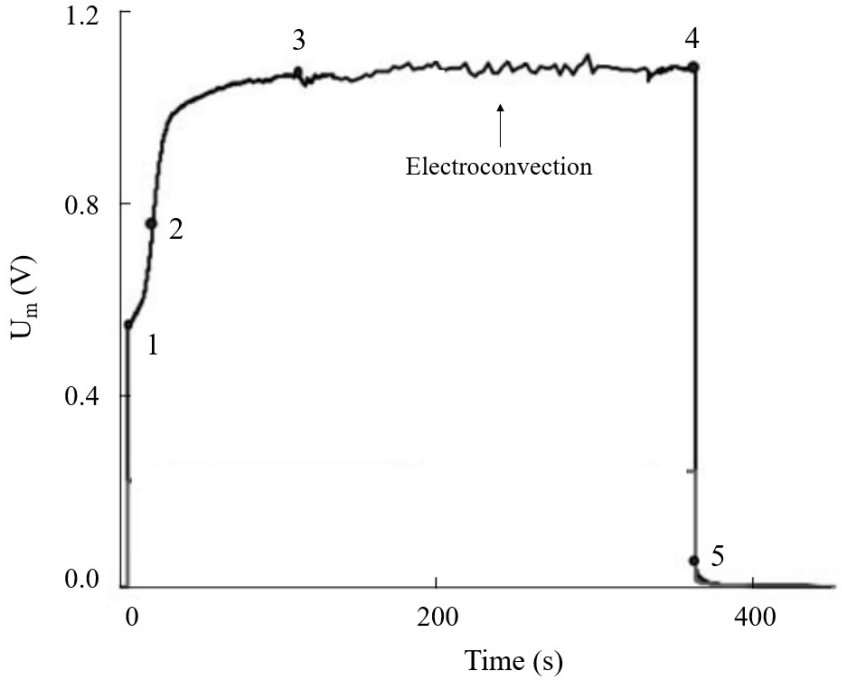

Figure 23

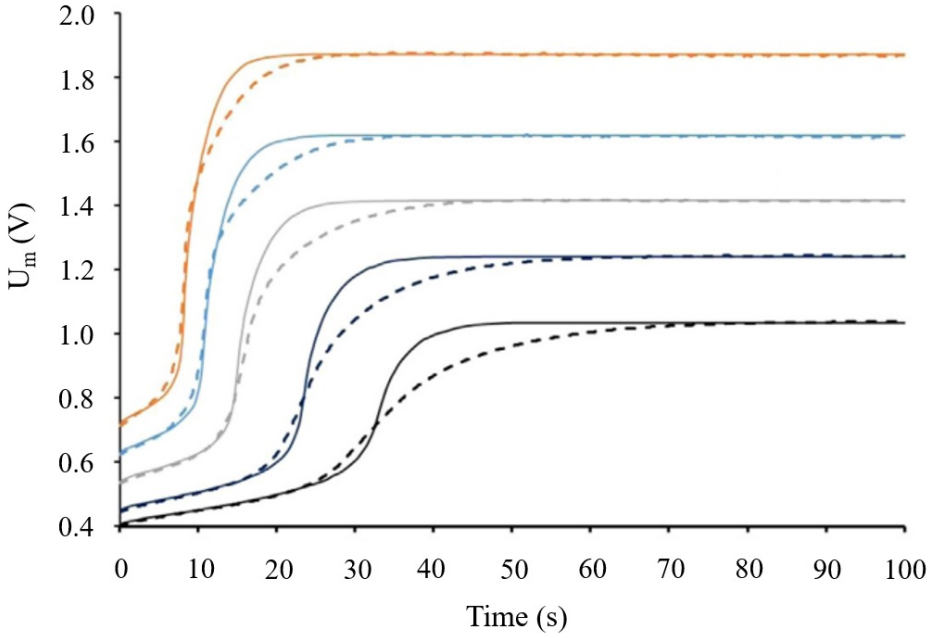

Figure 24

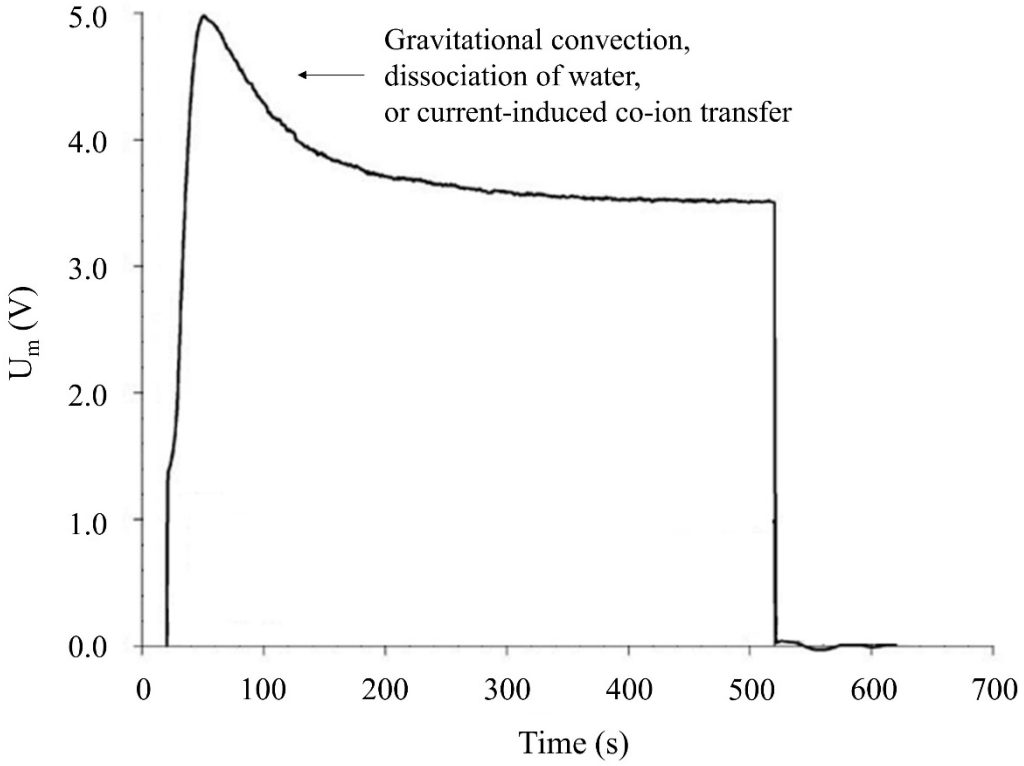
5.0
4.0
3.0
2.0
1.0
0.0
U_m (V)
0
100
200
300
400
500
600
700
Time (s)
Gravitational convection,
dissociation of water,
or current-induced co-ion transfer

Figure 25